SORPTION AND TRANSPORT IN HETEROGENEOUS POROUS MEDIA: APPLICATIONS OF FRACTAL AND STOCHASTIC APPROACHES

By

ITARU OKUDA

A DISSERTATION PRESENTED TO THE GRADUATE SCHOOL
OF THE UNIVERSITY OF FLORIDA IN PARTIAL FULFILLMENT
OF THE REQUIREMENTS FOR THE DEGREE OF
DOCTOR OF PHILOSOPHY

UNIVERSITY OF FLORIDA

1993

Copyright 1993

by

Itaru Okuda

ACKNOWLEDGEMENTS

The last four years that I spent working toward the Ph.D. were filled with excitement, frustrations, and challenges.

My research could not be accomplished without the understanding, guidance and the support of my major advisor, Dr.P.S.C. Rao. He gave me the opportunities and freedom to explore what I wanted to learn, which are probably the most precious things that a scientist can get. I am grateful to Dr. C.T. Johnston for his help in conducting vapor desorption experiments. I am indebted to Dr. R.D. Rhue, Dr. K. Hatfield, Dr. C.W. Park, and Dr. W.D. Graham for their valuable suggestions, and for serving on my dissertation committee.

I would like to thank Denie, Linda, Cheryl, Dong-Ping, Chris, and many other friends for their friendship and encouragement.

Finally, I am grateful to my parents for their understanding and support.

TABLE OF CONTENTS

Abstract of Dissertation Presented to the Graduate School
of the University of Florida in Partial Fulfillment of the
Requirements for the Degree of Doctor of Philosophy

SORPTION AND TRANSPORT IN HETEROGENEOUS POROUS MEDIA:
APPLICATION OF FRACTAL AND STOCHASTIC APPROACHES

By

Itaru Okuda

August 1993

Chairperson: Dr. P. S. C. Rao
Major Department: Soil and Water Science Department

The understanding and prediction of complex natural phenomena are essential to approach various environmental problems. This dissertation is focused on "how to deal with natural complexity."

In the first part of the dissertation, the molecular level geometry of natural and synthetic sorbents was studied. The main objective was to investigate how the complexity of the surface geometry affects the sorption behavior. In particular, the applicability and limitations of the concept of fractal dimension was used as the conceptual guideline. The surface fractal dimension was found to be a good measure of the geometrical heterogeneity of a surface as long as the surface is well-defined. The experimentally-estimated surface fractal dimensions of kaolinite and silica-gel were about 2.18 and 2.38, respectively. However, for energetically-

as well as geometrically- complex sorbents, the sorption behavior was also complex, and it could not be explained solely from the geometrical factors as a fractal object. Under such conditions, various controlling factors become compounded, and it is difficult to well-define surface parameters as measured from the sorption isotherms.

In the second half of the dissertation, solute transport in geometrically- and energetically-heterogeneous porous media was considered. Conceptually, solute transport phenomena in heterogeneous space may be approached from Langevin equation, Fokker-Planck equation, or Chapman-Kolmogorov equation. To study the effect of heterogeneity, hypothetical representations of complex media were created by imposing "self-organization" logic. Transport phenomena, such as diffusion-like transport in a heterogeneous medium, and desorption kinetics from a complex sorbed phase, were simulated using discrete Markov chain model, and compared with simplified differential equation models. The simulations revealed complex appearances of transport phenomena in heterogeneous hypothetical media. The proposed model seems to be an effective tool to investigate the details of solute transport in heterogeneous media.

CHAPTER 1
INTRODUCTION

One of the most challenging problems in environmental science is the description of processes occurring in complex natural systems. It is the complexities which obscure the connection between the cause and the outcome of environmental phenomena. Therefore, unlike mathematical and theoretical physics problems, many real phenomena in the environmental systems seem to be much more complex than something we can express with manageable mathematical expressions. Consequently, we are often forced to deal with problems in rather pragmatic, practical and semi-empirical ways focusing strongly on the predictable capabilities which meet our needs and demands of such predictions. However, over the years, I have encountered various ambiguities in environmental science. Such ambiguities make the communication and mutual understanding among environmental professionals difficult. I came to the point where I could not stand on such shaky ground in the name of applied science. I suspect such ambiguities are originated mainly from the complexity and heterogeneity of the systems. Therefore, I decided to explore some of the problems associated with complexities.

When I first started my studies in environmental science in semi-quantitative fashion, I came upon various questions;

(1) how many variables are needed to completely and uniquely specify the system,

(2) how many variables are required to perform a reasonable prediction,

(3) how do we choose those variables,

(4) accepting the fact that our idealized picture (model) is imperfect, how do we go about dealing with the factors which are not in the idealized picture.

I do not expect that for a large complex system these questions can be answered completely. In environmental, biological or social sciences, such questions are nontrivial. However, it was important for me to at least get the qualitative (conceptual) feel of the systems for which quantitative (idealized) pictures (or models) are developed. I found theorems in classical physics, which include the idea of phase space, Liouville theorem, Hamiltonian mechanics, and thermodynamics, to be very useful as guidelines to think through the problems posed by the first question. This is one area of science which I have to study more. For the second question, we often start from finding out what do we mean by a "reasonable" prediction. This is a rather practical question and it depends on the problem at hand. The next step is to choose variables. Generally we pick the relevant variables based on our educated guesses until the phenomena of interest

can be described to the accuracy we desire. As far as I see, this approach is usually the best we can do. However, there seems to be a discontinuity in attitude between the approaches in the basic science which evoke the question (1), and of the applied science which is primarily concerned with the questions (2) and (3) (e.g. a summary on experimental, theoretical, and the environmental applications aspects of adsorption is provided by Findenegg, Steele, and Weber in Myers and Belfort (1984)). Even when our predictive capability is high, it is important to contemplate the real meanings of such predictions.

The fourth question is also worth considering. It is probably true that most of the mathematical models used in environmental science require some sort of data fitting and/or the interpretation of the fitted parameters. Unfortunately, there seem to be many misuses and misunderstandings of the use of such idealized models by over-trusting the underlying mathematics, physics, and chemistry, and biological theories of the model (e.g. Sposito et al., 1983). Suppose the system can be described by 10 variables. However, due to various constraints, we can only measure the 5 variables which explain 95 percent of the phenomena of our interest. So we write a "reasonable" model based on these five variables. By fitting the parameters, we may be able to explain 99 percent of the phenomena, although such a procedure is, of course, incorrect in a strict sense. Then what happened to the rest of the five parameters? How do we know if the model is correct, and that the parameters represent what they should be representing? Over what range of parameter values does this approximation based on only five variables provide

adequate prediction? In particular, when the system has heterogeneity which is difficult to characterize, how do we deal with it? If the nature of heterogeneity can be characterized and parameterized, as is so often the case, how do we estimate appropriate "average" parameters and processes? These types of questions can be only answered by carefully examining the system and designing clever discriminating experiments. However, in many instances, it is not the case, and many theories and equations seem to be used without any doubt of their validity. Furthermore, we often use those ambiguous parameters as variables to obtain other parameters. Such encounters with ambiguities forced me to be skeptical, and made me realize the importance of the scientific reasoning.

As an applied scientist, I should learn to acknowledge the practical problems we are facing, and accept the imperfectness of our approaches. Nevertheless, I think we should not ignore any ambiguities. Since it is inevitable to deal with ambiguities coming from the natural complexity in environmental science, we should rather try to (1) identify the nature of the complexity and ambiguities, and (2) understand how complexity can affect our idealized picture. This is the motivation of my study toward the Ph.D. degree. Through my study, I wanted to learn how deep our scientific reasoning, or more specifically reductionism, can work in a complex world. As a subject of my contemplation and investigation, I found abiotic soil system to be ideal since it is exceedingly complex at an atomic level, but also simple compared to biological systems. It is worthwhile to mention

two books which influenced my philosophy. One is a book by Erwin Schrödinger entitled "What is Life? & Mind and Matter" (Schrödinger, 1967). Written in 1944-1958, the celebrated pioneer of quantum mechanics speculates physics of biological systems which inspired many early-day molecular biologists. The other book is "The Systems View of the World" by Ervin Laszlo (1972). These two rather contrasting attitudes toward life influenced my thinking significantly.

In the next two chapters, we will consider a few approaches to the problems of natural heterogeneities. In Chapter 2, the characteristics of sorption of organic vapors onto heterogeneous surfaces are considered as an example of a heterogeneous equilibrium system. In the past, most of our ideas of surface phenomena evolved around the assumption of a flat surface. For vapor sorption, the B.E.T. theory has been accepted as a simple mechanistic model for sorption onto a uniform, near flat surface, and has been widely applied in environmental science. However, a real natural surface is likely to be neither uniform nor flat. Most of the studies on the macroscopic sorption on heterogeneous surfaces have dealt with energetically-heterogeneous surfaces. However, the recent development of fractal theory enables us to deal with sorption onto geometrically-heterogeneous, rough surfaces. The main objective of Chapter 2 is to experimentally investigate the degree of molecular-level geometrical heterogeneity of natural sorbents using the concept of fractals. In this chapter, I have another objective that I wanted to achieve. Even though the experimental set-up used in this investigation is extremely simple, it will become obvious that the macroscopic

parameters which we can obtain from the macroscopic experiments provide only the blurry image of the corresponding microscopic (molecular-level) reality (Callen, 1985). First of all, whether a sorption isotherm can be uniquely defined for a given experimental system will be considered. Secondly, what B.E.T. equation represents in microscopic as well as macroscopic level will be demonstrated from statistical mechanical and kinetic derivations. Based on these arguments, it will be found that our scientific reasoning from macroscopic world to the molecular level pictures appears to be reasonable, but such logic is very naive. This research made me realize where I stand as an environmental chemist who deals with observations of macroscopic phenomena often from microscopic level consideration. Understanding this limitation, the molecular level fractal dimensions were obtained for various sorbents. I believe that this approach to heterogeneity is definitely a powerful tool as long as what it represents is correctly understood.

In Chapter 3, we will consider the problem of solute transport dynamics in heterogeneous systems in which the local solute transport parameters are highly variable from place to place. In Chapter 3, we will re-examine the three fundamental conceptual equations for solute transport phenomena; Fokker-Planck equation, Langevin equation, and the Chapman-Kolmogorov equation. Despite their fundamental nature, these approaches are not well accepted among many hydrologists who approach the transport processes mainly from models based on mass balance formulations of the convective-dispersive equation (CDE). Therefore, it was of interest for me to explore the connection, and reestablish the validity of

CDE as we learn. In the first part, the connection between the non-linear Langevin equation and the Fokker-Planck equation (or CDE) will be scrutinized from which the ambiguous nature of Eulerian flux in heterogeneous field will be illuminated. In the second part of Chapter 3, a discrete Markov chain model will be presented as an alternative approach to the solute transport in heterogeneous media. The connection between the transition probability and the finite-difference scheme will be demonstrated. The discrete Markov chain model is then applied to the problem of diffusional transport in geometrically- as well as energetically- heterogeneous media. Finally, the diffusion-limited desorption kinetics from heterogeneous porous sorbed phase to solution phase will be simulated using the discrete Markov chain model. This simulation will demonstrate the possible inadequacies of mass transfer or simple diffusion models to capture the characteristics of the desorption kinetics.

In this dissertation, I will introduce some approaches of basic sciences which may be rather foreign to many environmental scientists. However, the main goal of this dissertation is the understanding of the nature of the heterogeneous natural systems. I tried to make the dissertation to be self-explanatory. Many concepts are introduced to familiarize the readers with the ideas, i.e. the way of thinking. This dissertation was synthesized not only to gain knowledge, but also to pursue my curiosity, and the construction of my best scientific reasoning/logic applied to the environmental science. I hope I am successful in communicating my thoughts with the readers.

CHAPTER 2
MOLECULAR-LEVEL GEOMETRY OF NATURAL SURFACES

Introduction

The surfaces of natural materials are expected to be somewhat convoluted. However, many scientists considered that the geometrical complexity from such "non-flatness" is difficult to deal with for decades. Consequently, many conceptual/mathematical models of surface phenomena, such as ion-exchange, adsorption, etc., are developed under the assumption of a flat surface, or otherwise strictly from macroscopic perspective.

Consider a situation that a molecule is almost completely surrounded by convoluted surfaces. Such situation can be expected for some amorphous clays, inside organic matter, etc. In this case, the interaction of molecules with the surface can be viewed neither as two-dimensional nor as three-dimensional, but somewhat in between. Mathematical descriptions of convoluted surfaces (e.g. surface of a mountain) with a limited number of parameters are generally difficult in discrete Euclidian space. However, recently-developed fractal theory (Mandelbrot, 1982) enables us to describe complex shapes with characteristic fractal dimensions. This idea seems to be a valuable tool scientists who deal with geometrically- (e.g. pore geometry) as well as energetically-complex (e.g.

interaction energy is spatially variable) natural materials which include soils, rocks, and biological materials. Thus, the applications and limitations of fractal theory in describing geometrical complexities of natural sorbents was pursued toward a understanding of phenomena in complex spaces.

Fractal Dimensions

What Is Wrong With the Classical (Euclidian) Approach?

Soil is a highly complex medium and simplifications of the system are generally inevitable for mathematical model development and a conceptual understanding. Assumptions such as homogeneous (quasi-uniform), isotropic medium, spherical or cubic components, flat surface, are very common in many sub-disciplines of soil science and allied disciplines. For example, rudimentary transport equations often assume plug flow, complete mixing, or uniform, isotropic medium, constant unidirectional velocity, etc. Many theoretical equations used in soil chemistry, such as B.E.T. (Brunauer-Emmett-Teller) equation, Diffuse Double Layer theory, assume near-flat surfaces. The assumptions of a flat surface or uniform media are valid if the underlying variations, fluctuations or perturbations are "averaged out" at the macroscopic scale. However, complexities generally exist at all scales in natural systems. Fractal concept is one of the simplest model to deal with scaling properties of complexity, which assumes that the nature of complexity is similar at all scales.

Fractal - Its Central Concepts and General Application

The central idea of the fractal dimension is self-similarity. A self-similar object shows similar features when it is magnified or shrunk in size. A famous example is the length of coast line (Mandelbrot, 1982). Suppose we are interested in measuring the length of coast line between the two points on a coast. The length is longer if you measure it on a 1:1,000 scale map than that on a 1:100,000 scale map since we can see more small-scale inlets and outlets on the 1:1,000 scale map. In other words, the coast line length depends on the yardstick (scale) with which it is measured. It has been discovered that even though the length depends on the scale, the way the coast looks on maps of different scales is surprisingly similar. Such a structure is said to be self-similar.

If objects are self-similar, we can characterize them with the fractal dimensions. In short, the fractal dimension is a measure of geometrical complexity; and it is the simplicity and the intuitiveness of the concept which made this theory so attractive alternative for describing otherwise extremely complex objects. There are at least two types of objects which are important in environmental chemistry which possibly possess fractal properties. One is the size distribution of pores in which water and solutes are transported (Darcian scale or larger). The other is the surfaces where the interaction, retardation, and degradation take place (interfacial scale). We are also interested in the internal structure of sorbents if the sorption occurs inside the sorbent (sub-grain scale; see Chapter 3). It is the latter two scales I consider in my dissertation research.

The numerous studies of natural geometry as fractal object revealed that fractal-like objects are very common in nature (Mandelbrot, 1982). Researchers have been interested in why fractal-like objects are so common in nature. Fractal structures, as well as other interesting chaotic behavior, seem to emerge in open, nonequilibrium systems (Takayasu and Takayasu, 1988). "Open" means the system is open to the flows of heat and materials (energy). Although classical thermodynamics has been developed mainly for closed equilibrium systems, such open nonequilibrium systems are ubiquitous. For example, oceans, rivers, biological systems are all subjected to the flows of heat and materials. The earth receives energy continuously from the sun. Therefore, the occurrence of fractal structures is the natural consequence. "Repetitions" is the other key word for the development of a fractal structure. The study of fractal structure, such as Diffusion Limited Aggregation (DLA), has revealed that under certain conditions, the fractal structures appear when the underlying mechanism operates again and again under certain condition (Vicsek, 1989). In DLA, aggregates are formed by diffusing particles sticking to other particles. The repetition of this process yields repeating pattern over the scales which is self-similar, i.e. fractal.

At this point, let us consider how we can apply this concept of fractal to realistic natural science problems. It is helpful to imagine various computer softwares which draw various complex (almost-) natural objects using fractal theory.

Application-1: The application as a descriptive parameter of complex shapes

Shape (geometry) is a very important features of an object. However, beyond the concept of physical size (length, area, volume), other important shape factors, such as connectivity and branching, are not well recognized. This lack of recognition is partly attributed to the lack of an intuitive parameter. The use of fractal dimension seems to be a promising approach to the additional geometrical parameters other than the physical size. The fractal dimension may be incorporated into various classification schemes.

Application-2: The use of realizations as the surrogate model for realistic, natural geometry.

As exemplified by numerous computer softwares which draw complex natural objects using fractal dimensions, the fractal theory can be used to come up with numerous realizations of complex geometry which resemble real natural objects. The capability of describing complex natural geometry in detail is a major asset for natural scientists. Many static and dynamic phenomena, which include sorption phenomena as discussed in this chapter and transport phenomena as discussed in Chapter 3, occur in rather limited complex space. Therefore, one of our major tasks is to elucidate the processes which occur in complex space. With the progress of computer technology, it is now possible to run realistic, sophisticated simulations. As exemplified by molecular modeling programs, once the necessary parameters (such as distance, mass, and electrostatic

characteristics) and the relationships among the parameters (e.g. strength of interaction as functions of distance, valence, etc.) are specified, these programs can optimize the system so that the result is in accord with the laws of physics (minimization of energy, maximization of entropy, or minimization of time integral of the Lagrangian). These approaches (computer experiment method) seem to be ideal to study phenomena (e.g. sorption) in complex geometrical environment. Fractal theory can provide numerous realizations of complex spaces as examples of realistic natural geometry.

In addition, many natural phenomena, such as the precipitation patterns and the earthquake frequencies, tend to exhibit chaotic, fractal-like patterns. The idea of correlated noise rather than random white noise seems to be a key to such patter formation (Mandelbrot and van Ness, 1968). These patterns may be modeled as fractals. The spatial distribution of variables, such as thermal and hydraulic conductivity in nature may be modeled as fractal. In practice, much sophisticated fractal theories (e.g. multifractal) may be needed to come up with a realistic pattern. Although statistical techniques to come up with patterns (the use of correlation structure) are also widely available, fractal theory seems to connect the mechanistic aspects of formation processes with the resulting patterns.

Application-3: The Investigation of Formation Process

The idea of fractal dimension also promoted various levels of discussions on how natural structures are formed. They include the formation of aggregates,

crystals (e.g. snow-flakes), viscous-fingering, geological formations, etc (e.g. Vicsek, 1989). The fractal dimension has been also used to study how structures of materials (e.g. silica-gel) change with the manufacturing process and various chemical, thermal, or other treatments (Orcel, 1987; Wijnen et al., 1991).

Objectives

This study is motivated by the following objectives:

(1) Explain the effect of geometrical surface heterogeneity on sorption phenomena from the perspective of surface fractal dimension.

(2) Experimentally characterize the molecular-level surface geometry of natural and artificial sorbents in terms of the corresponding surface fractal dimensions.

Sorption phenomena are complex, macroscopic outcome of molecular level interactions of solute molecules with the surface. It is highly likely that the sorption phenomena are affected by both the geometric and energetic factors in highly compounded manner. Therefore, it is difficult to single out these effects independently. The next progress from simple, uniform-energy, uniform-geometry sorption models are uniform-energy, complex-geometry models or complex-energy, uniform-geometry models. As the surrogate guideline model for a uniform-energy, complex-geometry system, the concept of fractal dimension is considered.

We hypothesize that the sorbent surface has fractal-like geometry. As explained in detail in the following section, the fractal dimension can be estimated from the relationship between the monolayer value, $N_m(\sigma)$, and the probe molecule size, σ. The monolayer value, $N_m(\sigma)$, is an ideal parameter to test this hypothesis since it is relatively energy-independent. From the relationship between $N_m(\sigma)$ and σ, the experimentally determined surface fractal dimension is computed.

Definition and Classification of Fractal Objects
(Mandelbrot, 1982; Pfeifer and Obert, 1989; Falconer, 1990)

A "Deterministic fractal" is generated by operating a fixed procedure (generator) on the initiating shape (initiator). Famous examples of deterministic fractals are Koch curve, Peano curve, Cantor Dust, Sierpinski arrowhead, Sierpinski carpet, Menger sponge. Figure 2-1 illustrates the way to generate a Koch's curve. Mandelbrot (1982) provides numerous examples of fractal objects with initiators and generators.

The properties N(r) of fractal objects, such as length or area, are described by a simple power law:

$$N(r) = C\, r^{-D} \qquad (2\text{-}1)$$

where C is a constant, and r is the unit length (yardstick length) with which the property is measured. In fact, this is the generalization of properties in Euclidian space;

Koch Curve

$$D = -\frac{\log[4]}{\log[1/3]} = 1.262$$

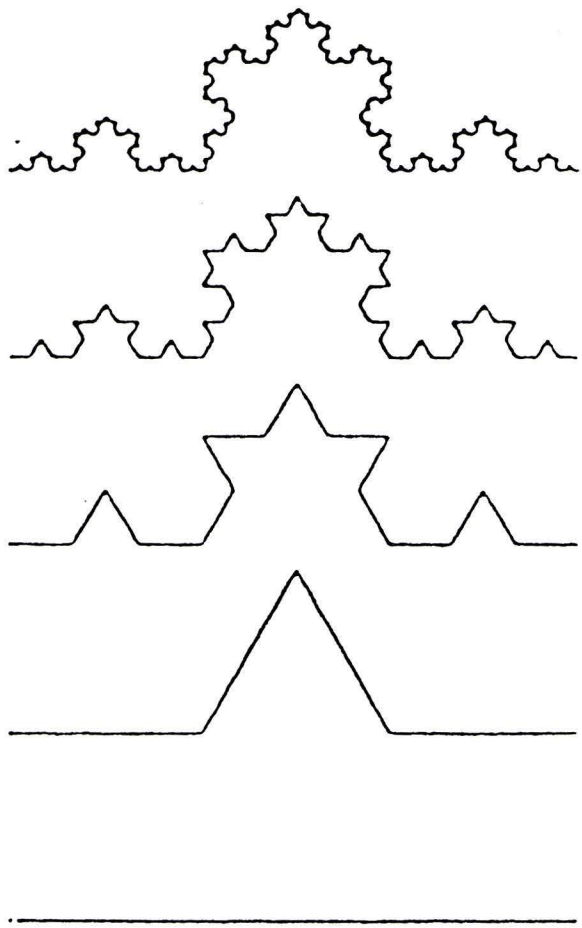

Fig. 2-1. Generations of Kock's curve.

Length $\propto r^{-1}$

Area $\propto r^{-2}$

Volume $\propto r^{-3}$

Notice that the exponent takes on integer values which correspond to the Euclidian dimensions. If the initiator and generator are known, the fractal dimension of the object is easily calculated. If the initiator and/or generator are complicated, or the object is fractal in a statistical sense as are most natural fractals, it is difficult to determine the fractal dimension by just looking for the initiators and generators. In this case, there are many ways to estimate fractal dimension by analyzing the scaling behavior.

Consider an object in space. The space in which the object exists is called the embedding space. Now, we divide this space into cells (for example, boxes for 3-dimensional space, squares for 2-dimensional space, etc.) of side r, and count the number of the cell, N(r), containing the object. Then, we continue this procedure with different size (r) of cells. If the number of the cells of size r containing the object diminishes with the size r as $N(r) = C\ r^{-D}$, then the surface fractal dimension of the object is D. Heuristically, a surface fractal dimension between 2 and 3 represents an object which is not flat (dimension of 2), and not volume-filling (dimension of 3), but somewhere in between, namely convoluted shape in Euclidian dimension of 3. The degree of complexity is generally reflected by the surface fractal dimension, i.e., larger the surface fractal dimension, more convoluted the surface is in fractal sense. It should be noted that most of the

natural fractal objects do not exhibit deterministic fractal relationship; they are fractal in a statistical sense (Mandelbrot, 1982).

Similarly, the surface fractal dimension can be defined as follows (Pfeifer et al., 1984; Farin and Avnir, 1989). Consider an estimated surface area, $S(m^2)$, measured with small spheres whose projected area is σ (m^2). If $N(\sigma)$ represents the number of this small spheres needed to completely cover this area (Fig. 2-2), we have

$$S = N(\sigma) \times \sigma \tag{2-2}$$

The surface is considered as a fractal if $N(\sigma)$ grows exponentially as $\sigma \rightarrow 0$, namely

$$N(\sigma) \propto \sigma^{-D/2} \tag{2-3}$$

where D is the corresponding fractal dimension. Here after, this concept is referred as the surface coverage method. If the surface is flat, $N(\sigma)$ is proportional to $1/\sigma$, which means that the dimension is 2. Besides the surface which consists of the interface between the mass (the body of the object itself) and the pores (voids), we can treat mass, pore, edge, and exposed interface in the same manner. Pfeifer (1987) classified the fractal objects based on the $D_{surface}$, D_{mass} , D_{pore} , and D_{edge} into four different categories (Fig.2-3):

(1) Surface fractals: A surface fractal has a fractal surface, but the body of the object and the pores are three dimensional. Examples are graphite, crushed quartz, carbon black, kaolinite, porous silica.

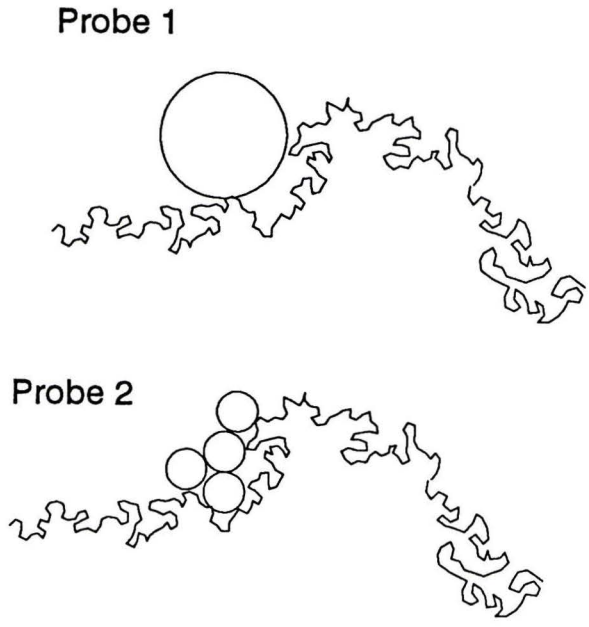

Fig. 2-2. Exploring a surface with probes of various sizes.

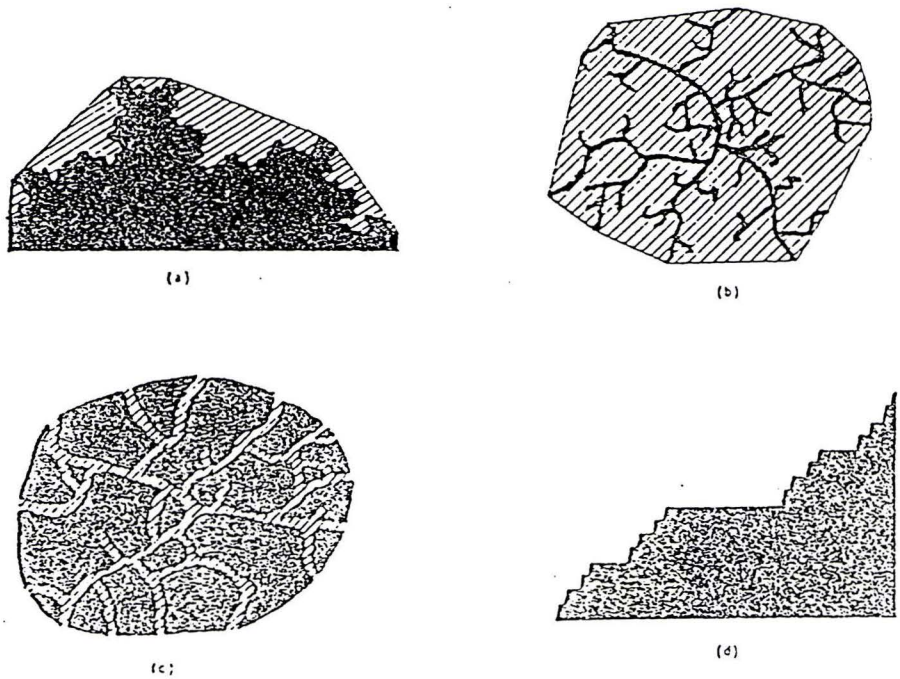

Fig. 3. (a) Surface fractals, (b) mass fractals, (c) pore fractals, and (d) subfractal surfaces. Black areas are mass sites, shaded areas are pore sites (see Pfeifer and Salli, 1987, for the general definition of the pore space). The boundary between the two makes the surface sites. The surface (d) with Cantor's staircase (Mandelbrot, 1982) as profile has $D = 2$ and $D_{edge} = 1 + \ln 2/\ln 3$.

Fig. 2-3. Classification of fractal objects (after Pfeifer (1987)). (A) surface fractal; (B) mass fractal; (C) pore fractal; (D) sub-fractal.

(2) Mass fractals: The object occupies only a small fraction of the space. The mass also exhibits fractal behavior as the surface, but the pores are three dimensional. Examples are silica aggregates, polymers, plant roots, fungal hyphae, etc.

(3) Pore fractals: This fractal is the opposite case of a mass fractal. The object occupies a large part of the space such that the D_{mass} is approximately 3. The surface and the pores show fractal behavior. Examples are zeolites, expandable clays, sandstones, vycor glass.

(4) Subfractals: This fractal has surface dimension of 2. However, the edges and/or corners show fractal behavior with $D_{edge} < 2$. Examples are pillared clays, platinum crystallites on SiO_2.

Fractal as Statistical Description of Surface Heterogeneity (Ogilvy, 1991)

In this section, we will consider the meaning of fractal dimension in comparison with other statistical methods for describing rough surface. Similar argument can be extended to the statistical description of complex pores, mass, etc. However, since this chapter deals exclusively with the surface characteristics, the statistical descriptions of rough surfaces are presented here.

In Euclidian space, a smooth surface is defined by two vectors which form a 2-dimensional plane. The roughness of the surface may be described as the statistical structure of the deviation from the mean plane, which is given by

introducing the third vector, namely the height. The probability of finding a height between h and h+dh is given by p(h)dh, where p(h) is the height probability density function. This probability distribution function reflects the surface formation processes. In general, when the formation of the surface is the result of a large number of local events, the probability distribution function asymptotically approaches to a Gaussian (normal) distribution.

Figure 2-4 shows three surfaces which have the identical height probability distribution function. The differences among these surfaces are due to the correlation structure of the surface. The autocorrelation function

$$C(r) = \langle h(x)h(x+r)\rangle \tag{2-4}$$

is generally used to describe the correlation structure. The notation, < > indicates the statistical expectation. The autocorrelation function is a measure of the similarity, and it is zero when the structure is not correlated.

In geostatistics, a variogram, 2γ,

$$2\,\gamma(r) = \langle [h(r) - h(r+h)]^2\rangle \tag{2-5}$$

is often used to describe the correlation structure. In this case, the same idea was applied to the surface height function. For a stationary surface, the following relation between the autocorrelation function and the variogram holds;

$$\gamma(r) = \sigma^2 - C(r) \tag{2-6}$$

The variogram has an advantage over the autocorrelation function in the sense that it is independent of the choice of the reference surface (height).

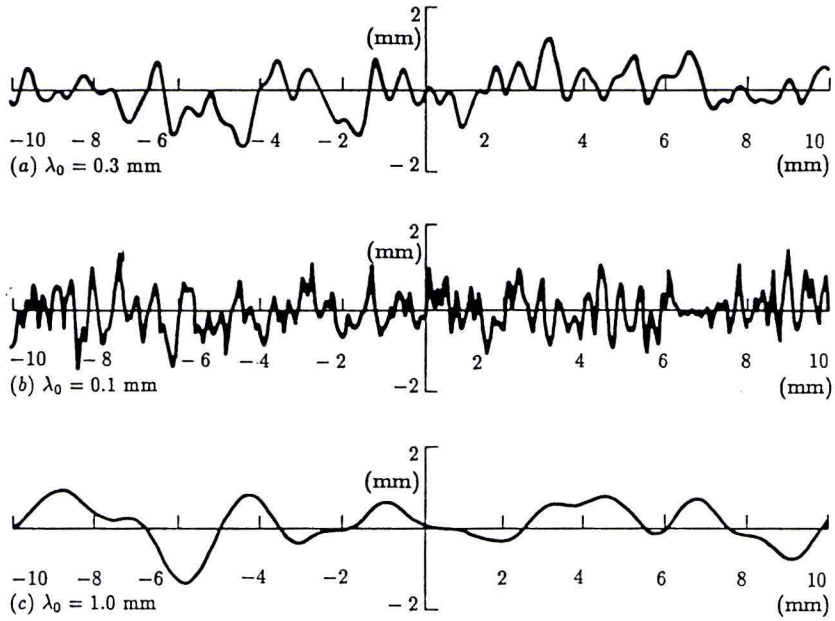

Fig. 2-4. Gaussian surfaces of the same identical height probability distribution. The differences are due to the differences in the correlation structures (after Ogiliy, 1991).

The characteristic functions and the moment generating functions are particularly helpful to obtain various statistical parameters such as the moments. The one dimensional characteristic function of a rough surface is:

$$\phi(\omega) = \int_{-\infty}^{\infty} p(h) e^{j\omega h} dh \tag{2-7}$$

Similarly, the moment generating function is

$$MGF(s) = \int_{-\infty}^{\infty} p(h) e^{sh} dh \tag{2-8}$$

The power spectrum (power spectral density function), $P(\omega)$ is defined as the Fourier transform of the autocorrelation function, C(r)

$$P(\omega) = \int_{-\infty}^{\infty} C(r) e^{-j\omega r} dr \tag{2-9}$$

A directional dependence of the property of the surface is often observed. Naturally-occurring surfaces often show such dependence, which is called anisotropy. When the property is independent of the direction, the structure is said to be isotropic. The isotropy/anisotropy may be examined by calculating the autocorrelation function in different directions. When all the statistical properties of the surface are independent of the shift in the origin (coordinate), the structure is called stationary in a strict sense. However, in practice, a much more relaxed condition is often considered in which the mean and the autocorrelation, C(r), are independent of the shift of origin. This condition is known as stationarity in a wide-

sense or 2nd-order stationarity (Papoulis, 1991). Fig. 2-5 depicts three realizations of surfaces which were generated from an identical statistical distribution (Gaussian height distribution /Gaussian autocorrelation distribution). The ergodic assumption states that any statistical moment taken over many different parts of one realization is the same as ensemble moment over many realizations.

Fractals: The statistical techniques discussed above section are not always appropriate for describing rough surfaces. In particular, when the surface has self-similar structure, the statistical property of the structure cannot be well defined. As an alternate, the surface may be described with the fractal dimension. For example, the property of the height of the surface may be described as

$$|h(x+\Delta) - h(x)| \sim \Delta^{\alpha} \qquad (2\text{-}10)$$

where α, known as the Lipschitz exponent ($0 < \alpha < 1$), is related to the fractal dimension, D, through $\alpha = (2 - D)$. A fractal surface is continuous but not differentiable. It cannot be described using the conventional statistical method mentioned above (variogram can be defined for a fractal object). For example, the average of the height $<h(x)^2>$ is infinite since the roughness exists down to the infinitely small scales. Furthermore, the correlation distance is infinite since the roughness also persists to the infinitely large limit. While such structures are difficult to deal with using conventional statistical approaches in Euclidian dimension, fractal-like structures are ubiquitous in natural systems.

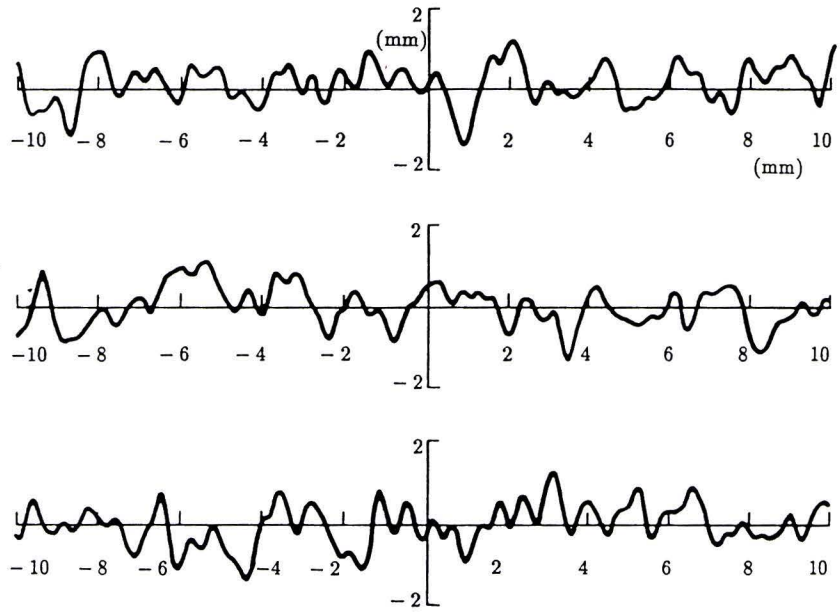

Fig. 2-5. Three realizations generated from identical height distribution and correlation structures (after Ogilvy, 1991).

Application of Fractal Theory in Surface Science

The fractal surface is represented by the repetition of disorder (geometrical heterogeneity) at all length scales. In other words, the disorder exists at any length scale. This results in variable surface area which has been considered to be an absolute quantity for centuries based on Euclidian geometry. In surface science, the surface area plays the fundamental role since the surface phenomena, such as adsorption, surface reaction kinetics etc., are generally linearly related to the surface area. The surface area is generally measured by counting the number of molecules of known size (for example, N_2 gas) required to cover the surface. Fractal theory revealed that the surface area seen by N_2 molecule is different from that seen by other molecules. The importance of this concept has been widely recognized (Avnir et al., 1983), and discussed in the recent edition of classical text book on surface chemistry by Adamson (1990).

Experimental Measurement of Fractal Dimension by Monolayer Adsorption Method

To investigate a surface at the molecular level, the resolution of the surface configuration by the technique should be in the order of molecular size, say 10^{-10} m. Adsorption and scattering techniques are widely used to determine the surface fractal dimension in this range of resolution (Pfeifer, 1988). In particular, we adopted the monolayer adsorption method (Pfeifer and Avnir, 1983) which is directly pertinent to the definition of surface fractal dimension, the surface coverage method, given above. The principle of the method is as follows:

(1) The sorbent surfaces are explored with probe molecules of various projected surface areas, σ, by means of adsorption. A series of vapor desorption (or adsorption) experiments are conducted to achieve this.

(2) The number of molecules required for monolayer coverage, $N_m(\sigma)$ (mmole/g) is estimated from the result of vapor sorption experiments, and

(3) From the relationship between $N_m(\sigma)$ and σ, the surface fractal dimension, D, is estimated as

$$N_m(\sigma) = C\,\sigma^{-\frac{D}{2}} \qquad (2\text{-}11)$$

In addition to the measurement of the surface fractal dimensions, the sorption phenomena are extremely important to the fate and transport of toxic chemicals in the environment.

Alternatively, in principle, it is possible to estimate the surface fractal dimension by varying the size of the sorbent rather than the solute. In this method, the sample is fractionated based on the particle size, R, and the monolayer value for each particle size fraction, $N_m(R; \sigma_{fixed})$ is determined by adsorption of probe such as nitrogen or argon. However, the particle fractionation often causes the compositional fractionation when applied to soils (Sokolowska et al., 1989), and therefore is not recommended.

Fractal Dimension of Natural Sorbents Measured with Monolayer Adsorption Techniques

Table 2-1 summarizes the fractal dimensions of natural sorbents measured by various researchers using mostly adsorption techniques. van Damme et al. (1985) suggested a fractal aggregation model for the microstructure of clays. The fractal dimensions of soils and clays have been studied by Avnir et al., (1984, 1985) and Sokolowska et al. (1989). Avnir et al. (1985) noticed abrupt changes in the fractal dimension of soil around size fraction of 25-45 μm from their fractal analysis. This shift in the dimension is probably due to a change in the mineralogical composition of size fractions. Smaller fractions contains mainly clay particles while large fraction contains quartz, feldspars or other primary minerals. An interesting point is the rather abrupt change in dimension (see Table VIII and Fig. 6 of Avnir et al. (1985)). Sokolowska et al. (1989) have also noticed abrupt shifts in dimension. The shift shows usually lower dimension for coarser fractions to higher dimension for finer fractions. This trend is consistent with the expected behavior based on the structures of clays and sand fractions. Based on the mineralogy, and the obtained fractal dimension of various materials, clays, especially expandable clays, have higher surface dimensions than primary minerals.

Since a soil consists of various materials, both organic and inorganic, various sizes and compositions, unique fractal dimension for a whole soil is not a good assumption. We must picture soil particles as having different dimensions

Table 2-1. Surface fractal dimensions of natural sorbents

Material	Method	D	Probe	Source
Madagascar quartz	P.S.	2.14±0.06	N2	1
Snowit quartz	P.S.	2.15±0.06	N2	1
quartz	P.S.	2.21±0.01	dissolution rate in HF	1
Iceland spar limestone	P.S.	2.16±0.04	N2	1
Niagara dolomite	P.S.	2.58±0.01	Kr	1
Mosheim limestone	P.S.	2.63±0.03	Kr	1
Ranport limestone	P.S.	2.81±0.04	Kr	1
Goodland limestone	P.S.	2.97±0.01	Kr	1
dolomitic rock	P.S.	2.91±0.02	Kr	1
carbonate	P.S.	2.90±0.01	N2	1
Pre-Shoal granite	P.S.	2.73±0.05	N2	1
Shoal-C granite	P.S.	2.88±0.02	Ar	1
pumice	P.S.	2.89±0.04	N2	1
Rainier rubble (tuff)	P.S.	3.03±0.05	N2	1
Rainier glassy rock	P.S.	2.46±0.11	Ar	1
Ottawa sand	P.S.	2.02±0.01	dissolution rate in HF	1
coal mine dust	P.S.	2.33±0.08	N2	1
coal mine dust	P.S.	2.52±0.07	N2	1
clays	I.A.	2.54-2.80	N/A	1 (Sarra)
Georgia kaolinite	M.L.	2.12±0.05	H2O,N2,MeOH,EtOH,etc.	2
Russian kaolinite	M.L.	2.40±0.1	H2O,N2,MeOH,EtOH,etc.	2
Wyoming bentonite whole	M.L.	2.10±0.06	N2,C6H12,benzene,etc.	2
Wyoming bentonite exter.	M.L.	2.30±0.07	H2O,MeOh,EtOH,PrOH	2
pillard montmorillonite	M.L.	1.89±0.09	N2,benzene,etc.	4
pillard montmorillonite	M.L.	1.94±0.10	N2,benzene,etc.	4
soil 1	P.S.	2.34-2.99	Malachite Green	1
soil (kaolinite)	P.S.	2.46-2.92	Malachite Green	1
soil 3	P.S.	2.37-2.90	Malachite Green	1
soil 4	P.S.	2.43-2.89	Malachite Green	1
soil 5	P.S.	2.19-2.89	Malachite Green	1
soil 6	P.S.	2.65±0.05	Malachite Green	1
soil 7	P.S.	2.59±0.04	Malachite Green	1
soil Orthic Luvisol A1	P.S.	2.28/2.35	N2/H2O	3
soil Orthic Luvisol A3B	P.S.	2.32/2.25	N2/H2O	3
soil Orthic Luvisol B	P.S.	2.40/2.30	N2/H2O	3
soil Orthic Luvisol BC	P.S.	2.31/2.30	N2/H2O	3
soil	P.S.	2.13	N2	2
soil	P.S.	2.21-2.61	N2	2
soil	P.S.	2.25-2.71	N2	2
soil org. matter (solid)	SAXS	2.3-2.8	N/A	5
soil org. matter (solution)	SAXS	1.6-2.5	N/A	5
soil aggregate C1	P.V.	2.75±0.10	N/A	6
soil aggregate C2	P.V.	2.95±0.03	N/A	6
soil aggregate C3	P.V.	2.93±0.03	N/A	6
soil aggregate B2	P.V.	2.93±0.02	N/A	6

Table 2-1. (continued)

References

1 Avnir et al., 1984 and/or Avnir et al., 1985; 2 Sokolowska et al., 1989; 3 Sokolowska et al., 1989; 4 van Damme and Fripiat, 1985; 5 Rice and Lin, 1993, 6 Young and Crawford, 1991

Methods

P.S.: particle size; M.L.: monolayer; I.A.: Image Analysis; SAXS: small-angle x-ray scattering; P.V.: pore volume

depending on the size and composition. The other interesting related topic is the type of fractality for these natural sorbents. Pfeifer (1987) suggested that quartz and kaolinite are surface fractals; zeolite and expandable clays are pore fractals; and pillared clays are subfractal.

Recent investigation revealed that a soil is not a pore fractal but a mass fractal (Bartoli et al., 1991). This distinction is important because it is also related to pore-related properties such as conductivity, dispersivity, etc.

Other Methods of Fractal Dimension Determination

There are number of ways to estimate the fractal dimension without relying on an adsorption experiment. Small-angle x-ray (SAXS) or neutron scattering (SANS) seems to be a powerful tool to investigate fractal surfaces (Bale and Schmidt, 1984; Schaefer et al., 1984; Pfeifer, 1988). Recently, Rice and Lin (1993) reported the surface fractal dimensions of humic materials as measured with SAXS method. Rojanski et al. (1986) and Ross et al. (1988) compared the results obtained from adsorption method with those from a scattering method. While Rojanski et al. obtained a good agreement, Ross et al. reported disagreement.

Image analysis is also a possible method (Kaye, 1989). In principle, pictures of the object are analyzed at different mesh sizes. Serra (1982) has analyzed magnified pictures of clays. The determined fractal dimensions were in the range 2.54 to 2.80 which agreed well with the results obtained from adsorption experiments. This method has been used to characterize the fractal dimensions of

plant root system (Tatsumi et al., 1991). If the image analysis technique is combined with Atomic Force Microscopy (AFM), it becomes possible to directly characterize molecular level geometry.

Porosimetry measures the distribution of pore volume as a function of pore diameter. The distribution of pore volume with respect to pore size is called a pore size distribution. The general relationship between the pore size distribution and the fractal dimension has been discussed by Pfeifer and Avnir (1983) and Fripiat (1989).

$$\frac{dV_{pore}}{dr} = C\, r^{2-D} \qquad (2\text{-}12)$$

The pore volume distribution is obtained by mercury porosimeter or by analyzing the multilayer adsorption isotherms. It should be noted that this method measures the pore fractal dimension rather than the surface fractal dimension.

On the Reliable Estimation of $N_m(\sigma)$ and σ

According to the definition of fractal theory, the surface fractal dimension can be calculated from the relationships between the projected molecular surface area, σ, and the monolayer number, $N_m(\sigma)$. Since none of these parameters can be directly measured, reliable methods are needed for estimating $N_m(\sigma)$ and σ. In this section, therefore, we will discuss how to estimate $N_m(\sigma)$ and σ values from the sorption isotherm and available information about the size of the molecule.

Estimating $N_m(\sigma)$ from Sorption/Desorption Isotherm

Presumptions

In the proceeding discussion, it was demonstrated that the surface fractal dimension can, in principle, be estimated experimentally from the monolayer value, $N_m(\sigma)$ and the projected surface area, σ, in analogous to the definition of the surface fractal dimension (equation 2-3). Our goal is, thus, to estimate the monolayer value, $N_m(\sigma)$, from the amount of the solute adsorbed at a given vapor pressure (isotherms). However, a real molecule is not a simple disc or sphere, and a real surface (sorbent) is not rigid and energetically uniform. On the other hand, the idea of a surface fractal dimension presumes that:

Presumption-(1): $N_m(\sigma)$ is well-defined;
Presumption-(2): the same surface is explored by probes of different sizes;
Presumption-(3): the estimated $N_m(\sigma)$ represents the true $N_m(\sigma)$.

To ensure the correct analysis of the surface fractal dimension, therefore, the these conditions have to be met.

For the first condition, it is desirable that the sorbent is not very flexible. When the sorbent is flexible, the probe molecule can penetrate into the sorbent. The degree of penetration is often strongly affected by the energetic interaction of the probe and the sorbent in addition to the size of the probe. Therefore,

depending on the reactivity of the probe, the probe may see an entirely different surface.

Suppose a monolayer value, $N_m(\sigma)$, can be well defined for a given probe. The second necessary condition for a correct analysis of fractal dimension is that the probe molecules see the same surface. Again, a flexible sorbent is not suitable since the penetration of the probe makes the $N_m(\sigma)$ to be dependent on the chemical properties of the probe molecule. In this case, different $N_m(\sigma)$s may be obtained for probes with the same σ depending on the physicochemical characteristics of the probe molecules. Fig. 2-6 depicts a hypothetical situation that the first and second presumptions are violated. It is obvious that for a penetrating probe molecules, $N_m(\sigma)$ is rather operationally defined. Furthermore, the $N_m(\sigma)$ itself is dependent on the physicochemical property of the probe other than σ. One of the typical example is expandable clays, e.g. montmorillonite. It is well known that polar probes (e.g. water, EGME) can penetrate into the interlamellar position of the expandable clay while non-polar probes (e.g. N_2) cannot penetrate into the interlamellar region (Sokolowska et al., 1989). Assuming that non-polar probes explore the external surface and polar probes explore both external and internal surfaces, Sokolowska et al. (1989) estimated the surface fractal dimensions of the external and total surfaces. However, for complex sorbent such as organic matter, it is likely that the differences between external and internal surfaces cannot be well-defined. In this case, the operationally defined accessible surface area depends strongly on the chemical characteristics of the probe molecule. Therefore,

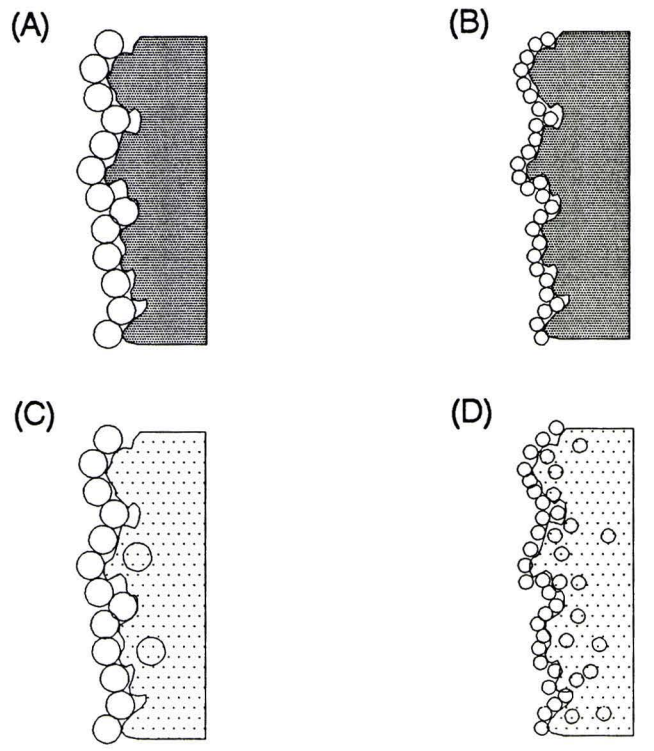

Fig. 2-6. Sorption of spherical probes by rigid ((A) and (B)) and flexible ((C) and (D)) sorbents. For a flexible sorbent, the monolayer value is not well-defined, and the probe molecules may see entirely different surface depending on the physicochemical properties of the probes.

it is expected that the experimental application of the fractal theory is most successful for chemically uniform and geometrically complex systems.

For a given set of a probe (polarity, size) and sorbent, let us postulate that the probes of different sizes see the same surface, and the dependency of true $N_m(\sigma)$ can be solely attributed to the size of the probe, although we have not discussed how to estimate the true $N_m(\sigma)$ from the available information. Therefore,the amount of probe adsorbed at a given relative pressure, $N(\sigma; p/p_o)$, is determined by (1) $N_m(\sigma)$ which is related to the accessible surface area of the sorbent, and; (2) other factors, mainly associated with the energetic interaction of the solute with the accessible portion of the surface.

The next task is to extract the $N_m(\sigma)$ from the sorption isotherm independently from other factors. In reality, sorption is a result of the complex processes of interaction of the sorbed molecule with the surface as well as the other sorbed molecules. Therefore, whether $N_m(\sigma)$ can be properly estimated or not depends on how well we can handle the other factors, especially the interaction energy related terms.

A distinct well-defined monolayer can be expected when the surface is energetically uniform and nearly flat, and the direct interaction of the sorbed molecule with the surface is significantly stronger than the interactions among the sorbed species. In this case, the $N_m(\sigma)$ value can be well-defined. However, under various realistic conditions, the distinct formation of the well-defined $N_m(\sigma)$ is masked by:

(1) formation of successive layers before the completion of the monolayer

(2) energetic heterogeneity effect

(3) irreversible sorption

(4) kinetic constraint (unable to attain the equilibrium due to the time constraint)

(5) hysteresis effect

(6) deviation from the expected behavior based on the adsorption on near-flat surface, such as partitioning-type sorption

Before the reliable estimate of $N_m(\sigma)$ can be done, these factors have to be removed, or otherwise avoided from the estimate of $N_m(\sigma)$. The following discussions are provided to deal with these constraints associated with the reliable estimates of $N_m(\sigma)$s and the surface fractal dimensions.

Sorption Time

To conduct an equilibrium sorption experiment, it is essential to estimate the time required to reach the equilibrium. A soil system is very complex, and it is practically impossible to reach the true equilibrium condition. For example, the reorientation of complex organic polymer (soil organic matter) is considered to take place slowly over years (Swalen et al., 1987). Furthermore, various irreversible transformations may take place. Therefore, it is important to set a practical time scale to conduct the sorption experiments. The processes which do not come to the equilibrium within this time scale are considered kinetically constrained. As a guideline estimation, we assume that the time which a molecule stays on the

surface is governed by the Boltzmann distribution equation.

$$\tau = \tau_o \exp\left[\frac{Q}{RT}\right] \qquad (2\text{-}13)$$

where τ is the time of stay, τ_o is in the order of 10^{-12} to 10^{-13} sec (molecular vibration), and Q is the molar energy of sorption. From this estimation, if Q is in the order of 10 kJ/mole (physisorption), the τ is in the order of 10^{-11} second (Little, 1966; Adamson, 1990). If Q is in the order of 150 kJ/mole, τ is in the order of 10^{13} seconds. Therefore, if the time scale of the experiment is approximately 10^4 seconds (hours), the most of the chemisorption with the interaction energy of 100 kJ/mole or higher (Little, 1966; Adamson, 1990) appear to have very slow kinetics or irreversible. In addition to this estimate, the transport process in the system also contributes to the kinetics of the sorption processes. In fact, sorption/desorption kinetics is generally considered to be a diffusion-limited process. In Chapter 3, the desorption kinetics from geometrically and energetically complex sorbed phase will be investigated in detail. Overall, an experiment with an equilibration time of 10^2 to 10^4 seconds was set as the practical equilibration time frame for the physisorption equilibrium.

Sorption Isotherm Equations

To achieve the accurate and practical estimation of a monolayer value, $N_m(\sigma)$, it is essential to account for the formation of multi-layer before the mono-layer coverage is achieved. In conclusion, despite the various unrealistic

assumptions (Gregg and Sing, 1982), we accepted the classical B.E.T. equation (Appendix A) as the practical working equation which gives consistent semi-quantitative estimate of the monolayer value, $N_m(\sigma)$. The classical B.E.T. equation is an equation which extracts and lumps geometric contribution and energetic contribution into only two parameters, $N_m(\sigma)$ and C respectively. Considering the complexity of the process, this simplification is elegant, although the simplification of the process requires some unrealistic assumptions. The detailed reasoning why the classical B.E.T. equation was selected from numerous sorption isotherm models are discussed in Appendix A from rather theoretical basis. The statistical mechanical derivation of the classical B.E.T. equation involves the following assumptions:

(1) The sorption is reversible.

(2) The sorption is localized.

(3) The surface is flat.

(4) The sorption occurs vertically, and there is no horizontal interaction between the sorbed molecules.

(5) The heat of sorption between the bare surface and the sorbed molecule in the first layer is uniform across the surface.

(6) The heat of sorption associated with the successive multilayer formation is uniform and does not depend on the distance from the surface.

Gregg and Sing (1982) give extensive discussion of the validity of B.E.T. equation. A real surface probably differs from this idealized picture for

(1) energetic factor: the heat of sorption (the potential well) is not uniformly distributed, and there is horizontal interaction between the sorbed molecules.

(2) geometric factor: the surface is not flat.

Many modified classical B.E.T. equations have been formulated to account for these discrepancies. However, even the modified versions of the B.E.T. equation, the modification is rather ad-hoc and they inherit the false assumption made in the B.E.T equation. Consequently, the parameters obtained from the isotherm inevitably include some ambiguities. The ambiguity is indeed frustrating not only because it is difficult to assess the true meanings of the obtained parameters, but also because every scientist has different standard and tolerance for such ambiguities.

However, despite such problems inherited in the model, it is the fact that the classical B.E.T. equation is one of the most successful equation which gives reasonable, semi-quantitative interpretation to the typical S-shaped vapor sorption isotherms in terms of the multi-layer formation. Therefore single gas physisorption measurements are still widely used for determining the specific surface area, the energy distribution of adsorption sites, and the pore size distribution of adsorbents. B.E.T. monolayer value of nitrogen at 77 K seems to be still recommended as the standard method of the surface area measurement (Adamson, 1990). After more than 50 years, the B.E.T. equation is still an extremely useful equation as long as

we interpret the equation correctly. Based on these critical reviews, the reasonable starting points for the study of complex sorbents appeared to be still single gas sorption experiments and the B.E.T. equation. Instead of using the rather ad-hoc modified B.E.T. equation, in this series of experiments, the classical B.E.T. equation is considered as a good semi-quantitative working equation to obtain the monolayer value, N_m, which is needed to estimate the surface fractal dimension.

Experimental Measurement of $N_m(\sigma)$ Using the Classical B.E.T. Equation (Gregg and Sing, 1982)

The B.E.T. method for calculation of specific surface area involves two steps: evaluation of the monolayer capacity $N_m(\sigma)$ and the conversion of $N_m(\sigma)$ to the surface area by means of the projected surface area σ. Even in the favorable case of nitrogen or argon, the divergence of at least 10 percent must be reckoned with. Besides the difficulties associated with the estimate of molecular level picture from macroscopic data, there are intra and inter laboratory experimental errors. Of interest is the cross-laboratory examinations of measured surface areas of standard sorbents conducted by 13 experienced laboratories in United Kingdom (see Gregg and Sings (1982), p 104). In addition, the uncertainty associated with the estimation of the projected surface area seems to be even larger. Depending on the orientation of the molecules, the projected area of the probe molecule varies considerably. Therefore, the estimation of the surface orientation of the probe molecule becomes very crucial, especially for larger flexible molecules.

Uniqueness of Isotherm

To estimate $N_m(\sigma)$, we implicitly assumed that at constant temperature, and the surface area, the system is uniquely specified if the pressure is known. From the Gibbs phase rule, this system may be viewed as follows. First of all, let us assume that the sorbent is inert, and it provides the interface for sorption to take place. We have one component, c, the solute for a fixed amount of sorbent. The number of the phases, p, are two, i.e. the vapor and the sorbed phases. The degree of freedom, f, is then

$$f = c + 2 - p = 1 + 2 - 2 = 1 \qquad (2\text{-}14)$$

Therefore, from this simple thermodynamic argument, it is assumed that the system is uniquely defined once the pressure of the solute vapor is defined.

However, in reality, a vapor sorption isotherm for porous media is not unique due to the hysteresis and kinetic effects. There are number of reasons why hysteresis occurs. One of the plausible explanations is attributed to the "bottle-neck" structure of pores. This effect is considered to take place at higher relative pressure regions (e.g. $p/p_o < 0.3$). The hysteresis in lower relative pressure regions may be explained from the trapping of solute molecule between the collapsed structure of the sorbent. During the adsorption process, the solute penetrates between the narrow region of the sorbent, and the sorbent expands (swells). During the desorption process, the rate of the desorption may be slower than the rate that the collapse of the sorbent structure which causes a part of

solute to be nearly irreversibly trapped in the sorbed phase structure. In addition to these mechanisms, the slow kinetics may cause apparent hysteresis effect. As discussed in the previous section, strongly held (chemisorbed) chemicals may not be desorbed from the sorbed phase to the final equilibrium value within the time frame set for the experiment. Slow transport (diffusion)-limited sorption/desorption kinetics produces a similar effect since the system does not come to the equilibrium within the reasonable time of experiment. In these cases, the sorption (adsorption) isotherm curve will be lower than the desorption isotherm curve although they should be the same line at equilibrium. Therefore, when there exists a strong hysteresis effect, the sorption isotherm (amount sorbed) is not well defined, and the application of simple thermodynamics becomes questionable. The development of macroscopic theories which can handle the non-uniqueness of the sorption/desorption isotherm is beyond the scope of this study. Therefore, we rather avoided this issue by choosing the simple sorbents as well as weakly reactive probe molecules which do not exhibit strong hysteresis or slow sorption/desorption kinetics effect. The significance of hysteresis will be considered again in the experimental section.

Partitioning-type Sorption

Sorption of organic solute into the organic matter is generally modeled as partitioning process. In the partitioning model, the probe (solute) is dissolved into the soil organic matter phase. Since the dissolved probe is surrounded by the

sorbent, the structure of a sorbed phase may be approximated with a volume-filing walls whose surface fractal dimension is close to three. The geometrical characteristics of such sorbent phase may be approached from the concept of surface fractal dimensions or pore fractal dimensions.

The difficulties of applying the surface fractal dimension to such sorbents are originated from the violations of the presumption-(1) and (2). Since the structure is generally not rigid, under what condition can $N_m(\sigma)$ be defined becomes an open question. Furthermore, the extension of the concept of surface fractal dimension to liquid-like sorbent does not produce correct physical picture of sorption behavior. For example, the fractal B.E.T. equations and fractal F.H.H. type equation generally produce very sharp knee (inflection) for an isotherm of near three surface fractal dimension (Pfeifer, 1988). However, the sorption isotherm of organic solute by organic matter generally produces near-linear isotherm.

Since the sorbent is assumed to be 3-dimensional, it is also possible to consider the characterization of the pore fractal dimension rather than the surface fractal dimension. The application of equation 2-12 may be one way of estimating the pore fractal dimension. Alternatively, an attempt has been made to describe the dependency of solubility in the sorbed phase on the molar volume of the probe in relation to the pore fractal dimension (Augustijn, 1993). However, it is difficult to separate the effect of energetic factor from the overall solubility. Consequently, the method overestimates the fractal dimension. The application of fractal theory to flexible sorbents such as organic matter is still questionable unless the method

measures the dimension without affecting the structure of the sorbent. In this sense, SAXS (small angle x-ray scattering) or SANS (small angle neutron scattering) approach seems to be a powerful tool, although the method does not give the geometrical characteristics of the sorbent as "felt" by the sorbed molecules.

σ : Projected Surface Area

As discussed in the discussion section, it was found that the estimation method for the projected molecular surface area, σ, significantly influences the surface fractal dimension. Therefore the uncertainty associated with the estimate of σ cannot be neglected. The projected surface area is determined by the size and the configuration of the molecule on the surface. The difficulties associated with the estimate of σ value come from

(1) The configuration (orientation) of the probe molecule on the surface is dependent on the nature of the surface and the probe molecule itself.

(2) Unless the surface is perfectly flat, there is no such thing as the absolute surface area due to the difference in the accessibility of probe molecules (Alymore et al., 1970). Therefore, the calibration of the σ value from an operationally defined standard surface area, such as the nitrogen B.E.T. surface area, involves a certain error in the estimate.

From these two points, it is obvious that the σ value is dependent on both the probe molecule itself as well as the characteristics of the surface. Therefore, in principle, it should be defined in terms of the combination of the probe and the surface, pressure and temperature. With this restriction in mind, the projected surface areas of probe molecules, σ (m^2/molecule), can be estimated from liquid density, calibration from the sorption on a surface of known surface area, or from molecular modeling programs.

In the case of liquid density method, the average configuration of the molecule is usually approximated by the spherical molecule which is hexagonal close-packed at the given temperature and liquid density. This assumption yields

$$\sigma = 1.09 \times \left(\frac{M.W.}{N_o \, \rho(T)} \right)^{2/3} \qquad (2\text{-}15)$$

where M.W. is the molecular weight of the probe molecules, N_o is the Avogadro number (6.02×10^{23} molecule/mole), and ρ (T) is the liquid density of the probe molecules at the temperature, T. This method does not account for the effect of surface on the conformation of probe molecules on the surface, but it rather approximates the averaged configuration of the molecule in liquid state. The projected surface area estimated from liquid density are often quite different from the estimate from the calibrated surface area partly due to the surface conformation. Therefore, when the heat of sorption for the first layer is high, and the B.E.T. C value is high for the combination of the probe and the surface, this method is not recommended. On the other hand, when the B.E.T. C value is low,

the adsorbed molecule tends to behave like two dimensional liquid, and the use of the liquid density method may be justified.

Under an assumption of flat surfaces, McClellan and Harnsberger (1967) compiled reported projected surface areas of various molecules as normalized to mostly nitrogen B.E.T. surface areas of the same sorbents. In reality, the assumption of flat surface could be wrong, and it is the prime motivation of this study. To account for both the surface accessibility and the surface configuration effects, one of the best available approaches is the calibration of σ value from the B.E.T. monolayer value on near flat surface. For example, Clint (1972) conducted a series of n-alkanes vapor sorption experiments on Graphon (graphitized Spheron 6 at 3000 ° C). Assuming the surface is flat and the surface area measured with nitrogen B.E.T. as the reference surface area, the projected surface areas of n-alkanes, C_5 - C_{12}, were estimated using classical B.E.T. equation. The obtained σ values indicate flat orientations of the n-alkanes on the surface. For benzene, McClellan and Harnsberger (1967) recommended the σ of 0.43 nm^2 from fifteen papers covering eleven adsorbents. This result can be interpreted as the flat orientation of benzene on surfaces (Gregg and Sing, 1982). However, the B.E.T. C value for benzene sorption seems to be generally low which introduces an element of uncertainty into the estimation of monolayer calculation (Gregg and Sing, 1982). McClellan and Harnsberger estimated the σ values by normalizing the experimentally observed $N_m(\sigma)$ value to the surface area of the same sorbent measured with nitrogen or other inert gas B.E.T. surface area. Fig. 2-7 shows the

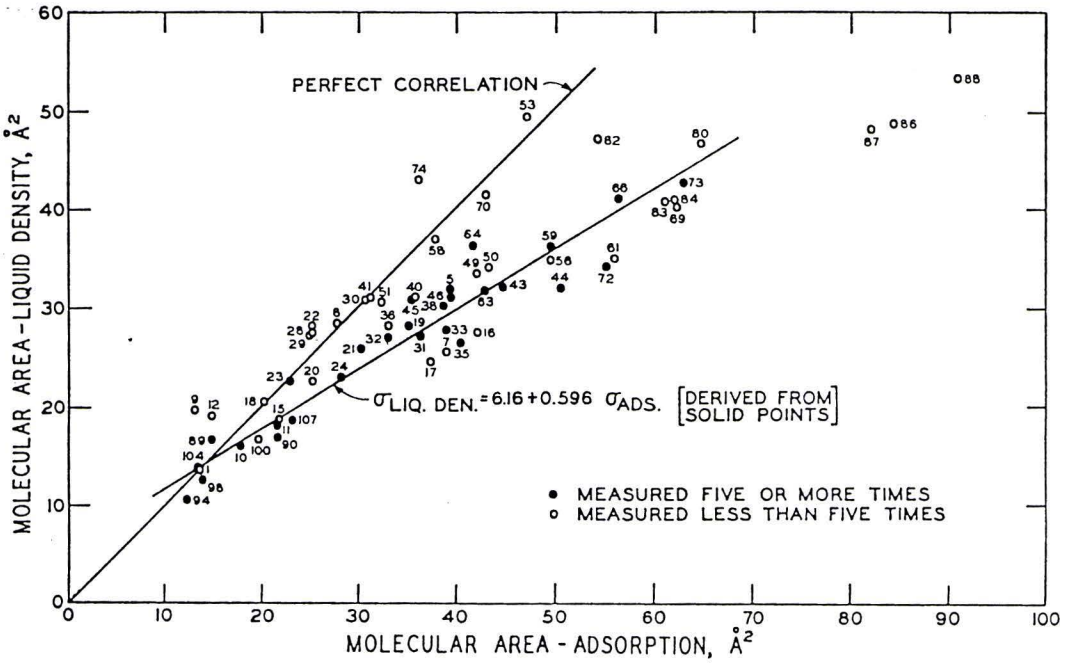

Fig. 2-7. The relationship between the σ estimated from the liquid density method and σ estimated by normalizing to the nitrogen B.E.T. surface area assuming the surfaces are flat (after McClellan and Harnsberger, 1967).

relationship between the observed (i.e. normalized) σ values and the σ values estimated from the liquid density method. It is obvious that the deviation of σ (normalized) from the σ (liquid density) increases with the size of the molecule. This deviation is partially attributed to the surface configuration of the probe molecule. However, this normalization does not account for the geometric heterogeneity of the surface.

To estimate the effect of the surface geometric heterogeneity, let us assume that a surface is approximated with a surface fractal structure. From the definition of the surface fractal dimension,

$$N_m(\sigma) = N_m(\sigma^*) \left(\frac{\sigma}{\sigma^*}\right)^{-\frac{D}{2}} \qquad (2\text{-}16)$$

where the asterisk * indicates the standard probe molecule such as nitrogen. σ is the true molecular surface area. However, the effect of the configuration of the probe molecule on the surface as well as the surface geometrical heterogeneity (fractal), it is not possible to estimate the both effect simultaneously. In the normalization scheme of McClellan and Harnsberger, the surface is assumed flat, and the σ is estimated from the standard probe surface area, $A_{standard} = N_m(\sigma^*)\ \sigma^*$. However, if the surface is fractal, the estimated molecular projected surface area, σ_{est}, becomes

$$\frac{N_m(\sigma)\ \sigma_{est}}{N_m(\sigma^*)\ \sigma^*} = 1 = \frac{N_m(\sigma^*)\left(\frac{\sigma}{\sigma^*}\right)^{-D/2}\ \sigma_{est}}{N_m(\sigma^*)\ \sigma^*} \qquad (2\text{-}17)$$

Consequently,

$$\sigma_{est} = \left(\frac{\sigma}{\sigma^*}\right)^{-D/2} \sigma^* \qquad (2\text{-}18)$$

This relation shows that the deviation of normalized σ from the liquid density σ is partly attributed to the surface geometrical heterogeneity. For example, when the surface fractal dimension is 2.5, and the nitrogen (σ =0.162 nm^2) is used as the standard probe, a probe of actual σ = 0.50 nm^2 is estimated as 0.66 nm^2. Therefore, the normalization procedure tends to overestimate the actual σ value. A significant part of the sorbents compiled by McClellan and Harnsberger (1967) are presumably flatter than D = 2.5. Therefore, the degree of the overestimation should be smaller. Nevertheless, the true projected surface area of a probe molecule, σ, is expected to be somewhere between the σ estimated with the liquid density method and the σ value recommended by McClellan and Harnsberger (1967) which is normalized to nitrogen B.E.T. surface area assuming flat surface area.

The molecular modeling programs have the flexibility of choosing best-approximated surface configuration. This method can be much preferred if detailed molecular configurations of the sorbent molecules and their interaction with the probe molecule are known. Furthermore, it is possible to simulate the full molecular level sorption phenomena using sophisticated molecular modeling program if the detailed structure of the sorbent surface is known. Even when the effect of the surface or other sorbed molecules on the configuration of a sorbed molecule

cannot be estimated, it is still feasible to investigate the approximate dimension of the molecule. In this research, SYBYL molecular modeling program was used to estimate the possible range of σ values of the probe molecules. At first, the structure of the molecule (single molecule) of interest was optimized by minimizing the interaction energy. Secondly, the volume of the molecule was estimated by estimating the electron distribution around the molecule. Then the molecule was rotated to find the maximum and minimum projected surface area. For a long alkane molecule, the minimum σ is expected when the molecule is adsorbed vertically, while the maximum σ is expected when the molecule is fully stretched, and horizontally (flat) oriented on the surface. This method directly estimate the projected size of a single molecule. Since this method does not account for the packing pattern of the sorbed probe at the monolayer formation, and molecules may not be very densely packed at the monolayer coverage, it is possible that this method tends to underestimate the actual area covered by a single molecule on the surface. Nevertheless, this method is useful to examine the range of uncertainty due to the surface orientation of the probe molecule. The liquid density σs generally lie between the minimum and maximum σ values estimated with SYBYL (except n-pentane and n-octane). It was found that there are a few-fold differences between the minimum σs and the maximum σs for some long-chain molecules.

The σ values estimated with four different methods, i.e. liquid density, recommended σ based on flat surface assumption, minimum and maximum σs

estimated with SYBYL, are given in Table 2-2. The uncertainty associated with the σ estimation is striking. For a long alkane (e.g. n-octane), the difference between the minimum σ, and the recommended σ is about four fold (0.6 on log scale). The effect of the uncertainty on the estimated surface fractal dimension will be discussed in Results section.

Materials

Sorbents

Georgia kaolinite (KGa-1, Clay Minerals Society), silica-gel SYLOID 244 (Davison Chemical), and Borden aquifer sand were used without pretreatment. These sorbents were chosen because their structures and the surface fractal dimensions have been well studied. Kaolinite is a dioctahedral 1:1 layer silicate clay mineral (Brown et al. 1985; van Damme et al., 1985). The chemical composition of Georgia kaolinite is close to the ideal structural formula (Jepson and Rowse, 1975), and considered to be well-crystallized (Clay Minerals Society). Therefore, the surface fractal dimension of this clay is expected to be close to 2 (Sokolowska et al., 1989). The reported surface fractal dimensions of kaolinite (well-crystallized to kaolinite rich soil) are in the range of 2.12 - 2.92 (Avnir et al., 1984; Fripiat et al., 1986; Sokolowska et al.,1989). On the other hand, silica-gel is considered to have much convoluted surface. The degree of the complexity is presumably determined by the silica-gel formation (sol-gel) process which may be modeled as diffusion limited aggregation (Orcel, 1987; Wijnen et al, 1991). Farin et al. (1985) tabulated

Table 2-2. Physicochemical Porperties of Probe Molecules

molecule	formula	mol. wt. g/mol	vap. press. *293 K mm Hg	$\sigma 1$	$\sigma 2$	$\sigma 3$	$\sigma 4$
					10^{-20} m^2		
n-pentane	C_5H_{12}	72.2	375	32.0	49.2	15	30
n-hexane	C_6H_{14}	86.2	108	39.4	56.2	16	37
n-heptane	C_7H_{16}	100.2	40.1	42.5	63.1	16	44
n-octane	C_8H_{18}	114.2	10.5	45.5	64.6	16	50
benzene	C_6H_6	78.1	81.8	30.5	43.6	18	34
p-xylene	C_8H_{10}	106.2	1.89	37.9	53.8	18	43
EGME	$C_4H_{10}O_2$	90.1		32.3	52.0**		
water	H_2O	18.0	17.5	10.8	12.5		
nitrogen	N_2	28.0		16.2	16.2		
krypton	Kr	83.8			20.2		

$\sigma 1$: Liquid density method assuming hexagonal close-packing at the given temperature.

$\sigma 2$: Recommended value by McClellan and Harnsberger (1967) based on the surface area measured with various probe molecules normalized to nitrogen B.E.T. surface area.

$\sigma 3$: σ values estimated based on the smallest projected surface area of the molecul (SYBYL). To estimate the configuration, MAXIMIN2 optimization was applied to a single molecule.

$\sigma 4$: σ values estimated based on the largest projected surface area of the molecul (SYBYL). To estimate the configuration, MAXIMIN2 optimization was applied to a single molecule.

*: CRC Handbook of Chemistry and Physics, 51st edit.

**: Carter et al. (1986)

the surface fractal dimension of silica-gel to be near 3. Recently Wijnen et al. (1991) investigated the effects of formation/aging process on the surface fractal dimension of aqueous silica-gel. The reported surface fractal dimensions of silica-gel vary considerably in the range of 1.5 to 3 (Rojanski et al., 1986; Orcel, 1987; Nakanishi and Soga, 1988; Farin and Avnir, 1989; Wijnen et al., 1991). The Borden sand was chosen as the example of real natural sorbent. Detailed analysis of Borden material has been given by Ball et al. (1990). We also conducted preliminary experiments with Arizona bentonite (SAz-1), Pahokee muck, Aldrich humic acid (Aldrich chemical), and Eustis soil.

Probe Molecules

The probe molecules were selected based on four criteria. These criteria are, 1) molecules of broad range in size with similar structure, 2) weak interaction with the surface to avoid specific interactions with functional groups on the surface, and 3) sufficient vapor pressure to conduct a vapor phase desorption experiment, and 4) rigid molecules are preferred over flexible, chain-like molecules since the problem associated with the estimate of the surface configuration may be smaller. While the first and last requirements were difficult to be fulfilled completely due to the other constraints, benzene, p-xylene, n-hexane, n-octane, and nitrogen were used as probe molecules (solutes). The physicochemical properties of the probe molecules are given in Table 2-2. All chemicals were of analytical grade, and no further purification/redistillation was employed.

Since fractal is a scaling concept, to establish a meaningful dimension, the same fractal relationship should hold over several orders of magnitude in size (Feder, 1988). This means that the large probe is desired to be several orders of magnitude larger than the small probe. However the saturated vapor pressure at a given temperature decreases sharply with the size of the molecule which makes the experiment difficult. Because of the analytical limitation (10^{-5} atm) of Pirani pressure gauge (Edward 1505), we did not investigate probe molecules larger than n-octane. The surface fractal dimensions investigated in this research are limited to this scale.

Methods

Cahn Desorption Study

The desorption of probe molecules other than nitrogen were measured at the University of Florida by means of weight of adsorbed probe molecules at given temperature and pressure. The experimental set-up consisted of 1) an electronically controlled microbalance in a closed system (Cahn D-200), 2) a vacuum pump (Precision DD195), 3) a personal computer (Zenith ZW248-82) for data acquisition/storage purpose, and 4) a Pirani pressure gauge (Edward 1505) to monitor the internal pressure of the system (Fig. 2-8). The detection limit of the balance was 10^{-4} mg. A thermocouple (Barnant 115) was attached to the (outside of the) system to measure the temperature. Since the pressure gauge determines the total pressure of the system, the experiments were restricted to single-probe

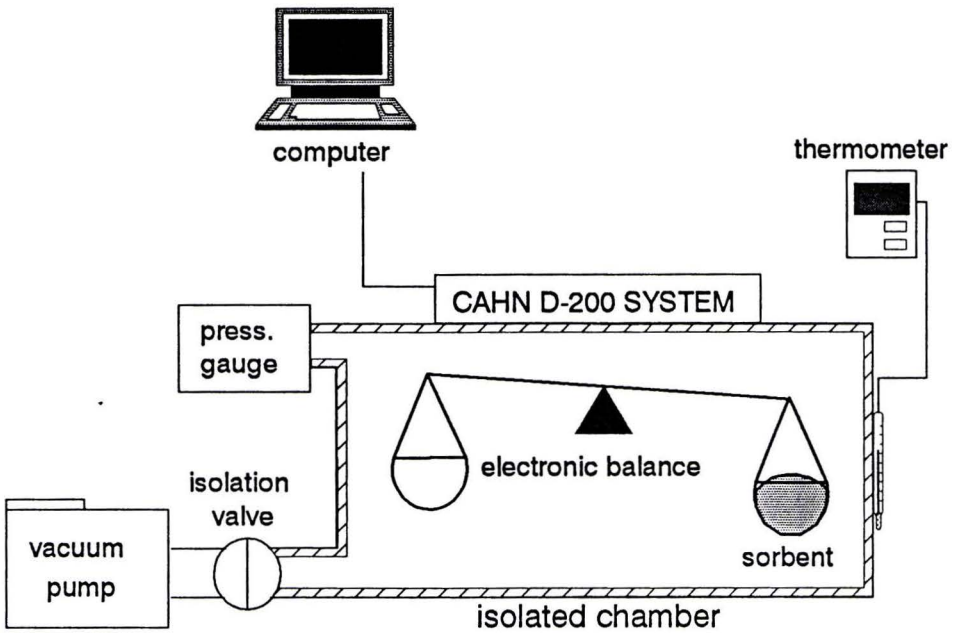

Fig. 2-8. The schematic of Cahn D-200 microbalance system.

molecule systems. The leak rate of the system was generally in the order of 10^{-5} to 10^{-4} atm per hour at pressure around 10^{-4} atm.

The desorption experiment was conducted in the following order. The system was evacuated with vacuum pump for 5 hours or more. After the system was dried and stabilized, the valve to the vacuum pump was closed. Then the leak rate was monitored for 5 to 60 minutes. If there was no excessive leak, the balance was tared. Preliminary blank experiments (experiments without sorbent) showed the system stayed in balance during the course of experiments at various vapor pressure conditions.

After taring the balance, the system was opened to introduce the sorbent. To ensure the significant weight changes by sorption, as much sorbent as the quartz glass cup could hold, which is about 40 mg of silica-gel, 100 mg of clays or 400 mg of Borden sand, was added to the quartz sample cup.

Since the relative vapor pressures of air components such as nitrogen and oxygen at room temperature were very low, the sorptions of most of the air components were considered to be negligible. However, certain components, especially water (relative humidity of 20-50 %, may exist in significant amounts on the surface of the sorbent. To investigate sorption characteristics including the surface area, the sorbent surface has to be free from molecules other than probe molecules. Therefore, degassing/drying is essential (Joy, 1953). In this research, the sorbent was evacuated down to 1×10^{-4} atm over night to degas the residual molecules on the surface. After the degassing, the valve to vacuum pump was

closed and the system was isolated. The leak rate was monitored for 5 to 60 minutes, and the dry-weight of the sorbent was recorded. The amount of sorption is expressed in this dry-weight basis.

The system was reopened to the ambient environment to introduce the probe molecules. Liquid state solute was placed under the sorbent, and frozen with liquid nitrogen (77 K). The amount of solute was decided so that saturated vapor pressure could be achieved at equilibrium. The system was evacuated at 2×10^{-4} atm for about 10 minutes to remove any undesirable molecules present in the system. Then the system was isolated, and allowed to come to the equilibrium for over night. Since the system was filled only by the solute vapor, the equilibrium vapor pressure was approximately equal to the saturated vapor pressure of the solute at the temperature (0.99 to 1.1 relative pressure).

The desorption experiment was initiated by lowering the vapor pressure. To obtain an isotherm, a few data points between 1 to 0.5 relative pressure, and 7 to 8 points between 0.5 to 0 relative pressure region, were taken. The general procedure is as follows. At first, the system was slowly evacuated down to the target pressure, and the new equilibrium was attained. To avoid unwanted effect of leakage, the system was considered to reach the equilibrium when the rate of the weight change is approximately less than 10^{-4} atm per hour and the weight change becomes negligible. After recording the weight of sorbent, vapor pressure, and temperature, the pressure was lowered to the next target pressure and same procedure was repeated.

In principle, the equilibrium is reached when the changes in pressure and weight is both zero. However, in practice, depending on the probe molecule and the sorbent, the time to reach the equilibrium was long enough so that the effect of leak became significant. Beside the slow desorption kinetics, (a) leakage, or intrusion of air into the system, (b) slow release of solute from the apparatus such as O-rings, and (c) temperature fluctuation cause changes in pressure and weight of the system. The experimental limitation for the systems of slow desorption kinetics are discussed later.

To construct a desorption isotherm, the relative pressure (p/p_o), where p is the vapor pressure and p_o is the saturated vapor pressure, has to be known. The saturated vapor pressure was estimated using the empirical three parameters fitting equations (Lange's Handbook of Chemistry). Since the vapor pressure is strongly affected by the temperature, the relative pressure was estimated for each data point using the corresponding measured temperature. The mass of the probe molecules in the sorbed phase (mg of probe molecules per unit mass of sorbent) was calculated from the weight difference between sorbed and dry state. The effect of temperature on the mass of probe molecules in the sorbed phase was neglected. An isotherm was then constructed by plotting the mass of probe molecules in the sorbed phase as a function of the relative pressures. The lower pressure region of the adsorption (p/p_o=0.05-0.35) isotherms were then fitted with classical B.E.T. equation, and the monolayer value, N_m (mmole/g sorbent) and the sorption energetic term, C, were obtained.

Nitrogen Sorption/Desorption Study

All nitrogen sorption experiments were conducted at Advanced Material Research Center using automated surface area analyzer, Autosorb-6 (Quantachrome) except the results of Borden aquifer material which was taken from the reported values (Ball et al., 1990). Both adsorption and desorption isotherms at 77 K were obtained from the gas phase volume change due to the sorption/desorption (Joy, 1953).

Experimental Considerations

Some experimental difficulties were also encountered in obtaining a reliable estimate of $N_m(\sigma)$. First of all, the energetic terms of the B.E.T. equation, C, were fairly small (Table 2-3) for KGa-1 and silica-gel. The isotherms are provided in Appendix B. Since this term is related to the difference in the heat of adsorption for the first and successive layers, small C term generally represents weak physical sorption. Weak interaction is ideal for the analysis of geometrical heterogeneity because the effect of energetic heterogeneity and strongly localized adsorption will be avoided. However small C value generally lessen the development of distinct monolayer. Consequently, the estimated $N_m(\sigma)$ becomes less reliable (Gregg and Sing, 1982). As long as weakly adsorbed molecules are used, this difficulty is inevitable. Based on the experimental results, however, the obtained $N_m(\sigma)$ values were consistent among the replicate experiments. Therefore, no correction was made on the estimated $N_m(\sigma)$. On the other hand, the C value for Borden aquifer

Table 2-3. B.E.T. parameters estimated by non-linear regressions to the desorption isotherms.

file	probe	sorbent	C	STD.(C)	N_m (mmole/g)	STD.(N_m)
I1019	octane	KGa-1	0.148E+2	0.571E+1	0.253E-1	0.238E-3
I1032	octane	KGa-1	0.132E+2	0.862E+0	0.277E-1	0.492E-3
I1049	hexane	KGa-1	0.219E-1	0.258E+0	0.293E-1	0.699E-4
I1051	hexane	KGa-1	0.625E+1	0.529E+0	0.302E-1	0.111E-2
I1106	p-xylene	KGa-1	0.203E+2	0.163E+1	0.372E-1	0.519E-3
I1110	p-xylene	KGa-1	0.133E+2	0.343E+0	0.345E-1	0.219E-3
I1113	p-xylene	KGa-1	0.136E+2	0.574E+0	0.349E-1	0.243E-3
I1116	benzene	KGa-1	0.744E+2	0.931E+2	0.392E-1	0.247E-2
I2039	H2O	KGa-1	0.228E+2	0.130E+1	0.261E+0	0.273E-1
I2042	H2O	KGa-1	0.376E+2	0.328E+1	0.247E+0	0.278E-2
	N2	KGa-1			0.837E-1*1	
I1067	hexane	SAz-1	0.699E+4	0.158E+6	0.352E+0	0.644E-2
I1073	hexane	SAz-1	0.739E+4	0.264E+6	0.393E+0	0.118E-1
I1083	octane	SAz-1	0.916E+4	0.181E+7	0.386E+0	0.604E-1
I1087	octane	SAz-1	0.384E+4	0.454E+6	0.293E+0	0.665E-1
I1097	hexane	silica-gel	0.222E+1	0.181E+0	0.588E+0	0.228E-1
I1100	hexane	silica-gel	0.394E+1	0.120E+1	0.438E+0	0.543E-1
I1103	octane	silica-gel	0.174E+1	0.288E+0	0.477E+0	0.380E-1
I1120	benzene	silica-gel	0.973E+3	0.181E+5	0.573E+0	0.659E-1
I1123	p-xylene	silica-gel	0.159E+2	0.410E+1	0.628E+0	0.374E-1
I2045	H2O	silica-gel			0.201E+1	
	N2	silica-gel			0.162E+1*1	
I2049	hexane	Borden	0.336E+3	0.186E+3	0.316E-2	0.307E-4
I2052	hexane	Borden	0.163E+3	0.160E+3	0.321E-2	0.101E-3
I2023	benzene	Borden	0.197E+4	0.100E+5	0.925E-2	0.145E-3
I2026	benzene	Borden	-.166E+3	0.548E+2	0.930E-2	0.135E-3
I2065	benzene	Borden	0.106E+3	0.149E+2	0.426E-2	0.333E-4
I2031	H2O	Borden	0.312E+2	0.311E+1	0.761E-1	0.115E-2
I2034	H2O	Borden	0.711E+2	0.130E+1	0.767E-1	0.107E-2
I2056	heptane	Borden	0.171E+2	0.443E+1	0.325E-2	0.171E-3
I2062	octane	Borden	0.540E+2	0.190E+2	0.318E-2	0.972E-4
I2070	p-xylene	Borden	0.167E+3	0.173E+3	0.472E-2	0.191E-3
I2074	pentane	Borden	-.118E+3	0.260E+2	0.378E-2	0.678E-4
	N2	Borden			0.470E-2	
	N2	Borden			0.480E-2*2	
	N2	Borden			0.388E-2*1	
	EGME	Borden			0.926E-2*2	

*1: AMRC; *2: Ball et al., 1990

Note: All desorption experiments were conducted at the room temperature (292-296 K) except the nitrogen experiments (77 K).

material, SAz-1 were very high. In general, these isotherms exhibited distinctive knees at very low p/p_o region. Negative C value was also observed for Borden aquifer material. Negative C value occurs when the inflection point (knee) is below the relative pressure of 0.05. It was found that the classical B.E.T. isotherm with small negative (large negative) C value ($C < -250$) behaves almost identical to the classical B.E.T. equation with the same absolute (positive) C value. Therefore, when the isotherm exhibit strong inflection at $p/p_o < 0.05$, the fitted C can be negative. In this case, regardless the sign of the C, the resulting N_m values are almost identical. However, the anomalous C values generally indicate that the sorption process cannot be described with weak physisorption as modeled with classical B.E.T. theory. In particular, irreversible sorption and hysteresis effects were of concern.

In principle, the sorption isotherms have to be analyzed at the equilibrium. However, the possible effect of contamination, especially with water and other components of air, had to be minimized since the experiments were conducted at sub-ambient pressure (as low as 10^{-5} atm). Generally, significant desorption occurred within the initial 5 minutes, and followed by very slow release. It was of practical importance to decide when the equilibrium was achieved. Each successive desorption step was initiated when the desorption rate becomes negligible (pressure change of approximately 10^{-4} atm per hours) which took about 20 minutes to 2 hours depending on the combination of probe molecules and sorbent. Typically 10 to 15 data points were taken per experiment, so the total time

for the entire desorption process was about 10 to 20 hours. Our preliminary results indicated soil organic matter and montmorillonite clay had rather slow desorption kinetics. Chiou et al. (1988) reported that the desorption process may extend over 48 hours or more. For such long desorption time, the intrusion of ambient air into the system is highly likely. The correction of the contamination effect by subtracting the blank experiment result, and/or estimating the infinite time behavior by extrapolating the desorption kinetics curves, were considered. However, the errors introduced by these corrections can be significant.

In addition, the nitrogen adsorption-desorption curves measured with Autosorb-6 surface area analyzer revealed that the systems with slow desorption kinetics often exhibited significant hysteresis (Fig. 2-9), while KGa-1 and silica-gel showed no hysteresis. Whether this hysteresis is due to the irreversible sorption or reversible but slow kinetics is not known. Because the Cahn system was dedicated for desorption study (see the section on the methods), we did not investigate the hysteresis of probe molecules other than nitrogen. Since reliable equilibrium data could not be obtained, the fractal dimensions of organic matters and montmorillonite clay were not analyzed here. Furthermore, the high B.E.T. C values of Borden desorption isotherms are the indication of irreversible sorption or hysteresis effect. As an alternative method, x-ray scattering technique (Schaefer, 1984) may be applied to estimate the surface fractal dimension of such sorbents. This method is not constrained by the slow kinetics, hysteresis, or sorption energetics. However, it may not reflect real (fractal) sorption environment.

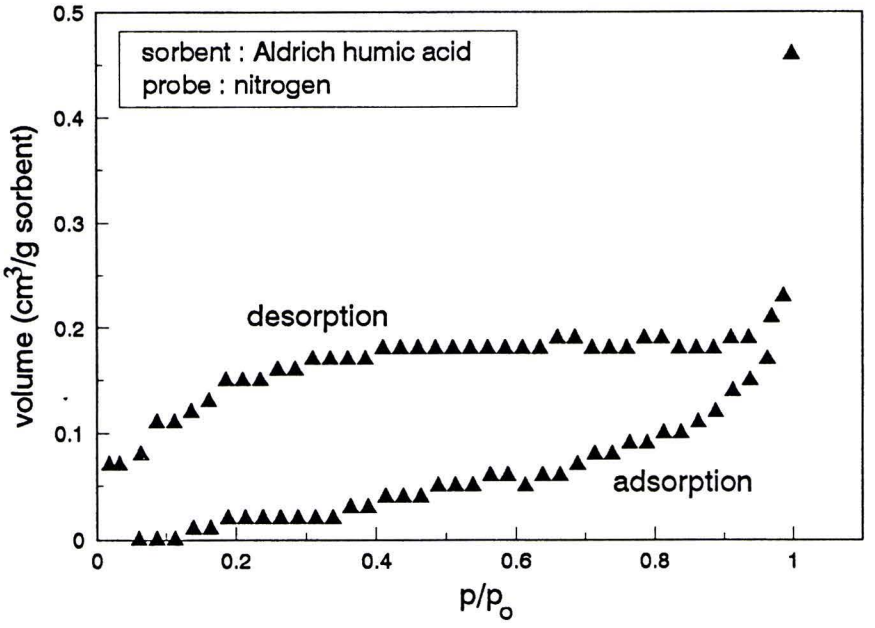

Fig. 2-9. Sorption/desorption of N_2 by Aldrich humic acid.

Results

Our investigations showed that kaolinite and silica-gel have minimum kinetic and hysteresis effects, and are least susceptible to the errors associated with the estimation of $N_m(\sigma)$. The isotherm data (Appendix B) for the lower relative pressure range (p/p_o 0.05 - 0.35) were fitted with the classical B.E.T. equation using non-linear least squares method (Table 2-3). As expected from the fractal theory, the linear relation between the natural log of the monolayer values, $N_m(\sigma)$, and the natural log of the estimated projected surface area of the probe molecule, σ, were obtained (Fig. 2-10, and 2-11).

The fractal dimension was estimated with a non-linear fitting program. Using the σ values estimated with liquid density method, the non-linear least-square estimations of these curves gave the fractal dimensions of kaolinite and silica-gel to be 2.18 ± 0.09 and 2.56 ± 0.26, respectively (Table 2-4). The $N_m(\sigma)$ values of H_2O were not used since H_2O is highly reactive with the surfaces. Similarly, the surface fractal dimensions of 1.56 ± 0.07 and 1.82 ± 0.14 were obtained for the same sorbents when the normalized recommended σ values (McClellan and Harnsberger, 1967) were used (Fig. 2-11; Table 2-2).

According to Pfeifer (1988), the fractal dimension as defined in the previous section can take the value between its topological dimension, D_{topo}, and thedimension of its embedding space which is 3 in this case. Assuming that the probe molecule is much smaller than the sorbent, the D_{topo} is the dimension of surface, 2.

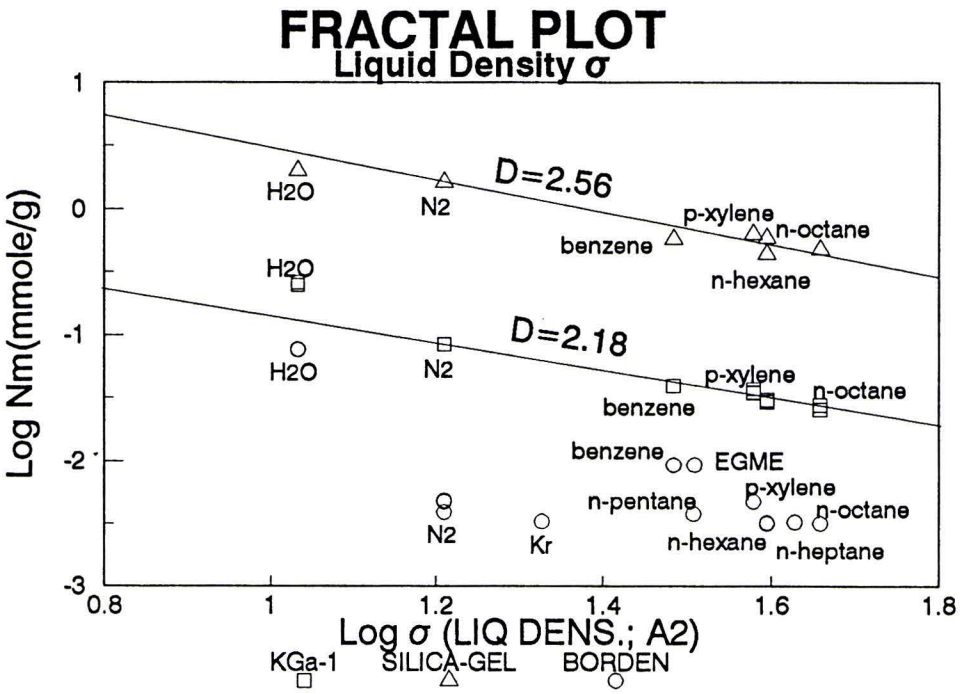

Fig. 2-10. The relationship between the monolayer values, $N_m(\sigma)$ and the projected surface area of probe, σ, for KGa-1, silica-gel (SYLOID 244) and Borden aquifer sand. For Borden aquifer sand, N2, Kr and EGME values were taken from Ball et al. (1990). The projected surface area of a molecule, σ, was calculated using the liquid density method. The estimated surface fractal dimensions for KGa-1 and silica-gel were 2.18± 0.09 and 2.56± 0.26, respectively.

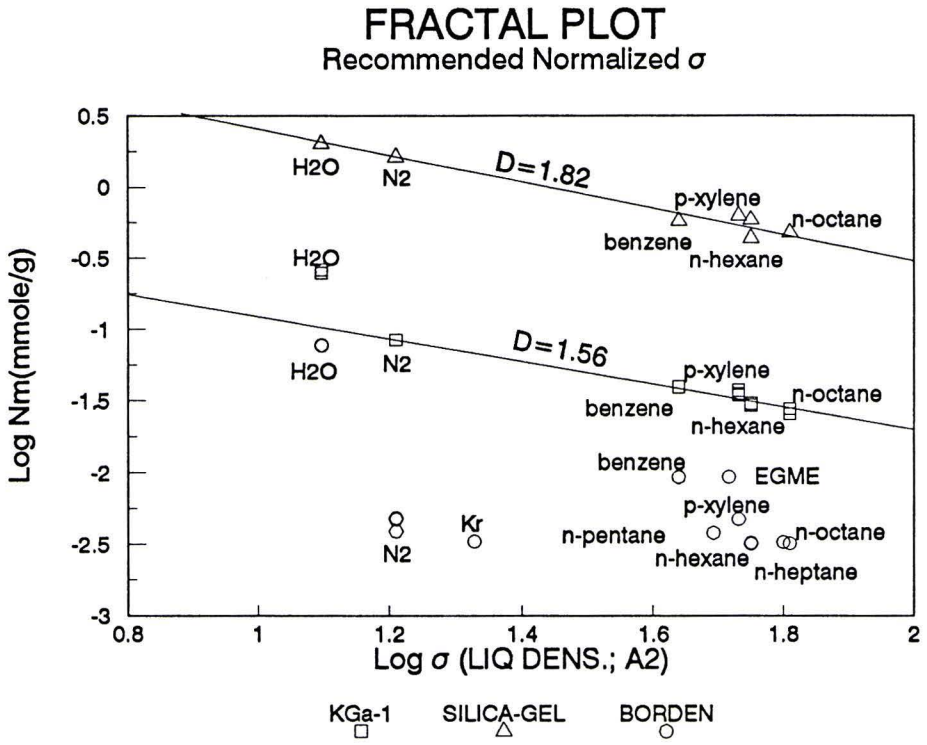

Fig. 2-11. The relationship between the monolayer values, $N_m(\sigma)$ and the projected surface area of probe, σ, for KGa-1, silica-gel (SYLOID 244) and Borden aquifer sand. For Borden aquifer sand, N2, Kr and EGME values were taken from Ball et al. (1990). The recommended projected surface areas of probe molecules, σs, (McClellan and Harnsberger, 1967) were used. The obtained surface fractal dimensions for KGa-1 and silica-gel were 1.56± 0.07 and 1.82± 0.14, respectively.

Table 2-4. The surface fractal dimensions of KGa-1 and silica-gel. The estimated monolayer value, $N_m(\sigma)$ and the estimated σ values were fitted with $N_m(\sigma) = C\,\sigma^{-D/2}$ using non-linear fitting program.

	Liquid Density Method		Recommended σ value	
Sorbent	D ± (stdev.)	C ± (stdev)	D ± (stdev.)	C ± (stdev)
KGa-1	2.18 (0.09)	1.74 (0.26)	1.56 (0.07)	0.737 (0.086)
Silica-gel	2.56 (0.26)	56.7 (22.6)	1.82 (0.14)	20.2 (4.6)

Therefore, we expect the surface fractal dimensions to behave as: 1) for convoluted surface, the dimension will be between two (topological dimension) and three (space filling); 2) the highly convoluted surface has higher fractal dimension than the surface with flatter surface. The surface fractal dimension lower than 2 obtained using the normalized σ values can be partially explained from the overestimation of the σ values due to the surface geometrical heterogeneity as explained previously.

The striking differences between the surface fractal dimensions estimated from the liquid density σ values and the recommended σ values is quite peculiar since this effect can be solely attributed to the σ estimation. Due to the large uncertainty of σ values, it is difficult to estimate the fractal dimensions of kaolinite and the silica-gel. To estimate the realistic σ values, the following two criteria were considered.

(1) Assuming that KGa-1 is well-crystallized kaolinite which has nearly flat surface structure, the surface fractal dimension of KGa-1 is closer to two. Therefore, under the assumption of fractal structure of KGa-1, the realistic σ may be closer to the liquid density σ ($D=2.18\pm0.09$) than the recommended σ ($D=1.56\pm0.07$), and possibly somewhere between these two estimates.

(2) The recommended σ tends to overestimate the actual σ because the effect of the surface roughness was not accounted for when the data were compiled

by McClellan and Harnsberger in 1967. On the other hand, the liquid density σ is based on the averaged configuration.

These criteria generally support the surface fractal dimensions estimated from the liquid density σs. However, the configuration of the sorbed molecule can be specific depending on the combination of the solute and the sorbent. The direct confirmation (e.g. spectroscopic studies) of the configuration of the sorbed species is essential to draw a definite conclusion.

In addition to the standard deviation estimated with the non-linear fitting program, the uncertainty associated with the estimate of fractal dimension was assessed using the propagation of error technique. Assuming that log $N_m(\sigma)$ and log σ are uncorrelated, the variance of D, Var[D], is given as

$$\begin{aligned} \mathrm{Var}[D] = {} & \mathrm{Var}[\log N_m]\left(\frac{\partial D}{\partial \log N_m}\right)^2 + \\ & \mathrm{Var}[\log\sigma]\left(\frac{\partial D}{\partial \log\sigma}\right)^2 + \mathrm{Var}[\mathrm{LogC}]\left(\frac{\partial D}{\partial \log C}\right)^2 \end{aligned} \qquad (2\text{-}19)$$

The standard deviation of the fractal dimension for KGa-1 about the point of log σ at 1.5, log N_m at -1.25, and log C at 0.239 was estimated from the estimated standard deviations 0.1 for log N_m, 0.1 for log σ, and 0.1 for log C, respectively. The estimated standard deviation for the D is 0.23. This estimate is rather conservative (possibly overestimating the uncertainty), and the actual uncertainty is presumably small. In practice, smaller molecules tend to have smaller uncertainty with respect to their size. Nevertheless, the uncertainty of about 10 % seems to be

inevitable. Therefore, the estimated fractal dimension should be interpreted accordingly.

To assess the reliability of our results, the obtained fractal dimensions were compared with reported values of similar sorbents. Georgia kaolinite (95%) has been studied by Sokolowska et al. (1989). It is not clear whether their kaolinite is equivalent to the KGa-1 we have used. Yet, it was of interest to directly compare the results assuming they represent well-ordered kaolinite. By applying fractal B.E.T. equation (Fripiat et al., 1986) and the recommended σ values (McClellan and Harnsberger, 1967), they estimated the surface fractal dimension of Georgia kaolinite to be 2.12 ± 0.05. However, their result of the classical B.E.T. monolayer values and the liquid density σ produces high fractal dimension (2.94 ± 0.3). This comparison pointed out the importance of the estimation of σ values on the resulting surface fractal dimension. Other examples of the reported surface fractal dimensions of kaolinite are $D = 2.40$ (monolayer sorptions of water - n-hexane) for Russian kaolinite as reported by Sokolowska et al. (1989), and $D = 2.92$ for a kaolinitic soil reported by Avnir et al. (1984) who estimated the fractal dimension from the dye sorption data of Cohen and Knight (1947). The degree of crystallization and other components seem to have significant impact on the surface fractal dimension.

For silica-gel, the literature value vary in the range between about 1.5 and 3 (Rojanski et al., 1986; Nakanishi and Soga, 1988; Farin and Avnir, 1989; Wijnen et al., 1991). The surface fractal dimension of silica-gel is likely to be affected by

the manufacturing process and storage conditions (Orcel, 1987; Wijnen et al, 1991). Therefore the results are not directly comparable, although it is important to consider whether the process of silica-gel formation is consistent with the measured fractal dimension. It was noticed that several earlier works (Avnir et al., 1984; Rojanski et al., 1986) reported the fractal dimension of silica-gel to be near 3. However, recent SAXS studies (Orcel, 1987; Wijnen et al., 1991) generally obtain the fractal dimension around 1.6 to 2.5. The dimension lower than 2 is generally interpreted that some silica-gels are mass fractals rather than surface fractals. As depicted in Fig. 2-3, a mass fractal has "entangled strings" like structure. It is not very clear whether the applicability of monolayer method can be extended to mass fractals. However, regardless the σ estimation method, the measured surface fractal dimension for silica-gel was higher than the surface fractal dimension of KGa-1, and KGa-1 is expected to have nearly flat surface, the silica-gel used in this research (SYLOID 244) seems to be a surface fractal rather than a mass fractal. Nakanishi and Soga (1988) conducted a series of alcohol vapor sorption experiments on silica-gels. The obtained fractal dimensions for two silica-gels were 2.14 and 2.4. Using the relationship between the film volume and the surface area, Pfeifer et al. (1991) experimentally measured the fractal dimension of porous silica to be around 2.5. Using the electronic energy transfer technique, Pines-Rojanski et al. (1987) measured the fractal dimension of various silicas. The obtained fractal dimensions were in the order of 2.05 to 2.82. The obtained fractal dimension of around 2.56 ± 0.26 (liquid density method) seems to be a reasonable estimate.

Given the uncertainties in the estimates of $N_m(\sigma)$ and σ, it should be concluded that the fractal dimensions measured with monolayer coverage method inherently have uncertainty in the estimated dimension. The uncertainty is associated with (1) the difficulty of measuring accurate monolayer value from experimental isotherms; (2) the difficulties of estimating the σ values as affected by the presence of the surface and other solute molecules; and (3) the statistical nature of the surface fractal dimension of the surfaces. To interpret the meaning of the uncertainty around the measured surface fractal dimension, it is especially important to discern the statistical characteristics of natural fractal dimensions from the uncertainties associated with the measurement technique. From the analysis of the propagation of errors, the estimated uncertainty associated with the monolayer coverage method is likely significant (10 %), and the monolayer coverage method should be considered as a semi-quantitative method. Thus it is difficult to assign definite surface fractal dimensions to KGa-1 and silica-gel as fractal objects.

However, it is truly remarkable that the experimental results followed the expected exponential relation very well, and the obtained surface fractal dimensions are in good agreement with the expected fractal dimensions based on their structures as well as the reported fractal dimensions of similar sorbents. Despite the complexity of sorption processes, the experimentally determined probe-dependency of the monolayer values can be reasonably explained from the geometrical complexity of the surfaces for kaolinite and silica-gel.

To investigate the applicability of fractal theory to natural environments, similar sorption experiments were conducted on a natural aquifer material, Borden aquifer sand. Borden sand was selected because: (1) it is a natural environmental sample, (2) the sample is relatively uniform, and (3) the material has been well-characterized (Ball et al., 1990). Figure 2-10 shows the ln $N_m(\sigma)$ against ln σ. The σ value was estimated from the liquid density and normalized values. In addition to the experimentally measured results, the reported values for nitrogen, krypton, and EGME (Ball et al., 1990) are also shown. From this figure, it became evident that the $N_m(\sigma)$ for non-reactive nitrogen, krypton, and alkanes are smaller than the $N_m(\sigma)$ values for reactive water, EGME and benzene. Nitrogen, krypton, and EGME data were measured independently (Ball et al, 1990). The anomalous behavior of water was also noticed for KGa-1 result. The failure of the simple surface fractal theory suggests that at least one of the presumptions was not fully satisfied. First of all, it is likely that the reactive probes such as water see different surfaces, and the difference in $N_m(\sigma)$ cannot be explained solely from the projected surface area, σ, in terms of the fractal structure (see Fig. 2-6).

The emergence of such effect can be partly attributed to the existence of flexible sorbents such as organic matter and clays. This possibility was also suggested from the relatively high cation exchange capacity (CEC = 0.67 cmole(+)/kg) of the Borden aquifer material as a sand material. Although the organic carbon content of Borden aquifer material is less than 0.1 % (Ball et al., 1990), it is still possible that small amount of organic matter affect the sorption of

organic solutes. It should be noted, however, from the results that we cannot conclude that the partitioning is primarily responsible for this deviation from the expected behavior from simple surface fractal dimension. Quite interestingly, in this anhydrous system, polar organic probes seem to interact with Borden aquifer sand much strongly than the non-polar alkanes do. Therefore, the polarity of the solute, or possibly weak electrostatic or dipole-dipole interactions can be important for the sorption of organic vapor solutes in anhydrous, and possibly in non-aqueous, sorbent systems. On the other hand, in an aqueous environment, the polar organic molecules are hydrated, and the interaction of water with the surface masks the interaction of the polar solute with the sorbent. The anhydrated system and hydrated system are very different. Therefore, it is difficult to apply the theories of hydrophobic partitioning directly to the anhydrated system since there is no driving force, i.e. water, in the anhydrated system. In addition to the possibility of penetration into the sorbent structure, a significant number of water molecules are expected to hydrate the surface cation and be held strongly. From the generally high C values (Table 2-3), hysteresis effect or irreversible sorption are also suspected. Many effects such as irreversible sorption, energetic heterogeneity, and slow kinetics are also expected to be compounded. Therefore, it became extremely difficult to single out the cause of the deviation from the simple surface fractal theory.

From this investigation, it was found that the surface fractal theory appears to be applicable to geometrically complex, yet still simple sorbents such as

kaolinite and silica-gel. However, real sorption processes by a natural soil material are even more complex than adsorption processes onto kaolinite and silica-gel. Real natural sorbents consist of various organic and inorganic components which have different geometrical and energetic heterogeneities. The sorption processes to natural sorbents cannot be modeled as covering geometrically complex, yet otherwise uniform rigid surface uniformly with spherical/disc-like probes. Each probe interacts with a sorbent in specific way, and even the monolayer value itself may be ill-defined or affected by the physicochemical character of the probe molecule other in addition to the probe size effect. Consequently, the domain where the sorption processes take place may markedly different from probe to probe. Although we cannot reject the hypothesis that Borden sand is a fractal object based on this experiment, it became clear that the sorption phenomena by Borden sand or any complex sorbents may not be solely explained in terms of fractal structure. To investigate the geometrical features of complex sorbent, therefore, alternative methods (e.g. SAXS) should be utilized.

Conclusions

Surfaces of well-crystallized kaolinite (KGa-1) and silica-gel (SYLOID 244) were explored with H_2O, N_2, benzene, p-xylene, n-hexane, and n-octane molecules to investigate the geometrical heterogeneity of the surfaces. From the monolayer value, N_m, estimated from the classical B.E.T. equation, and the projected surface areas of probe molecules, σ, the dependence of N_m values on the probe molecule

size was investigated. The relationship between the monolayer value, N_m, and the projected molecular surface area, σ, is well described by the power law, $N_m \propto \sigma^{-D/2}$, which is consistent with the fractal theory.

The obtained surface fractal dimensions were about 2.18 ± 0.09 and 2.56 ± 0.26 for kaolinite and silica-gel, respectively. These values were in good agreement with the expected roughness of the surfaces from the knowledge of molecular level surface structures as well as the literature values of the surface fractal dimensions for these sorbents. The uncertainty around the estimated surface fractal dimension is partly originated from the fact that a surface fractal dimension is merely a statistical measure of the average geometrical complexity of a real surface. In addition, the experimental uncertainty of ± 10 % should be generally reckoned about the surface fractal dimension estimated with the monolayer coverage method. This experimental uncertainty is attributed to: (1) the difficulty of accurately estimating the monolayer value, $N_m(\sigma)$, due to the complex nature of adsorption processes (formation of multi-layer, energetic heterogeneity effect, hysteresis, kinetic constraints, irreversibility, etc.); and (2) the uncertainty associated with the estimate of the projected molecular area, σ, at the monolayer condition.

The same procedure was also applied to sorption processes by a natural sandy aquifer material. The Borden aquifer material appears to be physically and chemically rather simple as a soil material. However, the sorption processes seemed to be much complex, and the sorption behavior could not be captured

from the simple fractal logic based solely on the probe size dependence of the sorption behavior at the operationally defined monolayer coverage. The results indicated that the each probe molecule could be interacting with the sorbent in quite different manner depending on the physicochemical character of the probe, and even the monolayer value, thus the specific surface area, may be ill-defined or operationally defined. Furthermore, the energetic heterogeneity, hysteresis effect, kinetic constraints, irreversible sorption make the probe-sorbent interactions compounded and even more complex.

This study showed that the idea of fractal dimension was a good conceptual guideline to the description of the complex natural geometry. This is a significant step toward the understanding of sorption processes since the geometrical heterogeneity has been often neglected in the past. As an experimental measurement technique, the monolayer coverage technique should be considered as "semi-quantitative" due to the experimental uncertainty on the estimated surface fractal dimension. Toward the better understanding of complex natural sorbents, therefore, the development of better measurement technique and the simultaneous characterizations with various techniques are desired.

CHAPTER 3

TRANSPORT PROCESSES IN HETEROGENEOUS POROUS MEDIA

Introduction

In Chapter 2, we investigated the macroscopic manifestation of the molecular level heterogeneity as measured by sorption phenomena. From the results of the experiments, it is evident that the surfaces of the natural materials have both geometrical as well as energetic heterogeneities at various scales. Recent investigations have also revealed that the pores of geological materials generally exhibit similar scaling properties of heterogeneity. For example, Tyler and Wheatcraft (1990), and Rieu and Sposito (1991) have proposed fractal-like pore geometry. There are a considerable number of findings that the patterns of river flows or shapes of mountain can be also modeled with fractals. Such discoveries generally lead to the conclusion that the natural objects generally have various degrees of heterogeneities over the spatial scales. Fractals are the special case of such heterogeneous structure which have the same degree and type of heterogeneity at all scales.

With the social attention to the environmental problems associated with groundwater quality, there is a need for establishing comprehensive understanding

and predictive capabilities of the fate and transport of pollutants, especially toxic organic chemicals, in complex natural porous media.

Let us generalize the problems of transport phenomena in heterogeneous media. Any modeling attempt of transport phenomena may be cast in the mathematical operator form. The objective is, given the initial condition of the material of interest, ξ_i, to predict the future distribution of the material, ξ_f, given the mechanisms of the transport and the boundary conditions. This is a mapping process

$$\Xi \xi_i = \xi_f \tag{3-1}$$

where Ξ is the operator (transport operator) which maps the initial distribution ξ_i, to the distribution at the later time, ξ_f (Fig. 3-1).

For any dynamic systems, the following three criteria (conservation laws) have to be incorporated into the transport operator, Ξ;

1. mass balance
2. energy balance
3. momentum balance

A set of conservation equations

$$\frac{\partial A}{\partial t} = -\nabla \cdot J_A \tag{3-2}$$

where "A" (e.g. mass of a chemical species) is the variable of interest whose quantity is to be conserved, J_A is the flux of this mass. A flux is often proportional to the gradient of a potential (thermodynamic intensive parameters) as

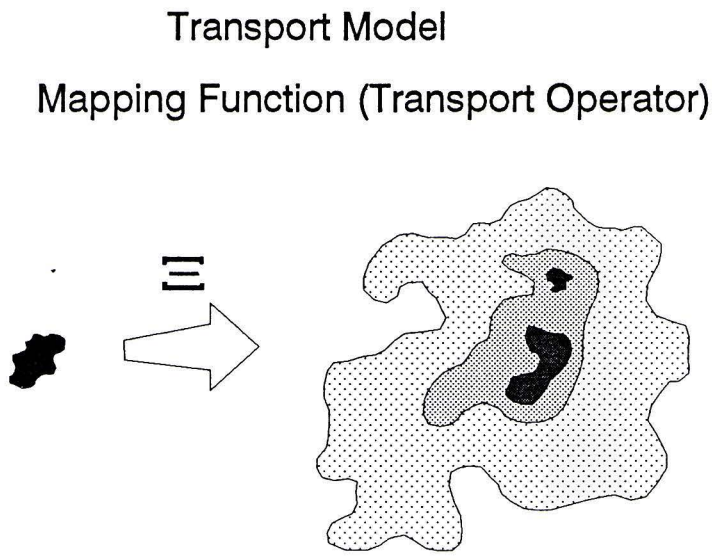

Fig. 3-1. Transport process as a mapping in time. Ξ is the transport operator for ξ.

$$J_A = - K \nabla B \qquad (3\text{-}3)$$

where "K" is the conductivity tensor of the variable "A", and "B" is the relevant potential. This type of flux equation is generally known as the constitutive law. Numerous examples of constitutive laws are known. For example, Fick's law of diffusion relates the diffusional flux to a diffusion constant and a gradient of concentration (chemical potential). A flux of heat is given by the product of a thermal conductivity and a gradient of temperature. Darcy's law, which explains the flux of water in porous media as the product of a hydraulic conductivity and a gradient of water potential, also belongs to the constitutive equation.

It is important to remember that the constitutive equation cannot be applied at any length scale. For example, a porous medium at grain scale may be inhomogeneous since there is a volume where grain exists, and a volume occupied by pore. Therefore, at grain scale, the conductivity changes extremely from a place to place. Thus the idea of "representative elementary volume (REV)" has to be introduced. REV is the volume at which the small scale inhomogeneity is averaged out. At such scale, parameters such as the conductivity are slowly varying in space, and a constitutive equation becomes a reasonable approximation of the actual flux. It is quite interesting to notice that the concept of REV is somewhat contradictory to the concept of fractal. In fractal, the heterogeneity exists at any length scale.

Conservation laws and the constitutive laws are generally coupled, and yield a set of equations. The Navier-Stokes type equation is of this type. The coupling

of water (mass) conservation equation and Darcy's law (a constitutive equation for water flux in porous media) gives Richards' equation. Richards' equation has been widely used by hydrologists to solve the problems of groundwater flow.

Applications of these formulations seem to be quite successful for homogeneous media. However, for heterogeneous porous media, a number of difficulties have been realized. For example, Richards' equation is a non-linear partial differential equation, and the non-linear, hysteric relationship between the mass of water (water content), water potentials, and the hydraulic conductivity makes this equation difficult to solve. In addition, real natural porous media often have complex initial and boundary conditions. Therefore, just solving these partial differential equations is a challenging task. The cellular automata method, which represents the continuous space and time in discrete manner, has proved to be a good alternative approach to the formulation of differential equations, and has been applied to the fluid flow problems in porous media (Wolfram, 1986; Rothman, 1988).

At this point, let us closely focus on the problems of solute transport processes assuming that we have a good handle on the overall fluid (water) transport. Before we accept this assumption, we should realize that the overall fluid flow determines the solute transport processes because it is the fluid which generally "carries" the solutes. First of all, the average location of solute is roughly determined by the average fluid (water) velocity and the interaction (sorption) of the solute with the porous media. The spreading characteristics of solutes

(dispersion) are dictated by the hydrodynamics dispersion (dispersion due to the differences in local fluid flow). Nevertheless, we will consider the solute transport process, and not the fluid transport per se because: (1) Solutes consist of an insignificant part of dynamic system. Therefore, the solute mass balance is the primary concern for solute transport. On the other hand, for fluid transport, the overall force balance has to be considered; (2) We are interested in how solutes (e.g. toxic chemicals or nutrients) move in porous media.

The following discussions on solute transport phenomena in heterogeneous porous media are developed upon the knowledge and understanding of fluid flow in porous media (This view is common among numerous solute transport models in which the average water flux and the dispersion coefficient are assumed to be known or measurable). In particular, we will mainly focus on the solute transport processes under the condition that the parameters of fluid flow (average flux, dispersivity, etc.) are spatially variable but close to being time-invariant (steady-state). Furthermore, most of the simulations conducted in this chapter do not have strong local convective flux (drift). This condition is imposed because, at least, we have a good handle on the local diffusional transport which generally produces a Gaussian-type local spreading pattern. On the other hand, the situation when a rapid flow of liquid suddenly encounters a low permeability region has to be studied more. The following discussion will demonstrate that the conceptual models are, however, focused on general solute transport processes in wide length scale range which spans from transport inside sorbed phase (in the order

of μm-mm scale, called mesoscopic) to solute transport with groundwater at field scale (m - km range).

Heterogeneity

We will consider the transport operator for the solute, Ω,

$$\Omega \phi_i = \phi_f \tag{3-4}$$

which describes the evolution of the distribution of solute from its initial state, ϕ_i, to its later state, ϕ_f. Therefore, our task is to find or approximate the solute transport operator, Ω, which is pertinent to the boundary conditions. Even when the solute transport operator, Ω, is not strongly dependent on the time, the spatial heterogeneity of the medium makes the prediction of solute transport processes nontrivial.

The governing solute transport equation can be, in principle, developed by combining the mass conservation equation with an appropriate equation for flux (e.g. a constitutive equation for the solute flux). However, to solve such equation in heterogeneous environment, the spatial and temporal distributions of the conductivities and the relevant potentials have to be known. For example, the distribution of diffusion coefficients has to be known for a problem of a diffusion in heterogeneous environment. To predict the solute transport in an aquifer, the average local groundwater velocity, and the local hydrodynamic dispersion parameters (2nd moment (dispersivity) and higher moments) are required. However, these variables are difficult to measure in real-life situations. First of all,

the measurements of these parameters can be economically very costly. Secondly, the measurements often require a destruction or disturbance of the system (e.g. taking a sample). Thirdly, the underlying assumptions (e.g. REV assumption) may not be true. For example, it is well recognized that under near-water-saturation condition, small root channels, worm holes, or cracks in a low hydraulic conductivity matrix (clay) can markedly influence the overall property of hydraulic conductivity. This phenomenon is known as "preferential flow" which leads to so-called "macro-dispersion" phenomena. The question is, "At which scale should the REV be taken?", or "if the heterogeneity effect is not averaged out at the scale of interest, then what do we do?"

In this chapter, we will re-examine the fundamental concepts of transport processes. The main goal of the chapter is the development of conceptual framework to describe the transport processes in heterogeneous media. There are three rather distinctive, yet very closely related, approaches to transport processes based on the following types of equations: 1) the Forward/Backward Kolmogorov equation, 2) the Langevin equation, and 3) Chapman-Kolmogorov equation. The Convective-Dispersive equation (CDE) is closely related to Fokker-Planck equation which belongs to the (Forward) Kolmogorov equation category (Mortensen, 1969; Serra et al., 1986).

CDE type equations are by far the most widely used by hydrologists. However, the application of the CDE type partial differential equation to heterogeneous porous media with complex boundary conditions is often

mathematically very difficult. As effective alternative strategies for the modeling of the transport processes in heterogeneous media, the other methods are attractive.

The main objectives of this chapter are:

1) Introduction to the fundamental concepts of the Langevin equation and Chapman-Kolmogorov based theories.
2) Clarification of the connection between the different conceptual approaches to solute transport phenomena.
3) Application of the discrete Markov chain model to the solute transport in heterogeneous media.

These transport theories are conceptual, and can be applied, in principle, to any scale of transport processes. As an example of application, we will simulate the desorption kinetics process from the view point of mesoscopic diffusion in energetically and geometrically heterogeneous media. Besides the importance of sorption/desorption non-equilibrium in large scale transport processes, this simulation is also directly pertinent to the desorption experiments conducted in Chapter 2.

Stochastic Representation

In this section, we will briefly review the basic theories of probability and stochastic processes which are pertinent to the solute transport modeling. Before

we begin, it is very important to understand the meaning of the probability. Failure to do so will result in confusion of the differences among the mass balance equation, stochastic transport equations as will be introduced in this chapter, and the stochastic theories applied to the mass balance equation (Chu and Sposito, 1980; Sposito et al., 1983). Roughly speaking, the stochastic transport theories discussed in this chapter govern the transport of a specified mass, namely the probability of finding the specified mass at given coordinate at given time. On the contrary, in mass balance equations, we are interested in the change in any mass at particular point in space and time. Therefore, the mass can enter and leave the system in mass balance equation. In stochastic transport equations considered here, the motion of particle is usually represented by two types of probabilities.

One type is called the first order or state probability density, $p[X(t=t)=x_j]$, which is the probability of finding the solute particle at x_j at time t. It should be very clear, however, that this probability does not mean the probability of finding any solute particle at X_j at time t. The first order probability in the stochastic transport equation generally describes: given the particle(s) were located at some location at time t, what is the probability of finding it (them) in the future (or may be in the past). Therefore, the mass associated with the equation (the system) is fixed. This is quite different from the mass balance formulation. The derivation of the mass balance equation from the probability balance equation will be discussed briefly later. However, the probability balance equation may be considered as a mass balance equation with Dirac (instantaneous) input function whose total mass is

normalized to unity. Therefore, by combining an appropriate mass and Dirac delta function, the mass balance equation can be recovered from probability balance equation.

The details of the local transport dynamics are incorporated into the other type of probability known as the transition probability density, $p[X(t=t)=x_j \mid X(t=t-1)=x_i, X(t=t-2)=x_h, \ldots]$. This is the probability associated with the movement of the particle from location x_i at $t=t-1$ to location x_j at $t=t$ given the history of the particle (memory) for time $t \leq t-1$. While the first order probability is a probability at a particular time, the transition probability connects these events which occur at different times. The theories of stochastic transport processes are concerned with the properties and the governing equations of these probabilities. In particular, Fokker-Planck type equation, Langevin type equation, and Chapman-Kolmogorov or the master equation will be discussed as the three general approaches to the solute transport models in porous media.

While the probability balance in the stochastic transport equation is not quite equivalent to the mass balance in the mass balance equation, as long as the meaning of the probability and the mass associated with the description are clear, they can describe the same transport processes.

Non-linear Langevin Equation Type Approach

In this section, the approach based on the non-linear Langevin equation will be presented. We will consider an equation of Langevin type

$$\frac{dx(t)}{dt} = f(x,t) + g(x,t)I(t) \qquad (3\text{-}5)$$

as the representative model. This is a first order stochastic differential equation. The meanings of the parameters x, f(x,t), g(x,t), and I(t) are yet to be discussed. At this point, we realize that this equation has both the deterministic part, f(x), as well as the stochastic part, g(x,t)I(t). The stochastic nature of the equation comes from the introduction of fluctuation (noise), I(t), which is in this case a Gaussian white noise. It is very important to identify what is fluctuating in the equation because similar, but physically incorrect, equation can also be formulated. For example, to model Brownian motion, the following form of the Langevin equation

$$\frac{dv(t)}{dt} = -\gamma v(t) + G(v,t)I(t) \qquad (3\text{-}6)$$

(where v(t) is the velocity, γ is the viscosity of the medium, and G(v,t) is the diffusion coefficient) was historically developed first. The mathematical form of the equation (3-6) is similar to the equation (3-5). However, the equation (3-6) represents the fluctuation of the force which cause the fluctuations of the velocity. This idea is originated from the Newton's law of dynamics. For Brownian motion, therefore, the displacement of the particle, x(t), can be solved by

$$x(t) = x(0) + \int_0^t v(t')dt' \qquad (3\text{-}7)$$

where v(t) is obtained from the solution of Langevin equation with fluctuating force. On the other hand, to model transport of solute, it is also possible to assume that

the fluctuation of the local velocity causes the fluctuation of the location of the fluid particle (Durbin, 1983). We choose variables in the equation (3-5) so that f(x,t) is related to the mean particle velocity or the first moment and the g(x,t)I(x,t) explains the spreading around this mean particle velocity, i.e., dispersion which involves the second and the higher moments of the statistics of the motion of the particle. Roughly speaking, the mean particle velocity part and the dispersion part are considered to be the deterministic and stochastic in nature, respectively. Such choices of variables are in fact naive since no physical justification is given. In particular, much detailed observation is needed to conclude that the displacement of the particle can be modeled as Markovian process. Therefore, we treat this non-linear Langevin equation as a trial model.

However, the importance of this choice of variables comes from the possible connection between the Lagrangian and Eulerian formulation. So far we have seen that the Langevin type approach deals with the motion of each particle. On the other hand, the convective dispersive equation (CDE) or Fokker-Planck equation expresses the transport process as the concentration or probability of finding the solute particle at a particular location and time, which is an Eulerian formulation. It is, thus, desired to relate these two distinct formulations. For a uniform medium, this linear Langevin model (g(x) in equation (3-5) is constant) produces a Fokker-Planck (forward Kolmogorov) equation which is mathematically closely related with CDE. However, the extension of CDE type equation to heterogeneous system is indeed dubious since the applicability of constitutive equation (the dispersive flux

$$\frac{\partial \theta(x,t)C(x,t)}{\partial t} = \frac{\partial}{\partial x} D(\theta,x,t) \frac{\partial C(x,t)}{\partial x} - \frac{\partial q(x,t)C(x,t)}{\partial x} \qquad (3\text{-}8)$$

equation) in heterogeneous media (the medium in which the spatial variation of the dispersion coefficient is considerable) is not certain. Therefore, the connection of the Fokker-Planck equation to the Lagrangian formulation is considered in this section. We start from the non-linear Langevin type equation (3-5). Then we attempt to establish the connection between the non-linear Langevin type stochastic differential equation and the Fokker-Planck equation for heterogeneous systems from Markovian statistics. Furthermore, we would like to point out the danger associated with the use of a non-linear Langevin equation which produces a pathological paradox (van Kampen, 1981b) as explained in the following section.

The main difficulty of stochastic modeling of real systems comes from the understanding of the nature of the fluctuation and its mathematical description, I(x). There are many different types of physical processes which produce such fluctuations. According to van Kampen (1981a), the source of the noise can be external or internal. The external means 1) the noise source is not influenced by the system itself; 2) there is a parameter which permits, in principle, to turn off the noise. The internal noise is due to the fact that the system itself consists of discrete particles. Therefore, collision between the molecules may be considered to be the internal noise. Like the Dirac delta function, we use idealized noise to approximate real world fluctuation. This noise is known as the Gaussian white noise and it satisfies the following conditions.

(i) $<I(t)> = 0$.

(ii) $<I(t_1)I(t_2)> = \delta(t_1-t_2)$.

(iii) Higher moments are given by the rules of the Gaussian processes (e.g. all odd moments vanish).

The first condition states that the mean is zero. The second condition indicates the delta correlated function, i.e., each event is independent of each other at the time scale of the interest. The process has very short memory which is related to the Markovian statistics. This function has a flat power spectrum, and may be viewed as a random sequence of small pulses, both positive and negative. Like the Dirac delta function, the Gaussian white noise is an idealized model for rapid fluctuation.

The integral of the I(t) is so called Wiener-Levy process, w(t)

$$w(t) = \int_0^t I(t')dt' \tag{3-9}$$

We write the equation (3-5) in the following form.

$$dx = f(x)dt + g(x)dw(t) \tag{3-10}$$

To obtain the time evolution of the x(t), we integrate over the time as

$$x(t) = x(0) + \int_0^t f(x)d\tau + \int_0^t g(x)dw(\tau) \tag{3-11}$$

(This equation is sometimes referred as the Ito equation (Bhattacharya et al., 1990)). Therefore, the displacement of the particle is expressed in terms of the location dependent average particle velocity, f(x), and the local particle dispersion,

g(x). Note this expression is related to a generalized random walk

$$x(t) = x(0) + \sum_{i=1}^{n(t)} x_i = x(0) + \sum_{i=1}^{n(t)} \xi(x)\beta \qquad (3\text{-}12)$$

in which the statistical mean of each random walk step, x_i, can be non-zero (due to the average flow or drift).

Now we are ready to integrate the equation which has a stochastic term. This integration is not as straight forward as an ordinary integration due to the stochastic nature of the variables which are generally non-differentiable. While the equation (3-5) appears to be a first-order differential equation, it is meaningless unless an interpretation is given.

The non-linear Langevin equation (equation (3-5)) is not a complete equation by itself, and this fact makes the modeling approach from equation (3-5) ambiguous. In mathematics, there are two well-known interpretations of stochastic integration, known as Ito and Stratonovich calculi. The bottom line is that depending on which formulation is taken, the resulting Fokker-Planck equation, which is the most familiar formulation of the transport equation, appears to be different. As long as f and g are not dependent on x, there is no complication. However, a paradox arises when the function g(x) is dependent on x (van Kampen, 1981b). Since the parameters for heterogeneous natural systems generally have dependence on x, so we cannot avoid this mathematical problems. From the mathematical point of view, both representations are self-consistent as long as they are interpreted correctly. However, which convention represents the true physics,

namely which stochastic calculi gives f(x) and g(x) consistent with the macroscopic observable, is another issue.

Ito Stochastic Integral

We consider a finite-difference approximation to the last part of the right hand side of equation (3-11). Ito interpreted the stochastic integration as follows.

$$\sum_{i=0}^{n-1} g(t_i)\ [w(t_{i+1}) - w(t_i)] \tag{3-13}$$

This convention was taken so that $\Delta w(t)$ is independent of w(t), and has mean zero and variance Δt. This convention is preferred in the sense

$$<\int_0^t g(t')dw(t')> \ = \ \sum_{k=1}^{n} <g(t_{k-1})><w(t_k) - w(t_{k-1})> \ = \ 0 \tag{3-14}$$

which is the desired property for the stochastic integral. The corresponding transition probability of the Markov process obeys the Fokker-Planck-Kolmogorov equation.

$$\frac{\partial P}{\partial t} \ = \ - \ \frac{\partial}{\partial x} f(x)P \ + \ \frac{1}{2}\frac{\partial^2}{\partial x^2} g(x)^2 P \tag{3-15}$$

The derivation of the Fokker-Planck equation consistent with the Ito's interpretation is as follows (Durbin, 1983)

Assume a Markov process. Since the probability density at time t is determined by the probability density at time t-dt and by the transition probability;

$$p(x,t) = \int^{\Omega dx} p(x-dx,t-dt)\,dp_T(dx;x-dx) \tag{3-16}$$

in which p(x,t) is the first order probability density and the $p_T(dx;x-dx)$ is the probability density associated with the transition from x-dx to x in time step dt.

Since we adopt the Ito's convention, for the expected values in unit time, $<dw(t)> = 0$, $<dw^2(t)> = dt$, and $<dw^n(t)> = O(dt)^{n/2}$ (O () means in the order of),

$$<dx(t)> = <f(x)dt + g(x)dw(t)> = f(x)dt \tag{3-17}$$

$$<dx^2(t)> = <[f(x)dt + g(x)dw(t)]^2> = g^2(x)dt + O(dt^2) \tag{3-18}$$

$$<dx^n(t)> = O(dt^{n/2}) \quad n > 2 \tag{3-19}$$

We expand the equation 3-18 in a Taylor series in dx and dt. Also

$$\int dp_T(dx;x) = 1 \tag{3-20}$$

$$\int (dx)^n dp_T(dx;x) = <(dx)^n>_x \tag{3-21}$$

$$\int (dx)^n \frac{\partial\, dp_T(dx;x)}{\partial x} = \frac{\partial}{\partial x}\int (dx)^n dp_T(dx;x) = \frac{\partial <(dx)^n>_x}{\partial x} \tag{3-22}$$

By substituting equations 3-21 and 3-22 into the expanded equation, and keeping the terms up to dt, we obtain

$$p(x,t) = p(x,t) - \langle dx\rangle \frac{\partial p(x,t)}{\partial x} + \frac{1}{2}\langle (dx)^2\rangle \frac{\partial^2 p(x,t)}{\partial x^2} - dt\frac{\partial p(x,t)}{\partial t}$$
$$-\frac{\partial \langle dx\rangle}{\partial x} p(x,t) + \frac{1}{2}\frac{\partial^2 \langle (dx)^2\rangle}{\partial x^2} p(x,t) + \frac{\partial \langle (dy)^2\rangle}{\partial x}\frac{\partial p(x,t)}{\partial x} + O(dt^2) \quad (3\text{-}23)$$
$$= p(x,t) + dt\left[\frac{1}{2}\frac{\partial^2 [f^2(x)p(x,t)]}{\partial x^2} - \frac{\partial p(x,t)}{\partial t} - \frac{\partial [g(x)p(x,t)]}{\partial x}\right] + O(dt^2)$$

Thus the resulting Fokker-Planck equation is

$$\frac{\partial p(x,t)}{\partial t} = \frac{1}{2}\frac{\partial^2 [f^2(x)p(x,t)]}{\partial x^2} - \frac{\partial [f(x)p(x,t)]}{\partial x} \quad (3\text{-}24)$$

Stratonovich Stochastic Integral

Stratonovich calculated the integral by taking the midpoint

$$\sum_{k=1}^{n-1} g\left(\frac{x(t_k)+x(t_{k+1})}{2}\right)\left[w(t_{k+1})-w(t_k)\right] \quad (3\text{-}25)$$

such definition leads to an integral that is symmetric in time, and consistent to the integral of ordinary calculus. This rule of the integration does not give zero expected value, but rather

$$\left\langle \int_0^t g(t')dw(t') \right\rangle = \frac{1}{2}\left\langle g(x)\frac{\partial g(x)}{\partial t}\right\rangle \neq 0 \quad (3\text{-}26)$$

The corresponding Fokker-Planck-Kolmogorov equation is

$$\frac{\partial P}{\partial t} = \frac{1}{2}\frac{\partial}{\partial x} g(x)\frac{\partial}{\partial x} g(x)P - \frac{\partial}{\partial x} f(x)P \quad (3\text{-}27)$$

The interrelation between the two integral equations are

$$x_s(t) = x_s(0) + \int_0^t [f(x_s(t')) + \frac{1}{2}g(x_s(t'))\frac{\partial g(x_s(t'))}{\partial x}]dt' + (I) \tag{3-28}$$

where the subscript s and (I) indicate the Stratonovich and Ito's conventions. As far as the mathematics is concerned, they are both self-consistent and correct. Because of the non-zero expected value in equation (3-26), Ito's integral is generally preferred by mathematicians.

However, Ito's calculus is not completely consistent with the ordinary differential calculus (Riemann calculus). For example, suppose we are interested in the non-linear transformation of a stochastic (Wiener) process.

From the chain rule, the total differential is

$$dF(w(t)) = \frac{dF(w(t))}{dw(t)}dw(t) \tag{3-29}$$

The use of this kind of calculus is permitted in Stratonovich convention. However, if Ito's stochastic is used, this becomes

$$dF(w(t)) = \frac{dF(w(t))}{dw(t)}dw(t) + \frac{1}{2}\frac{d^2F(w(t))}{dw(t)^2}dt \tag{3-30}$$

Therefore, once Ito's stochastic calculus is used, it should not be mixed with the ordinary calculus.

The Comparison of Fokker-Planck Equations

It is possible to rewrite the Stratonovich's Fokker-Planck equation as

$$\frac{\partial P}{\partial t} = -\frac{\partial}{\partial x}[f(x) + \frac{1}{2}g(x)\frac{dg(x)}{dx}]P + \frac{1}{2}\frac{\partial^2}{\partial x^2}g(x)^2P \qquad (3\text{-}31)$$

Therefore two formulations are almost identical except the first part of the right hand side of the equation. We can cast the Fokker-Planck equations to the conservation equation form. By denoting $g^2(x)/2 = K(x)$,

from Ito's convention

$$\frac{\partial P}{\partial t} = \frac{\partial}{\partial x}K(x)\frac{\partial P}{\partial x} - \frac{\partial}{\partial x}\left[\left(f(x) - \frac{\partial K(x)}{\partial x}\right)P\right] \qquad (3\text{-}32)$$

and from Stratonovich's convention

$$\frac{\partial P}{\partial t} = \frac{\partial}{\partial x}K(x)\frac{\partial P}{\partial x} - \frac{\partial}{\partial x}\left[\left(f(x) - \frac{1}{2}g(x)\frac{\partial g(x)}{\partial x}\right)P\right] \qquad (3\text{-}33)$$

Therefore the velocity terms (Eulerian velocity) are different. The difference is sometimes called "spurious" or "noise induced" flow. If the medium is homogeneous, the difference between the two formulations disappears. The question is "which one of these two equations is the correct interpretation of the actual physical process ?". Or is any of these equations physically correct ? Unfortunately, no answer has yet been given in the hydrology literature, and further work is needed. However, it is worth noticing that no real fluctuation is strictly a white noise Markovian process. In reality, any natural fluctuation has a finite

correlation time. Since the introduction of Ito's convention is motivated by the mathematical strictness to idealized white noise, sometimes, the Stratonovich approach is preferred by physicists to model real systems (van Kampen, 1981a). Even then, there is no reason to prove any of these equation is indeed physically correct. In the end, it has to be emphasized again that the non-linear Langevin equation should be considered as a pre-equation which requires an interpretation to apply to solute transport modeling. While the non-linear Langevin equation can be integrated, how we integrate it becomes a physics question rather than a mathematical question; i.e. what type of integration method is consistent with the laws of physics. According to van Kampen, Chapman-Kolmogorov and the master equations are the equations which make sense in non-linear space, and the use of the non-linear Langevin equation or Fokker-Planck equation has to be denounced. Many detailed studies of fluid flow and solute transport processes in heterogeneous porous media are needed to understand the real natural systems.

The Dispersion Coefficient in Heterogeneous Environments

This mathematical paradox casts a question of the validity of CDE applied to heterogeneous media. The CDE is the most widely accepted equation among hydrologists, and is derived from the mass balance in a representative control volume. It is a second order partial differential equation:

$$\frac{\partial \theta C}{\partial t} = \frac{\partial}{\partial x} D\theta \frac{\partial C}{\partial x} - \frac{\partial}{\partial x} qC \qquad (3\text{-}34)$$

where C is the solute (non-reactive) concentration, x is the spatial coordinate, D is the dispersion coefficient, θ is the water content, and q is the water flux.

The general derivation is as follows;

From the mass balance consideration

$$\frac{\partial M}{\partial t} = \frac{\partial \theta C}{\partial t} = -\nabla \cdot J_M \qquad (3\text{-}35)$$

where M is the solute mass, J_M is the flux of solute.

The flux of the mass is defined as

$$J_M = -\theta(x,t)D(\theta,x)\nabla C + q(x,t)C \qquad (3\text{-}36)$$

in which the flux consists of the local dispersive and convective flux. By combining these equations, the CDE is derived. It is well-established that this equation does describe real solute transport process as long as the medium is homogeneous. However, the parameters such as D and q can be highly spatially dependent in heterogeneous environment.

The semi-variogram of such medium generally increases with the distance without reaching to a sill at (semi-variogram becomes independent of the distance because there is no correlation between the two points separated by the given distance) at the length scale of interest. Then, when the local dispersion coefficient, D(x), is strongly spatially variable, should the D(x) be outside of ∇ operator or should it be inside as given in equation (3-34)? Is there a convective flux induced

by the heterogeneity of the system? Initially, I thought I was not understanding the meaning of CDE correctly, and the derivation from Fick's first and second law type argument as given in equations (3-39, 3-40) was indeed the correct interpretation of the physics of solute transport. However, I found a similar, and very interesting discussion in van Kampen's book (1981a), in which the author discusses which of the

$$\frac{\partial \rho(x,t)}{\partial t} = \frac{\partial^2}{\partial x^2} D(x) \rho(x,t) \tag{3-37}$$

$$\frac{\partial \rho(x,t)}{\partial t} = \frac{\partial}{\partial x} D(x) \frac{\partial}{\partial x} \rho(x,t) \tag{3-38}$$

is the correct form of the diffusion equation in heterogeneous medium.

From the Fick's law, it is obvious that the equation (3-42) is the correct formula since,

$$J = -D \frac{\partial}{\partial x} \rho \tag{3-39}$$

$$\frac{\partial \rho}{\partial t} = - \frac{\partial J}{\partial x} \tag{3-40}$$

However, the author says this argument is not decisive. To find out if equation (3-38) is indeed the correct diffusion equation or not, the underlying mechanism is modeled, and Ω expansion is carried out. According to the author, one cannot make an a priori choice without examining the underlying mechanism. Then, is the CDE correct? Moreover, if we have made any logical mistake in deriving equation

(3-34) or if we have relied on any improper logic, I would like to know what was wrong even if equation (3-34) happens to be the correct interpretation in the case of diffusion in heterogeneous environment. From these confusions I had, Chapman-Kolmogorov based approaches will be considered next.

Chapman-Kolmogorov Equation Type Approach

In the previous section, we attempted to derive the Fokker-Planck equation from the Langevin equation in which the local transport process is described with both convective as well as dispersive motions. In this section, we attempt to re-establish our conceptual connection between the local and macro-scale solute transport process through a stochastic equation known as the Chapman-Kolmogorov equation.

The Chapman-Kolmogorov Equation and The Markovian Statistics (van Kampen, 1981a; Serra et al., 1986; Papoulis, 1991)

The importance of the particle's history is now of concern (Fig. 3-2). The particle's history is dependent on the nature of the transport mechanisms, and the time/spatial scale of interest. In this model, we assume that the motion of the solute particle has a very short memory compared to the respective motion at the local scale. This process is known as the Markov process. In reality, no natural fluctuation phenomenon is Markovian. Non-Markovian models may be developed; however, the Markovian process assumption offers a good approximation of the

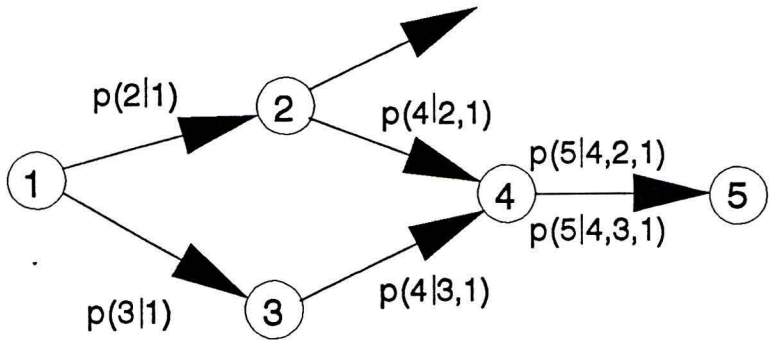

Fig. 3-2. The motion of a particle in discrete time/space expressed in terms of the transition probability densities. The numbers, 1,2,.. indicates the location of the particle. For a Markov process $p(5|4,2,1) = p(5|4,3,1)$. However this equality does not hold for non-Markovian process because the history of the particle is not independent of the transition from 4 to 5.

fluctuation phenomena with relatively short correlation time, and simplifies the transport equation significantly.

Markov Process

A Markov process is a stochastic process whose past has no influence on the future. When the time scale of interest is much longer than the underlying fluctuation time scale (or correlation time), the process may be considered as Markovian.

A Markov process is defined as, for $t \leq t_n$,

$$p[X(t_n)=x_i \mid X(t),t\leq t_{n-1}] = p[X(t_n)=x_i \mid X(t_{n-1})] \tag{3-41}$$

where p[a|b] is the conditional probability for a given b. The probabilities are defined as the density functions rather than the cumulative distribution functions. Equation 3-45 infers that the stochastic process at $t=t_n$ is completely determined by the state at $t=t_{n-1}$ which is the time right before t_n. Therefore, for a discrete-time process

$$p[X(t_n)=x_n \mid X(t_{n-1}),\cdots X(t_1)] = p[X(t_n)=x_n \mid X(t_{n-1})] \tag{3-42}$$

According to Papoulis (1991), the general properties of the Markov process are as follows:

(1) If we denote $X(t_n)=x_n$ as X_n, then

$$p(X_n|X_{n-1},\cdots X_1) = p(X_n|X_{n-1}) \tag{3-43}$$

Applying the chain rule gives

$$p(X_n,\cdots X_1) = p(X_n|X_{n-1})p(X_{n-1}|X_{n-2})\cdots p(X_2|X_1)p(X_1) \qquad (3\text{-}44)$$

where the last p.d.f. is a first order density.

(2) For the mathematical expectation

$$E[X_n|X_{n-1},\cdots X_1] = E[X_n|X_{n-1}] \qquad (3\text{-}45)$$

where E[] is the expected value.

(3) If the present is specified, then the past is independent of the future in the sense for $k<m<n$,

$$p(X_n,X_k|X_m) = p(X_n|X_m)p(X_k|X_m) \qquad (3\text{-}46)$$

The Chapman-Kolmogorov Equation

The probability associated with the transition beyond the one step process is formulated with the Chapman-Kolmogorov equation. For a Markov process, it states that the conditional density $p(X_n | X_k)$ can be expressed in terms of $p(X_n | X_m)$ and $p(X_m | X_k)$ for any $n>m>k$;

$$p(X_n \mid X_k) = \int_{-\infty}^{\infty} p(X_n \mid X_m) p(X_m \mid X_k) dX_m \qquad (3\text{-}47)$$

The integral is over the entire possible intermediate paths. Under the Markovian assumption, the transition probability $p(X_n|X_m)$ is independent of the transition probability $p(X_m|X_k)$. Each transition probability represents the transport of the solute particle in a short time interval as governed by the local scale physics law and the local boundary conditions. However, by applying the Chapman-Kolmogorov equation numerous times, in principle it is possible to predict the behavior of the system in large time/space scale. If we take time $k=0$, then the left hand side of the equation can be interpreted as follows: the probability of finding the solute particle at location x_n at $t=t_n$ given the initial location $x(t=0)$. This is the solution to the solute transport equation as expressed by the transition probability with given initial condition. The state probability density, namely the probability of finding the particle at X_n at $t=t_n$, is then calculated as

$$p(X_n) = \int_{-\infty}^{\infty} p(X_n \mid X_o) p(X_o)\ dX_o \qquad (3\text{-}48)$$

Clearly the state probability is related to the volume based concentration. The Chapman-Kolmogorov equation and its differential form equation known as the master equation are widely used in physics (van Kampen, 1981a). At least in non-linear heterogeneous space, the Chapman-Kolmogorov equation is considered to be the fundamental and preferred interpretation over a non-linear Langevin

representation or its Fokker-Planck counter part (see, van Kampen, 1981a). We make use of the Chapman-Kolmogorov equation in discrete form to approximate the continuous solute transport processes.

The Master Equation and Fokker-Planck Equation (van Kampen, 1981a)

The master equation is the differential version of the Chapman-Kolmogorov equation. For the first order probability of stationary Markov process,

$$\frac{\partial}{\partial t}p(x,t) = \int W(x|x')p(x',t) - W(x'|x)p(x,t)dx' \qquad (3\text{-}49)$$

where W(x x') is the transition probability per unit time from x' to x. Like the mass balance, this equation may be considered as the probability balance equation: the change in the probability of finding the particle at location x at time t is the difference of the probability coming in (the firs term) and the probability leaving out (the second term). It is possible to derive the Fokker-Planck equation as the approximation of the master equation as follows. Let's represent the transition probability W as a function of the size r of the jump and of the starting point:

$$W(x|x') = W(x'; r) \qquad r = x-x' \qquad (3\text{-}50)$$

The master equation is now written as

$$\frac{\partial\, p(x,t)}{\partial\, t} = \int W(x-r;\, r)\; p(x-r,t)\; dr - p(x,t) \int W(x;\, -r)\; dr \qquad (3\text{-}51)$$

Let assume that W(x'; r) is a sharply peaked function of r and it varies slowly with x'.

This may be stated that there exists r_δ such that

$$W(x'; r) \approx 0 \qquad for\ |r| > r_\delta \tag{3-52}$$

$$W(x'+\Delta x; r) \approx W(x'; r) \qquad for\ |\Delta x| < r_\delta \tag{3-53}$$

The second assumption is that the solution p(x,t) also varies slowly with x. It is then possible to expand the first integral in Taylor series up to the second order

$$\begin{aligned} \frac{\partial p(x,t)}{\partial t} &= \int W(x;r)p(x,t)dx - \int r\frac{\partial}{\partial x}[W(x;r)p(x,t)]dr \\ &+ \frac{1}{2}\int r^2 \frac{\partial^2}{\partial x^2}[W(x;r)p(x,t)]dr - p(x,t)\int W(x;-r)dr \end{aligned} \tag{3-54}$$

The first and the last terms cancel each other. Define the moments

$$a_v(x) = \int r^v W(x;r)\, dr \tag{3-55}$$

Then the result is

$$\frac{\partial p(x,t)}{\partial t} = -\frac{\partial}{\partial x}[a_1(x)p(x,t)] + \frac{1}{2}\frac{\partial^2}{\partial x^2}[a_2(x)p(x,t)] \tag{3-56}$$

which is the Fokker-Planck equation. This derivation showed that the Chapman-Kolmogorov equation, the master equation, and the Fokker-Planck equation are also closely related. In fact, it is possible to include all terms of the Taylor expansion as

$$\frac{\partial p(x,t)}{\partial t} = \sum_{v=1}^{\infty} \frac{(-1)^v}{v!}\left(\frac{\partial}{\partial x}\right)^v [a_v(x)p(x,t)] \tag{3-57}$$

which is known as the Kramers-Moyal expansion. Therefore, the Fokker-Planck equation derived in this subsection is a special case of the Kramers-Moyal

expansion where the all terms higher than v=2 are negligible. In real physical system, especially in heterogeneous media, however, this is not true.

Discrete-time Markov Chain

To simplify the structure of the model, we approximate the transport process as a series of events which occurs at a certain time interval. A discrete-time Markov chain is a Markov process X_n having a countable number of states, x_i. A Markov chain is specified in terms of its state probabilities

$$p_i[n] = P[X_n=x_i] \tag{3-58}$$

and the transition probability

$$\Pi_{ij}[n_1,n_2] = P[X_{n2}=x_j \mid X_{n1}=x_i] \tag{3-59}$$

Also note

$$\sum_j \Pi_{ij}[n_1,n_2] = 1 \tag{3-60}$$

$$\sum_i p_i[k]\Pi_{ij}[k,n] = p_j[n] = P[X_n=x_j] \tag{3-61}$$

The last equation means that the probability of finding the solute particle at x_j at time step n can be calculated from the first order densities at a previous time step k, and the second order transition probability density to x_j from any coordinate in space. The transition probability density serves as the mapping function from the previous time step to the next time step. In the continuous-time Markov chain

model (Knighton and Wagnet, 1987; Papoulis, 1991), the time derivative, i.e. the rate of such transition probability, is used. However, the discrete-time Markov chain is adopted here simply because it is even easier to comprehend. For time steps $n_1 < n_2 < n_3$, the discrete Chapman-Kolmogorov equation becomes

$$\Pi_{ij}[n_1,n_3] = \sum_r \Pi_{ir}[n_1,n_2]\Pi_{rj}[n_2,n_3] \qquad (3\text{-}62)$$

This equation states that the transition probability for going from x_i at n_1 to x_j at n_3 can be calculated from the probabilities for transition from x_i at n_1 to x_r at n_2 and the transition from x_r at n_2 to x_j at n_3.

Homogeneous Process

If the process X_n is stationary in time, then the function $p(X_n)$ and $p(X_n | X_{n-1})$ are invariant to a shift of the origin in time. In this case, the statistics of X_n are completely determined in terms of the second order density, $p(X_1,X_2)=p(X_2 | X_1)p(X_1)$. A Markov process X_n is called "homogeneous" if the conditional density $p(X_n | X_{n-1})$ is invariant to a shift of the origin, but the 1st order density $p(X_n)$ might depend on n. Solute transport under steady state groundwater flux conditions may be modeled as a homogeneous process.

If the process X_n is homogeneous, then the transition probability depends only on the difference $m=n_2-n_1$. Thus,

$$\Pi_{ij}[m] = P[X_{n+m}=x_j \mid X_n=x_i] = \Pi_{ij}[n_2,n_1] \qquad (3\text{-}63)$$

Setting $n_2-n_1=k$, $n_3-n_1=n$, the discrete Chapman-Kolmogorov equation is

$$\Pi_{ij}[n+k] = \sum_r \Pi_{ir}[k]\Pi_{rj}[n] \tag{3-64}$$

for a finite-state Markov chain, this can be written in matrix form

$$\Pi[n+k] = \Pi[n]\ \Pi[k] \tag{3-65}$$

where $\prod[n]$ is a Markov matrix with elements $\prod_{ij}[n]$.

$$\Pi[n] = \Pi^n \ ; \ \Pi = \Pi[1] \tag{3-66}$$

$$\Pi = \begin{bmatrix} \Pi_{11} \cdot \cdot \Pi_{1N} \\ \cdot \cdot \cdot \\ \cdot \cdot \cdot \\ \Pi_{N1} \cdot \cdot \Pi_{NN} \end{bmatrix} \tag{3-67}$$

Then

$$P[n] = P[n-k]\Pi^k = P[0]\Pi^n \tag{3-68}$$

where P[n] is a matrix whose elements are $p_j[n]=P[X_n=x_j]$, and P[0] is the initial state row matrix (vector). This matrix may be solved for $p_j[n]$s which are the probabilities of finding the solute particle at x_j at time step n. Therefore, the concentration distribution of the solute particle after n time step, P[n], for a given initial distribution, P[0], is solved if the transition probability density matrix, Π, is known. For steady state solute transport problem, $P[1]=P[2]=....=P[n]=P$. Then $P\prod=P$ is solved for p_j which is an eigen vector of its transition matrix with the eigen value equals one.

Transient Process

If the parameters are time-dependent and non-homogeneous, e.g. transient water flow, the transition probability density matrix becomes time dependent. In this case, we cannot take the power of the transition probability density matrix. Instead, the transition probability density is evaluated at each time as

$$P[n] = P[0]\Pi[0,1]\Pi[1,2]\cdot\Pi[n-1,n] = P[0]\prod_{i+1}^{n}\Pi[i-1,i] \qquad (3\text{-}69)$$

Clearly the first multiplication $p[0]\Pi[0,1]$ yields the distribution of the solute at t=1. The next multiplication $p[0]\Pi[0,1]\Pi[1,2] = p[1]\Pi[1,2]$ is the estimate of the distribution at t=2 from the distribution at t=1, and the transition probability from t=1 to t=2.

The Relationship Between Discrete Markov Chain And Finite Difference Approximation

Let's consider the finite difference approximation of the following equation

$$\frac{\partial P}{\partial t} = A\frac{\partial^2 P}{\partial x^2} - B\frac{\partial P}{\partial x} \qquad (3\text{-}70)$$

Please note that this equation is a probability balance equation, and not mass balance equation. The explicit forward-time, centered-space finite difference scheme is

$$\frac{\partial P(x_\alpha,t_\beta)}{\partial t} \simeq \frac{P(x_\alpha,t_\beta+\Delta t)-P(x_\alpha,t_\beta)}{\Delta t} \tag{3-71}$$

$$\frac{\partial^2 P}{\partial x^2} \simeq \frac{P(x_\alpha+\Delta x,t_\beta)-2P(x_\alpha,t_\beta)+P(x_\alpha-\Delta x,t_\beta)}{(\Delta x)^2} \tag{3-72}$$

$$\frac{\partial P(x_\alpha,t_\beta)}{\partial x} \simeq \frac{P(x_\alpha+\Delta x,t_\beta)-P(x_\alpha-\Delta x,t_\beta)}{2\Delta x} \tag{3-73}$$

Then the finite difference equation for this partial differential equation becomes

$$\begin{aligned} P(x_\alpha,t_\beta+\Delta t) = \\ &+\left[\left(\frac{A}{(\Delta x)^2}-\frac{B}{2\Delta x}\right)\Delta t\right]P(x_\alpha+\Delta x,t_\beta) \\ &+\left[1+\left(-\frac{2A}{(\Delta x)^2}\right)\Delta t\right]P(x_\alpha,t_\beta) \\ &+\left[\left(\frac{A}{(\Delta x)^2}+\frac{B}{2\Delta x}\right)\Delta t\right]P(x_\alpha-\Delta x,t_\beta) \end{aligned} \tag{3-74}$$

This finite difference equation may be considered as a random walk in which the transition probability is everywhere zero except for two nearest neighbors and the self transition. The Crank-Nicholson scheme (implicit forward-time, centered-space finite difference) implicitly uses the nearest neighbor random walk in space (Fig. 3-3). In the discrete Markov chain model, we do not limit the transition to the nearest neighbor (Fig. 3-3), and the model is explicit. As long as the difference equation is explicit in time, it is possible to write the difference equation as

$$P(x_\alpha,t_\beta+\Delta t) = \sum^{\forall x} P(x_\alpha,t_\beta+\Delta t)\,|\,x,t_\alpha)P(x,t_\beta) \tag{3-75}$$

which is equivalent to equation 3-61. In the finite difference scheme, there is a

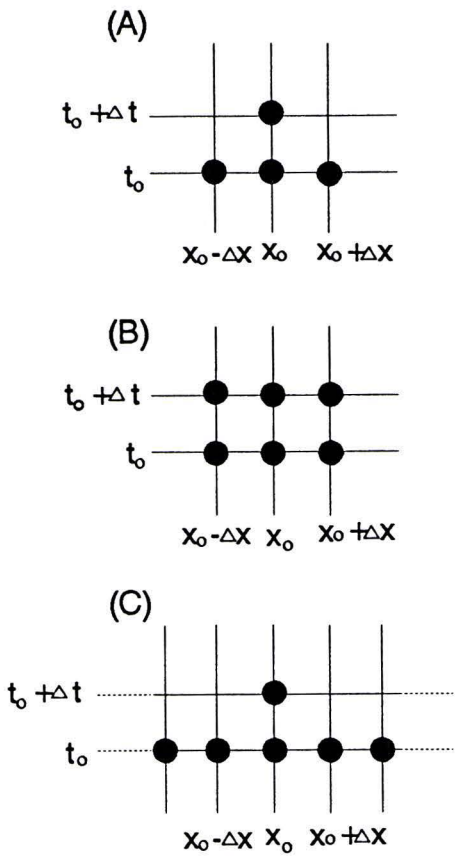

Fig. 3-3. The comparison of finite difference schemes ((A) = explicit forward-time centered-space, (B) = Crank-Nicholson) and discrete Markov chain model in discrete-time/space. The space (x-axis) and time (y-axis) are represented by two-dimensional, discrete, coordinates. While the numerical schemes use the nearest-neighbor for the estimation of the first order probability at (x_o and $t_o + \Delta t$), the discrete Markov chain is not limited to the nearest neighbor.

macroscopic governing equation, and the space and time are discretized to approximate the continuous process with nearest-neighbor random walk. On the other hand, in the Markov chain model, the local, mesoscopic transport process is integrated to the macroscopic transport behavior by eliminating the need for a macroscopic governing equation. While the formulation of a simple governing equation is elegant, the flexibility of the Markov chain model gives a certain advantage under various conditions such as for complex boundaries and spatial variable parameters. Furthermore for educational purposes, the assignment of transition probability gives us some insight of the underlying physics, and clarifies the connection to various other approaches which include Fokker-Planck type, linear/non-linear Langevin equation type, random walk type, non-Markovian type, and other stochastic approaches such as transfer function models (Jury et al., 1986).

The Relationship Between the Discrete Markov Chain Model and the Transfer Function Model

Jury et al. (1986) developed the transfer function model based on the solute life-time probability. In the transfer function model, the mass flux of the solute at the outlet at time t, $Q_{outlet}(t)$, is estimated from the mass flux of the solute at the inlet at time t', $Q_{inlet}(t')$, and the probability that the solute reaches to the outlet during the time interval t-t', $p_{trans}(t-t')$.

$$Q_{outlet}(t) = \int_0^t p_{trans}(t-t')\, Q_{inlet}(t')\, dt' \qquad (3\text{-}76)$$

$p_{trans}()$ serves as the transition probability for the transport from the inlet(t') to the outlet(t). From the previous sections, the first order density is calculated as

$$\int_{outlet} p(x_2(t))\,dx_2 = \int_{outlet}\int_{inlet} p[x_2(t)|x_1(t')]p(x_1(t'))\,dx_1\,dx_2 \qquad (3\text{-}77)$$

where the transition probability is defined as the probability of the transport from x_1 to x_2 during the fixed time interval t-t', and the integration is in space rather than in time. It is evident that these formulations are very closely related. However, in the transfer function model, the mass inside the system is variable in time since the mass is coming into the system at the rate of $Q_{inlet}(t)$ and leaving the system $Q_{outlet}(t)$. This shows that the transfer function model is indeed the mass balance equation. On the other hand, the probability balance equation governs the transport of the mass which is defined in the initial condition, P[0], and it does not apply for the any mass which is not defined in the P[0]. Therefore, the first order probability, p(x,t), is not the probability of finding any solute particle at location x and time t (i.e. normalized concentration), but it is the probability of finding the solute particle which is described in P[0] at location x and time t. To expand the probability balance equation to mass balance equation, the initial distribution function may be modified as

$$Q_{inlet}(\tau) = M_{inlet}(\tau)\,P_o[\tau]\,\delta(t-\tau) \qquad (3\text{-}78)$$

where $M_{inlet}(\tau)$ is the total mass of the chemical introduced into the system at time

t. In this equation, the time-dependent source is replaced with a series of Dirac input with the instantaneous mass of $M_{inlet}(\tau)$. For x_1 and x_2 to be the inlet and outlet domains, the transfer function model may be expressed as

$$Q_{outlet}(t) = \int^{outlet} p(x_2(t))\,dx_2$$
$$= \int_{t'=0}^{t'=t} \int^{outlet} \int^{inlet} p[x_2(t-\tau)\,|\,x_1(\tau)]\,M_{inlet}(\tau)\,p(x_1(\tau))\,\delta(t'-\tau)\,dx_1\,dx_2\,dt' \qquad (3\text{-}79)$$

Application of Discrete Markov Chain Model

In this section, we discuss possible applications of this discrete Markov chain model to natural systems, and their limitations. In the first part, the assignment of transition probability densities is considered, followed by the inverse time problem in the second part. The objective of the inverse time problem is the estimation of the solute particle distribution at $t<t_f$ from the solute distribution at $t=t_f$ given the transition probability density matrix. This means that we may be able to estimate the source of the contamination from the distribution of contaminants at a later time provided with the transition probability density matrix.

Transition Probability

The central issue of the application of the discrete Markov chain model is the realistic assignment of the transition probabilities. This model is descriptive rather than mechanistic. Therefore, despite the fact that the transition probability

is the reflection of underlying solute transport mechanisms and the boundary conditions, the primary goal is to express the best approximation/estimation of the real local transport phenomena in terms of the probability rather than the idealized but not realistic one. In fact, one of the advantages of this model is its flexible nature in which it is not constrained by any mechanistic models. The model rather requires the understanding of the principle mechanisms of solute transport and the estimation of errors around the idealized mechanistic model due to the simplifications imposed by the model. Another very important advantage is the fact that we do not have to express the spatial/temporal structure of the system in mathematical function forms. It is practically impossible to express complex natural geometry with a simple mathematical function. Therefore, even if a Fokker-Planck type governing differential equation is derived, a numerical solution will be required.

As an example, let us consider the transition density for a general case with a convective-dispersive type local transport process. Again, the transition probability density is defined as follows: "given the particle was found at $X(t=t_{n-1})$ at time step n-1, the probability of this particle moving from $X(t=t_{n-1})$ to $X(t=t_n)$ at time step n", or $p[X(t=t_n) \mid X(t=t_{n-1})]$. Figure 3-4 depicts such transition in 1-D space. In this case, the transition can be characterized by the spatial moments (Freyberg, 1986).

The first moment is related to the average local convective motion. The second moment is related to the average dispersive motion which is related to the local dispersivity. The third moment represents the deviation from the symmetry.

The task is to approximate this local process with discrete sets of transition probabilities. As an example, the transition probability densities for the local convective-dispersive type transport are represented by 5 discrete states (Fig. 3-4). The accuracy of the description of such local level approximation will be determined by the system of the interest.

To demonstrate how this model can be applied, a very simple example is provided so that interested readers can reproduce the result easily with a mathematical computer package like Mathematica. We represent the 1-D field with 15 nodes. The transition probability density matrix is thus 15 by 15, and given in Fig. 3-5. The diagonal elements of the matrix represent the self transition probability densities, i.e., the probability that the solute particle stays the same position at the next time step. The sum across the row equals one which means the mass is conserved. We also have the reflective boundaries at the node 1 and 15. The transition to the right (higher node number) is generally preferred which means there is a flux or drift to the right. Notice that such average flow and spreading characteristics are different from one location to another, i.e., spatially variable. Now we release a particle at node 3 at time 0. This initial condition is given as row vector p[0]. By employing the matrix operation given in equation 3-68 for 15 time steps, we will obtain the distribution of the particles as given in Fig. 3-6. To write a realistic model, the system should be represented in much more detail than with 15 nodes and 15 time steps, because the assumption of a near-Markov process may not be true for such a coarse approximation.

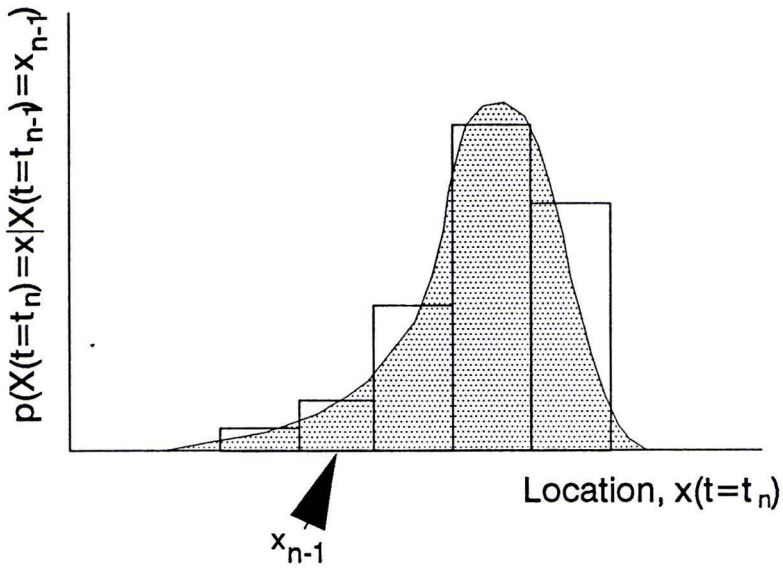

Fig. 3-4. A representation of 1-D solute transport process with 5 discrete transition probability densities.

$$\pi = [\pi_{ij}[1]] = \begin{bmatrix}
0.50 & 0.30 & 0.15 & 0.05 & 0.00 & 0.00 & 0.00 & 0.00 & 0.00 & 0.00 & 0.00 & 0.00 & 0.00 & 0.00 & 0.00 \\
0.05 & 0.15 & 0.50 & 0.25 & 0.05 & 0.00 & 0.00 & 0.00 & 0.00 & 0.00 & 0.00 & 0.00 & 0.00 & 0.00 & 0.00 \\
0.00 & 0.10 & 0.20 & 0.40 & 0.20 & 0.10 & 0.00 & 0.00 & 0.00 & 0.00 & 0.00 & 0.00 & 0.00 & 0.00 & 0.00 \\
0.00 & 0.00 & 0.05 & 0.35 & 0.45 & 0.10 & 0.05 & 0.00 & 0.00 & 0.00 & 0.00 & 0.00 & 0.00 & 0.00 & 0.00 \\
0.00 & 0.00 & 0.05 & 0.20 & 0.35 & 0.25 & 0.10 & 0.00 & 0.00 & 0.00 & 0.00 & 0.00 & 0.00 & 0.00 & 0.00 \\
0.00 & 0.00 & 0.00 & 0.05 & 0.15 & 0.35 & 0.35 & 0.10 & 0.00 & 0.00 & 0.00 & 0.00 & 0.00 & 0.00 & 0.00 \\
0.00 & 0.00 & 0.00 & 0.00 & 0.05 & 0.10 & 0.30 & 0.40 & 0.20 & 0.00 & 0.00 & 0.00 & 0.00 & 0.00 & 0.00 \\
0.00 & 0.00 & 0.00 & 0.00 & 0.00 & 0.10 & 0.20 & 0.30 & 0.35 & 0.05 & 0.00 & 0.00 & 0.00 & 0.00 & 0.00 \\
0.00 & 0.00 & 0.00 & 0.00 & 0.00 & 0.00 & 0.10 & 0.25 & 0.35 & 0.20 & 0.10 & 0.00 & 0.00 & 0.00 & 0.00 \\
0.00 & 0.00 & 0.00 & 0.00 & 0.00 & 0.00 & 0.00 & 0.10 & 0.15 & 0.35 & 0.30 & 0.10 & 0.00 & 0.00 & 0.00 \\
0.00 & 0.00 & 0.00 & 0.00 & 0.00 & 0.00 & 0.00 & 0.00 & 0.05 & 0.10 & 0.20 & 0.45 & 0.15 & 0.05 & 0.00 \\
0.00 & 0.00 & 0.00 & 0.00 & 0.00 & 0.00 & 0.00 & 0.00 & 0.00 & 0.05 & 0.20 & 0.30 & 0.35 & 0.10 & 0.00 \\
0.00 & 0.00 & 0.00 & 0.00 & 0.00 & 0.00 & 0.00 & 0.00 & 0.00 & 0.00 & 0.05 & 0.15 & 0.35 & 0.40 & 0.05 \\
0.00 & 0.00 & 0.00 & 0.00 & 0.00 & 0.00 & 0.00 & 0.00 & 0.00 & 0.00 & 0.00 & 0.15 & 0.20 & 0.35 & 0.30 \\
0.00 & 0.00 & 0.00 & 0.00 & 0.00 & 0.00 & 0.00 & 0.00 & 0.00 & 0.00 & 0.00 & 0.10 & 0.20 & 0.30 & 0.40
\end{bmatrix}$$

$$p[0] = [0, 0, 1, 0, 0, 0, 0, 0, 0, 0, 0, 0, 0, 0, 0]$$

Fig. 3-5. A example of transition probability density matrix for 15 discrete states, and a initial probability density vector.

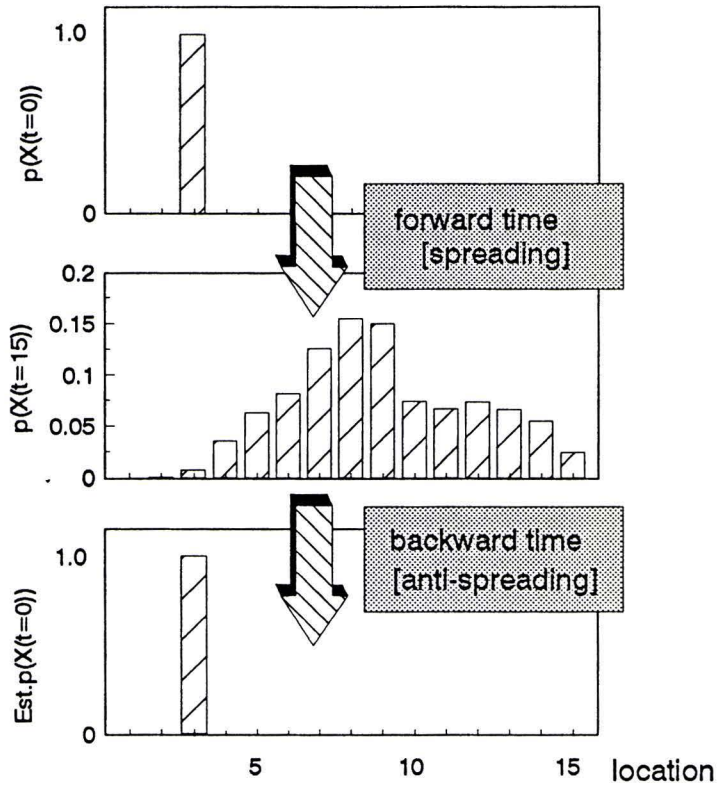

Fig. 3-6. The result of a discrete Markov chain simulation of solute transport process given by the initial and transition probability density matrices given in Fig. 3-5. The inverse-time operation was carried out by inverting the transition probability density matrix.

Inverse Time Problem

In this section, the inverse-time problem will be discussed. The goal of time-inversion is to extract the information of the past (e.g. the initial condition) from the information at a later time. The time-inversion technique discussed here is not based on sound physical/mathematical proofs. Despite our need for time-inversion in environmental, geological, and other natural sciences, considerable difficulties exist, and further validation is needed to prove whether such an operation is indeed permitted or not. The main purpose of this section is to facilitate discussion on the use of time-inversion in environmental science with an emphasis on its limitations to avoid misuse of the ideas presented.

In the forward-time problem, the concentration distribution at $t=t_n$, $P[t=t_n]$, was estimated from the initial distribution, $P[t=0]$, and the transition probability density matrix, $\mathbf{\Pi}[n]$. If we multiply this equation from the right with the inverse matrix of $\mathbf{\Pi}[n]$, we obtain

$$P[n]\ \Pi[n]^{-1} = P[0]\ \Pi[n]\ \Pi[n]^{-1} = P[0] \qquad (3\text{-}80)$$

This means, as long as we know $\mathbf{\Pi}[n]$, and provided $\mathbf{\Pi}[n]$ is non-singular, we can obtain the concentration distribution at an earlier time from the concentration distribution of a later time. We can, in principle, get the concentration distribution at any time prior to the observation at $t=n$.

It should be understood that what we are doing is not a reverse random walk to the origin. As assured by the second law of the thermodynamics, the

entropy for a spontaneous reaction is generally produced for the forward-time direction. The stochastic justification of the second law of thermodynamics from quantum mechanical reasoning is known as H theorem.

Information Entropy and Boltzmann H Theorem (Reif, 1965)

The differential version of Chapman-Kolmogorov equation, the master equation, is given as

$$\frac{dp_r}{dt} = \sum_s p_s W_{sr} - \sum_s p_r W_{rs} \tag{3-81}$$

where W_{sr} is the probability of transition from s to r per unit time. It is a gain-loss equation for the probability. In the previous discussion, the probability is defined for a particular coordinate in space. The transition probability was not necessarily symmetric. It should be noticed, however, the transition in the model is not for the accessible state, but rather for the accessible coordinate.

At molecular level, a transition is considered between the accessible quantum states. Due to the hermitian character of the Hamiltonian operator, the symmetry of transition probability density

$$W_{sr} = W_{rs} \tag{3-82}$$

is assured. If this symmetry holds, the master equation becomes

$$\frac{dp_r}{dt} = \sum_s W_{rs} (p_s - p_r) \tag{3-83}$$

Now we introduce the quantity H, which is an expected value of the ln p_r

$$H \equiv \sum_r p_r \ln p_r \tag{3-84}$$

Differentiate H with respect to the time

$$\frac{dH}{dt} = \sum_r \left(\frac{dp_r}{dt} \ln p_r + \frac{dp_r}{dt} \right) \tag{3-85}$$

$$= \sum_r \frac{dp_r}{dt} (\ln p_r + 1) \tag{3-86}$$

From the master equation with symmetric transition probability density

$$\frac{dH}{dt} = \sum_r \sum_s W_{rs} (p_s - p_r)(\ln p_r + 1) \tag{3-87}$$

We can also define the same quantity from s

$$\frac{dH}{dt} = \sum_r \sum_s W_{sr} (p_r - p_s) (\ln p_r + 1) \tag{3-88}$$

From the symmetry property, dH/dt can be written as

$$\frac{dH}{dt} = - \frac{1}{2} \sum_r \sum_s W_{rs} (p_r - p_s) (\ln p_r - \ln p_s) \tag{3-89}$$

The transition probability, W, is a positive quantity for the forward process. Furthermore, since ln p is a monotonically increasing function of p, it follows that if $p_r < p_s$ then ln $p_r < p_s$. These conditions assure the negativity of the time derivative of the quantity, H.

$$(p_r - p_s)(\ln p_r - \ln p_s) \geq 0 \tag{3-90}$$

$$\frac{dH}{dt} \leq 0 \tag{3-91}$$

This theorem is known as H theorem. If we define the information entropy as

$$S = -H = -\ln \sum_r p_r \ln p_r \tag{3-92}$$

the entropy increases for forward in time. This is the probabilistic interpretation of the second law of the thermodynamics. The formal treatment of relations between the thermodynamics and underlying quantum mechanics which is stochastic in nature is given in statistical mechanics. However, a discussion of the extent to which we can extend these arguments at mesoscopic or macroscopic level, especially the definition of the entropy in non-equilibrium state, and the relationship between the thermodynamic entropy and the information entropy, is beyond the scope of this study.

Inverse Time Transformation and Ill-Posed Problem

As assured by the H theorem, the spontaneous processes which are governed by the discrete Markov chain generally produce entropy and the information is diminished. On the other hand, the inverse time operation of the irreversible process, if it is possible by any means, should be opposite in terms of the entropy/information. The inversion of the transition probability density matrix, thus, creates a process which decreases the entropy and gains the information.

However, intuitively, once we loose the information, it is impossible to recover the lost information. To clarify this difficulty, consider the general forward-time transport process as follows: given the initial distribution of the particles, p_i, and the operator associated with the transport of the particle forward in time, Ω, obtain the distribution of the particle in the later time, p_f.

$$\Omega \; p_i = p_f \tag{3-93}$$

In the discrete Markov chain approach, the operator Ω is a transition probability density matrix. To find the inverse-time operation, we look for the time-inverse operator of Ω, Ω^{-1}. However, the p_i and p_f are not necessarily 1:1. Suppose that p_f is the equilibrium distribution of the particles. The system will eventually approach to this final configuration no matter what kind of initial distribution, p_i, it started with. If the relationship between p_i and p_f is not 1:1, the inverse-time operation cannot be well-defined. In terms of the Markovian process, the Markovian particles do not remember where they came from after one time step. Therefore, it becomes progressively difficult to retrieve the history of the particle as time passes. Mathematically, this type of process is called "ill-posed" (Tikhonov and Arsenin, 1977). The process, if operable, is extremely sensitive to the initial condition. Therefore, numerical errors, such as the round-off errors, make the operation to be unacceptable. For example, to obtain the inverse of a matrix with the Cramer's rule, the determinant of the matrix has to be calculated. It is known that to get the determinant of n-order matrix, approximately n^3 algebraic operations are needed. Furthermore, despite the fact that the inverse-time operation is very sensitive to the

initial condition, p_f, it is often difficult to obtain the exact knowledge of p_f for various real environmental situations. Therefore, the time-inversion of an irreversible process means the estimation of quasi-solution from the approximated initial condition knowing that the inverse operation is extremely sensitive to any small perturbation of the operation. In fact, these ill-posed problems are generally avoided in ordinary mathematics.

Given these severe limitations, several preliminary calculations of inverse transition matrices were attempted. As an example, the transition matrix given in the previous section was inverted using Mathematica with 150 significant digits. Using this inverse matrix, we could successfully go back in time starting from the distribution of the solute at time step 15 by "anti-spreading" the process. The estimated source (time step=0) is given in Fig. 3-6 which is identical to the initial distribution we have started with. It was found that the inverse-time operation can produce the probability in the past time for relatively short time steps (in this case 15 time steps). If we reverse the time more than the initial time, then negative first order densities (p_r), i.e. negative concentrations, occur. This is also forbidden from the physical intuition. It should be noticed that the inverse operation should be done only on the particle of the identical initial condition. In other words, the inverse operation is the pure reproduction of the forward process whose initial and transition properties are well defined. Therefore, if the time-inverse process is considered, the entropy should decrease and the information has to be obtained by the process.

This approach is different from the method of the Kolmogorov backward equation (Uffink, 1989), and the true nature of this time-inverse operation is beyond the scope of this study. Given the mathematical difficulties of ill-posed problems, the regularization method (Tikhonov and Arsenin, 1977) seems to be an promising approach if much stable time-inversion is desired.

Diffusion-type Transport in Heterogeneous Environment

In this section, we will apply the discrete Markov chain model to simulate diffusion-type transport in a two-dimensional, heterogeneous, mesoscopic medium from a point source. The term "mesoscopic" refers to the length scale of a sorbed phase which is between the molecular scale and the large pore scale (μm - mm). The objective of the study is to simulate the path of diffusional transport of the particle from the origin in a heterogeneous medium in which the diffusional characteristics are spatially variable, and there are complex impermeable boundaries. The general features of diffusion in heterogeneous environments have been studied by physicists (see Halvin and Ben-Avraham (1987)). This study was focused on the diffusional transport of organic solute in mesoscopic, heterogeneous, soil environment. The local environment of the sorbed phase is soil organic matter-rich, yet it is not uniform, and some pore and impermeable solid regions also exist. The goal of the study was to pinpoint the features of heterogeneity, such as tortuosity and distribution pattern of diffusion coefficient, which affect the macroscopic behavior of solute transport. To achieve this goal,

various realizations of hypothetical heterogeneous porous media were created using a Diffusion-Limited Aggregation type aggregation logic. Attempts were made so that the constructed structure, or the architecture, of the media has the expected characteristics of heterogeneous porous sorbed phase for organic solutes. The diffusion-like solute transport process in the created realizations were studied using nearest-neighbor (von Newman neighbour) random walks which were solved directly with the discrete Markov chain model.

Creating the Heterogeneous Medium with Cooperative Processes

The objective of this section is to come up with hypothetical structures of heterogeneous porous media whose characteristics resemble natural soil media. In particular, we are interested in the region of soils in which hydrophobic organic solutes are sorbed (sorbed phase). Hydrophobic organic solutes in soils are often associated with the organic matter rich environment of soil due to the hydrophobic interactions. This environment (the sorbed phase environment) is formed by the intricate interactions of various kinds of organic matter (hydrophobic to hydrophilic) with the mineral components. Numerous pore spaces which are filled with water and air are also expected. Our goal is to create hypothetical structures of sorbed phase, and study the solute transport processes in the sorbed phase environment.

One of the primary constituents of the sorbed phase, organic matter, has been characterized chemically (e.g. the elementary composition and chemical functional groups). In order to understand the transport phenomena inside the

organic matter, however, the structure of the sorbed phase has to be estimated in addition to the chemical/energetic characteristics. Furthermore, the locations of pores and mineral components also play important roles in the solute transport processes. Therefore, it is not the local components (chemical characteristics) of the medium which are important; but the manner in which the solute of the interest interacts with the local environment that determines the local transport processes. Accordingly, the local environment is defined in terms of the diffusion coefficient, or more specifically, the transition probability densities, rather than the chemical composition.

The detailed experimental studies of mesoscopic sorbed phase structure are still limited. Therefore, this attempt of creating hypothetical sorbed phase environment was aimed at the recognition of the important features of natural sorbed phase heterogeneity. There are many ways to create the hypothetical heterogeneous media. The most direct way is to characterize a real soil environment at a mesoscopic level, and use the real information. However, due to the technical difficulties of such characterizations, the investigation of the mesoscopic level soil structure has just begun.

The second approach is to imitate the process that the natural mesoscopic soil environment is developed. This involves the partial decomposition of plant tissues, the microbial alteration of the chemical components of the early stage soil organic matter, association of the soil organic matter with mineral components of the soil, polymerization and re-synthesis of new structures, etc. Obviously, this

process is extremely complex. Therefore, a great simplification is definitely needed if we try to mimic the natural processes.

As exemplified by the success of molecular biology, one of the most promising techniques of estimating the molecular level structure is the use of molecular dynamics programs. Recently, Tisccot and Ungerer (1989) discussed the possible molecular level structure of natural organic matter by using the quantitative analysis of functional groups as input into a molecular dynamics program. A molecular dynamics program can estimate and/or optimize the energy associated with a particular structure of the macro-molecule based on molecular orbital theories. A rigorous estimation of microscale structure is possible with a molecular dynamics approach. However, we are interested in the structure of sorbed phase under the influence of a solvent, the mineral components, etc. We felt this is beyond the scope of the current objective which is to create a simple mesoscopic model of natural soil structure, and not the microscopic one.

As alternative simple approach, the diffusion-limited aggregation (DLA) and cellular automata (CA) were also considered. DLA imitates the aggregation process which occurs by diffusion-limited transport. The sorbed phase environment, which can be viewed as aggregates, may be modeled as DLA. It has been known that many DLA structures can be well-described by fractal dimensions (Vicsek, 1989). CA are discrete space-time models which were studied by von Newmann in the late 1940s. In general, the space is divided into small discrete units (cells), and values are assigned to these cells. Rules local to specific cells determine the value

of that cell in the next time step. The resemblance of CA to the discrete Markov chain is obvious. The concept common to the DLA, CA, and the discrete Markov chain model is that the dynamics of the system are determined by the local rule. Based on these considerations, several trial programs based on DLA type and CA type (Rietman, 1989) logics were developed. To develop a structure-emergence logic, The following assumptions were implemented. First of all, hydrophobic-hydrophobic and hydrophilic-hydrophilic interactions among the components of organic matter can be expected. Secondly, the formation of organic matter presumably involve aggregation type processes. Thirdly, there may be regions which cannot be accessible for the solute. Therefore, we created the hypothetical mesoscopic sorbed phase structure using diffusion-limited aggregation or cellular automaton type approach (Rietman, 1989). The hypothetical medium thus created is not completely random but has a weak correlation structure. Recent experimental verification of the fractal structure of humic materials (Rice and Lin 1993) also partially support this approach. The computer codes developed in VAX C, P0607BM.C, is listed in the Appendix C.

In P0607BM.C, the medium is represented by 25 × 25 cells. This size was determined by the memory requirement and the CPU time available on IFAS VAX for the simulations. To eliminate the boundary effect, 27 by 27 cells were initially defined. The heterogeneity of the field is represented with 5 discrete numbers, 60, 70, 80, 90 and 0 to which 170, 160, 150, 79 and 170 cells were assigned, respectively. The numbers, 60 to 90, are related to the self-transition probability

(called the self-transition number), or more generally the diffusion coefficient used in the diffusion simulation program, P0607BD.C.

The detail of the assignment of the transition probability densities are given in the next section. However, it is necessary to describe how the medium was created with P0607BM.C. For example, a cell with the self-transition number 90 has the self-transition probability per Monte-Carlo step time is 0.90 unless its nearest neighbor is an impermeable cell. Therefore, for numbers between 60 and 90, higher the number, the particle tends to stay in the same position for longer time, i.e., the low diffusion coefficient case. The diffusion coefficient includes the interaction of solute with the local environment (e.g. hydrophobicity) and the local tortuosity factor (Appendix D). Therefore, the distribution of transition numbers is the consequence of the joint distribution of various parameters such as the distribution of tortuosity factor and the distribution of interaction energy between the solute and the medium.

The self-transition number 0 is assigned for the boundary cells. The transition into a boundary cell is forbidden in this simulation (impermeable space). Since the particles cannot exist in the forbidden region, it is possible to exclude any cells with the self-transition number 0 from the model. However, for the flexibility of the developed model, they were kept in the computer program.

To create a heterogeneous, weakly-correlated hypothetical sorbed phase, we assigned the aggregation-formation rule as follows. The location of the self-transition numbers 0 to 90 are assigned in the order of 90, 80, 70, 60, and 0. At

first, 79 cells are randomly selected, and the self-transition number 90 was assigned to them. After the random allocation of these 76 cells, 2000 (agg_time) locations were selected randomly. If the chosen cell had the self-transition number 90, then it was moved to one of its 4 nearest neighbors or to the same position with equal probability unless the newly selected location is already occupied. To reduce the boundary effect, the boundary at the minimum X (Y) coordinate is connected with the boundary of the maximum X (Y) coordinate. After this process, the locations of the cells with the self-transition 90 were fixed, and they are not allowed to move anymore. Then 150 cells were randomly selected from the unoccupied locations, assigned a self-transition number of 80. The same process was repeated again for 2000 (agg_time) steps. It was repeated until 729-170=559 cells were occupied with the self-transition numbers between 60 to 90. The self-transition number 0 was assigned for the rest of the 170 cells.

These processes produce media which are not random, but somewhat ordered. Since the order of the allocation of the self-transition number is from the high to low, there is a weak tendency that many aggregates are formed where the cells with high self-transition numbers become the center (core) of the aggregates. After the assignments of self-transition numbers, the boundary cells (row 1 and 27, column 1 and 27) were truncated to minimize the boundary effect. Three realizations are shown in Fig. 3-7.

At this point, it was desired to statistically characterize the hypothetical realizations. Since the detailed structure of the heterogeneous medium is given as

the spatial coordinate and the self-transition number at the spatial coordinate, it is possible to extract various statistical measures of the medium. The following statistical parameters are given.

The Statistical Average of the Self-Transition Numbers:

The means of the self-transition numbers are 56.6, 57.0, and 57.4 for P0607B1, P0607B2, and P0607B3, respectively.

The Standard Deviation of the Self-Transition Numbers:

The standard deviations of the self-transition numbers are 31.3, 31.0, and 30.7 for P0607B1, P0607B2, and P0607B3, respectively.

The Frequency Distribution of the Self-Transition Numbers:

Although the truncation of the boundary cells made the frequency distribution to be slightly different from one realization to another, they are practically identical (Fig. 3-8). The frequency distribution of the self-transition numbers reflect the chemical composition of the media. In real systems, the distribution of the self-transition numbers are continuous. However, they are represented with discrete distribution of 0, 60, 70, 80, and 90. Appendix D is provided to discuss how the distribution of the self-transition numbers is determined. The equilibrium behavior of the system (e.g. the equilibrium distribution coefficient, Kd) is generally determined by the distribution of the self-transition

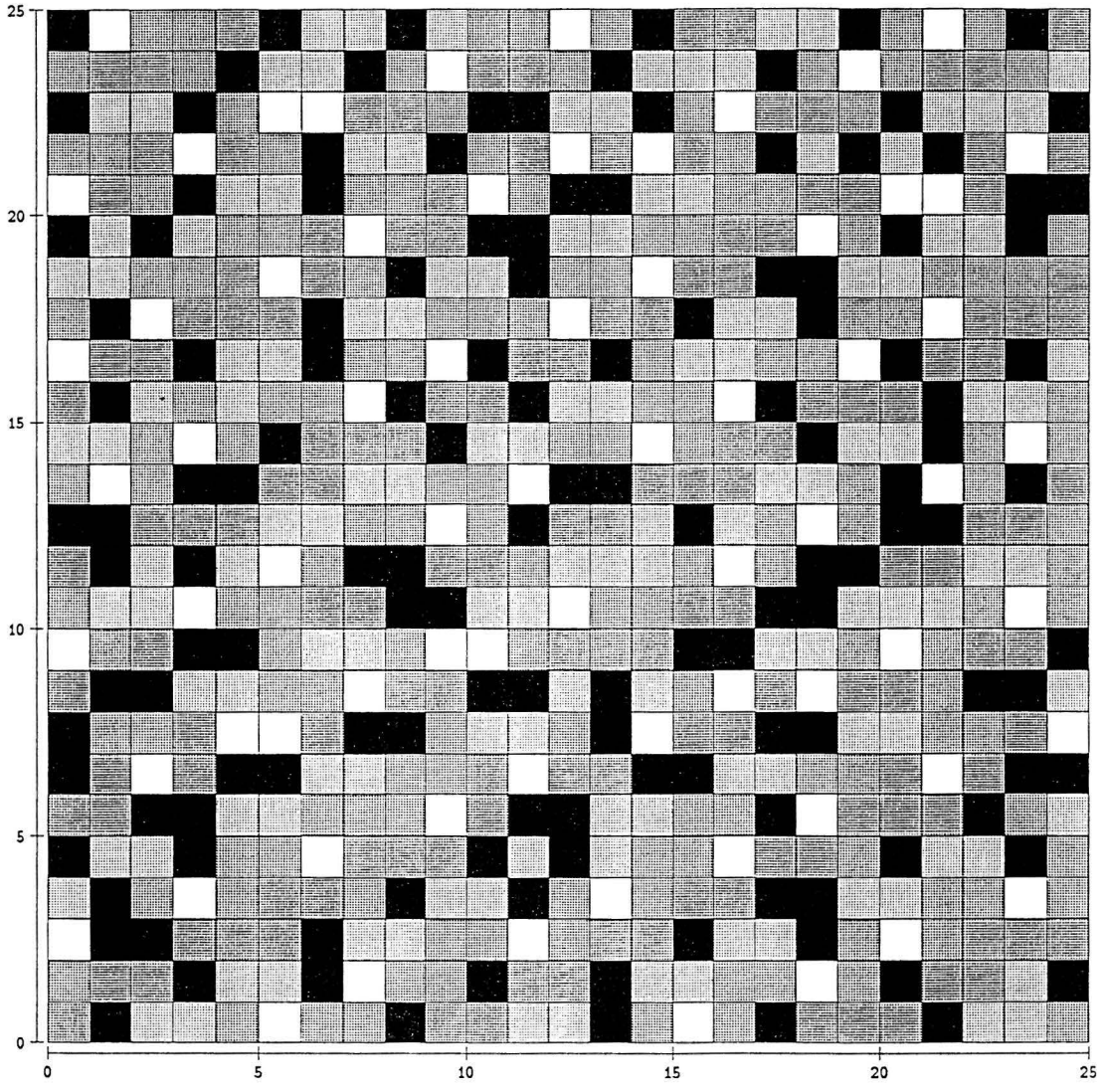

Fig. 3-7-A. A realization of heterogeneous media represented by 25 ×25 cells (P0607B1). The black cells are the impermeable boundary cells. White cells represent the local environment with low diffusion coefficient (high self-transition number of 90). Lighter the color, the higher is the self-transition number.

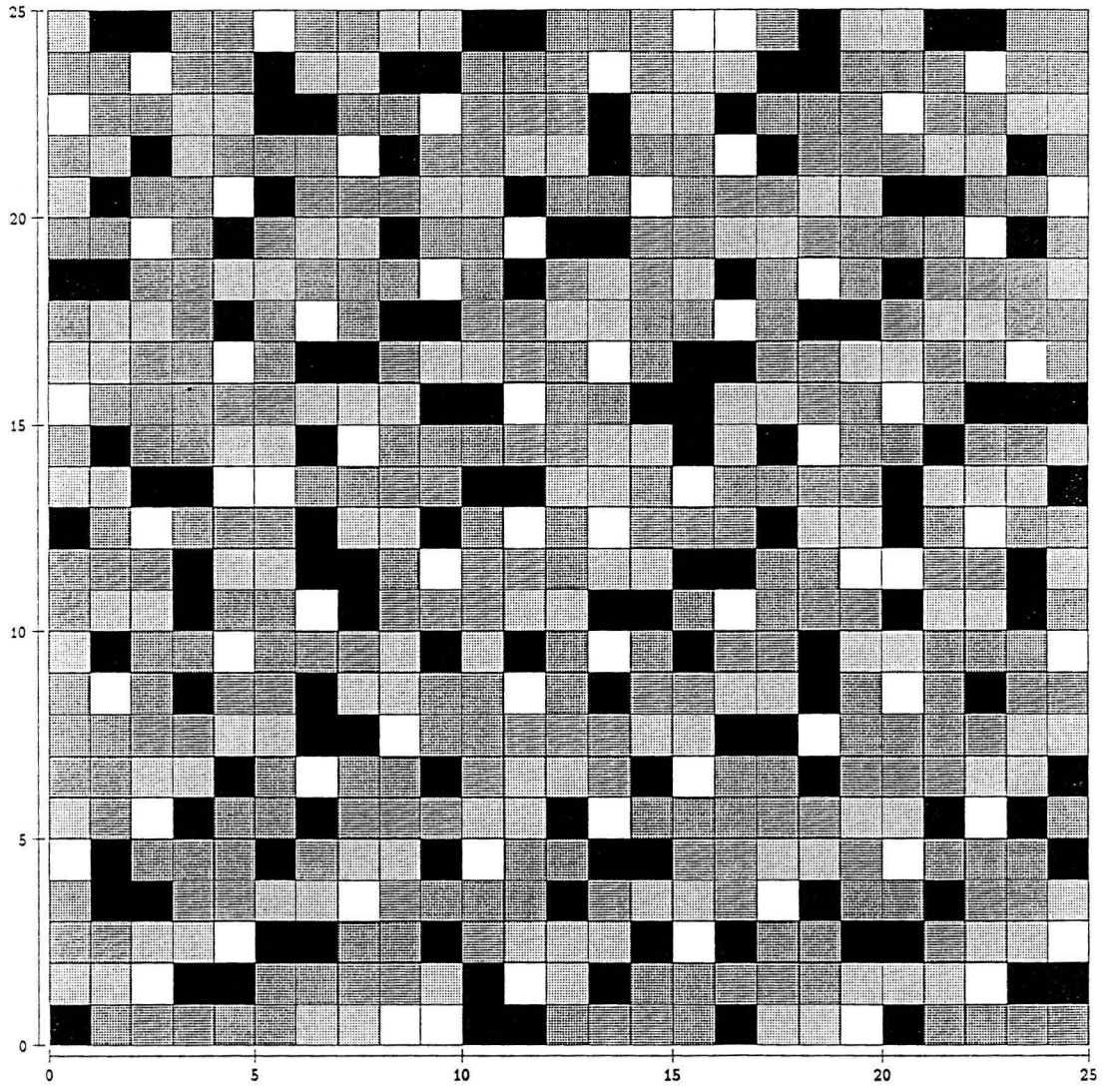

Fig. 3-7-B. A realization of heterogeneous media represented by 25 ×25 cells (P0607B2). The black cells are the impermeable boundary cells. White cells represent the local environment with low diffusion coefficient (high self-transition number of 90). Lighter the color, the higher is the self-transition number.

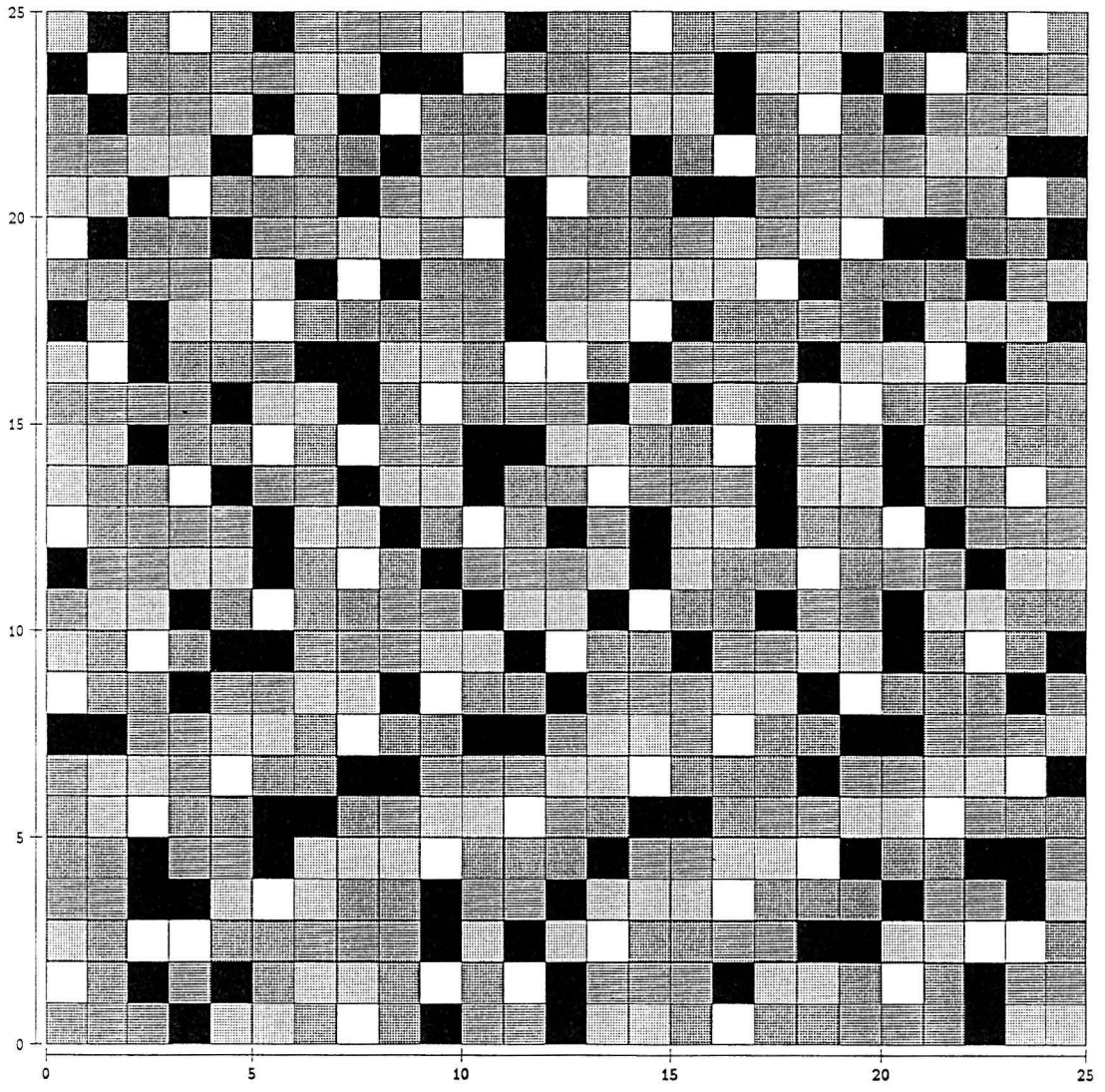

Fig. 3-7-C. A realization of heterogeneous media represented by 25 ×25 cells (P0607B3). The black cells are the impermeable boundary cells. White cells represent the local environment with low diffusion coefficient (high self-transition number of 90). Lighter the color, the higher is the self-transition number.

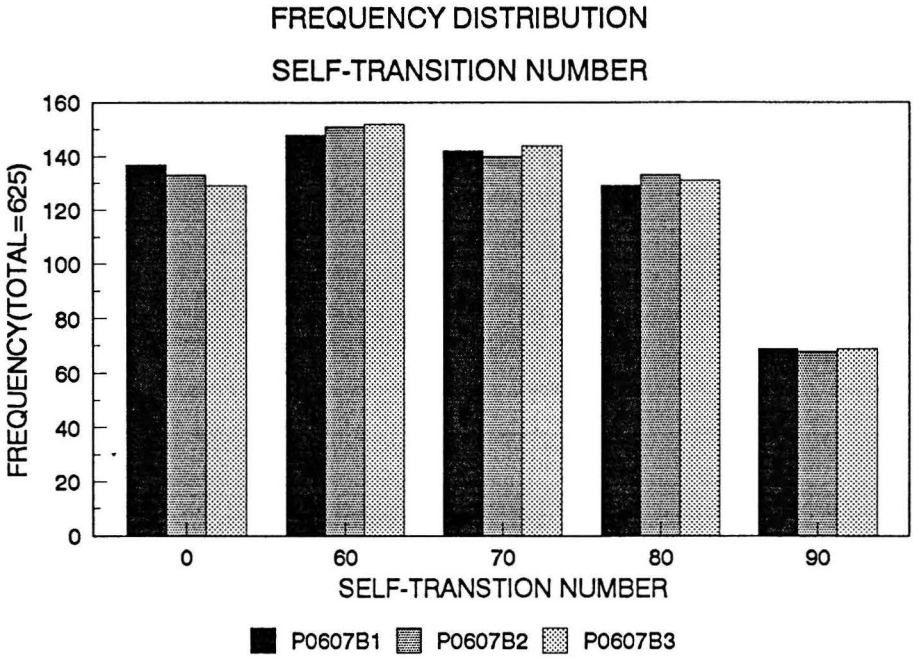

Fig. 3-8. The frequency distributions of the self-transition numbers. The three realization (Fig. 3-8-A, B, and C) have nearly identical frequency distributions.

numbers (and not the spatial correlation structure) provided that the space (sites)characterized by the statistics is accessible. However, when the kinetic aspects of the behaviors are of interest, further information is needed in addition to the distribution of self-transition numbers.

The Semi-variogram of the Self-Transition Numbers:

To estimate the degree of statistical correlation structure of the medium, the semi-variogram

$$\gamma(h) = \frac{1}{2} < [STN(X) - STN(X+h)]^2 > \qquad (3\text{-}94)$$

was calculated using a computer software GEOPACK (Yates and Yates, 1990). STN is the self-transition number, X is a coordinate in 2-D, X+h is another coordinate whose distance from X is h.

The impermeable cells were eliminated from the semi-variogram calculation for the following reason. The impermeable regions are completely isolated from the permeable region since no solute can enter the impermeable region as discussed in the following section. It is still possible to assign the self-transition numbers assuming the situation that the solute can move inside the impermeable region; even the solute cannot enter from the permeable region (e.g. the solute was initially (at time=0) inside the impermeable region). Therefore, any number between 0 to 100 could be assigned to the impermeable cells just like for the permeable cells. However, since these two spaces (i.e., permeable and

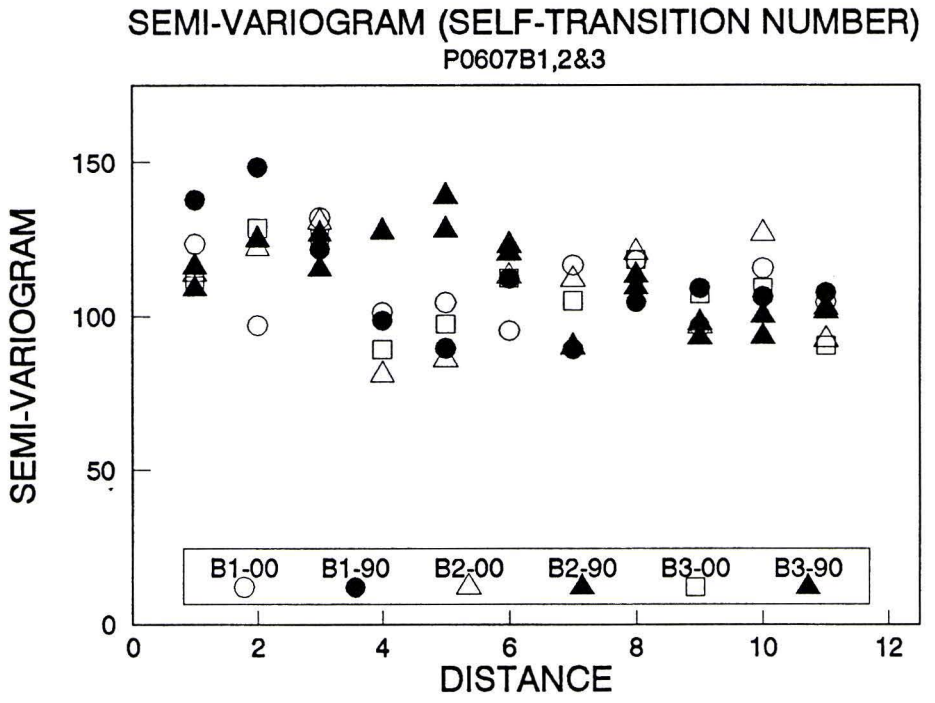

Fig. 3-9. The semi-variograms of the heterogeneous medium given in Fig. 3-7. B1, B2 and B3 correspond to the media in Fig. 3-8-A (P0607B1), 3-8-B (P0607B2) and 3-8-C (P0607B3), respectively. To study the anisotropy, two directions, 0° ± 10° (-00; x-axis) and 90° ± 10° (-90; y-axis), were examined.

impermeable spaces) are not connected at all, the properties inside theimpermeable space are irrelevant to the solute in thepermeable spaces. To obtain a meaningful parameter for the solute transport, therefore, the impermeable regions were eliminated from the calculation.

Figure 3-9 shows the semi-variogram of the self-transition numbers used in the simulation. From the semi-variogram, it is apparent that the degree of the aggregation (spatial correlation) is weak, and the created medium is almost uncorrelated at the length scale of solute spreading (10 cell unit). There was no apparent anisotropy effect since there was no mechanism which lead to the directional (anisotropic) structure of the medium.

The Simulation of Diffusional Transport in the Heterogeneous Medium

To perform the discrete Markov chain simulation of a diffusion-like process in heterogeneous medium, a computer program P0607BD.C was developed in VAX C (see Appendix C).

The transition probability densities for a single time step are calculated in the subroutine PImatrix(), and stored in the array, transit_1[ ][ ]. In this program, the self-transition probability density, p, is given as the 1/100 of the self-transition number assigned in the program P0607BM.C. Since there are 150 impermeable boundary cells, the transition to/from the boundary cells determines the boundary conditions.

CASE 1 : From permeable cell to 4 nearest permeable cells

The self-transition probability, p (0.6, 0.7, 0.8 or 0.9), is given to the self-transition. The rest of 1-p probability is assigned evenly to the transition to the 4 nearest neighbors.

CASE 2 : From impermeable cell to 4 nearest permeable cells

If $p=0$, which happens when the selected cell is the impermeable boundary cell, the transition probability of 0.25 is assigned for the transition to the nearest neighbor. However, the transition from the impermeable cell to permeable/impermeable cell is irrelevant to the particle transport since the transition from permeable to impermeable cell is not allowed. Therefore, there is no possibility that the particle penetrate into the impermeable cell. When any one or more of the 4 nearest neighbor is impermeable cell(s), the rule given in CASE 3 is applied.

CASE 3 : From permeable cell to nearest impermeable cell

This transition is concerned with the boundary problem. Any transition from a permeable cell to the nearest permeable cell is strictly forbidden in this model. When the particle approaches to the boundary, the particle is assumed to be reflected back to the permeable space. In this case, the transition probability is assigned as follows. At first, the self transition probability, p, is assigned as usual, and the transition probability other than the impermeable boundary cell(s) is (1-

p)/4. Since there is at least one transition to the impermeable boundary cell, the sum of the transition probabilities is less than 1. Therefore, the transition probability is renormalized by dividing the sum of the transition probabilities.

To minimize the numerical error, the 20th power of the transition probability density matrix was first calculated using double-precision, and the longer time step distribution was calculated from this matrix. The total CPU time required for the simulation was about 12 hours on the VAX computer. If higher accuracy and speed are required, it is possible to adopt a more sophisticated scheme for numerical matrix multiplication than the basic row-column operation.

Using the transition probability densities assigned above, we simulated the diffusional transport from the single origin at the center of the medium. To define this initial condition, the first order probability density matrix at time 0, P[X(t=0)], i.e., the probability of finding the particle at location X at time 0 was set so that this probability is everywhere zero except the source where the probability is one.

The results of the simulations at time steps of 200 are given in Fig. 3-10. The maximum time steps for this simulation was limited to 200 time steps since the solutes started to reach the edges of the medium. The model successfully simulated a possible first-order probability density profile in discrete 2 dimensional space. Since the particle movement into the impermeable boundary layer was forbidden, the probability of finding the particles (the first order density) inside the boundary (impermeable space) is zero. The simulation also shows the complex appearance of the first order probability density profile as affected by the boundary

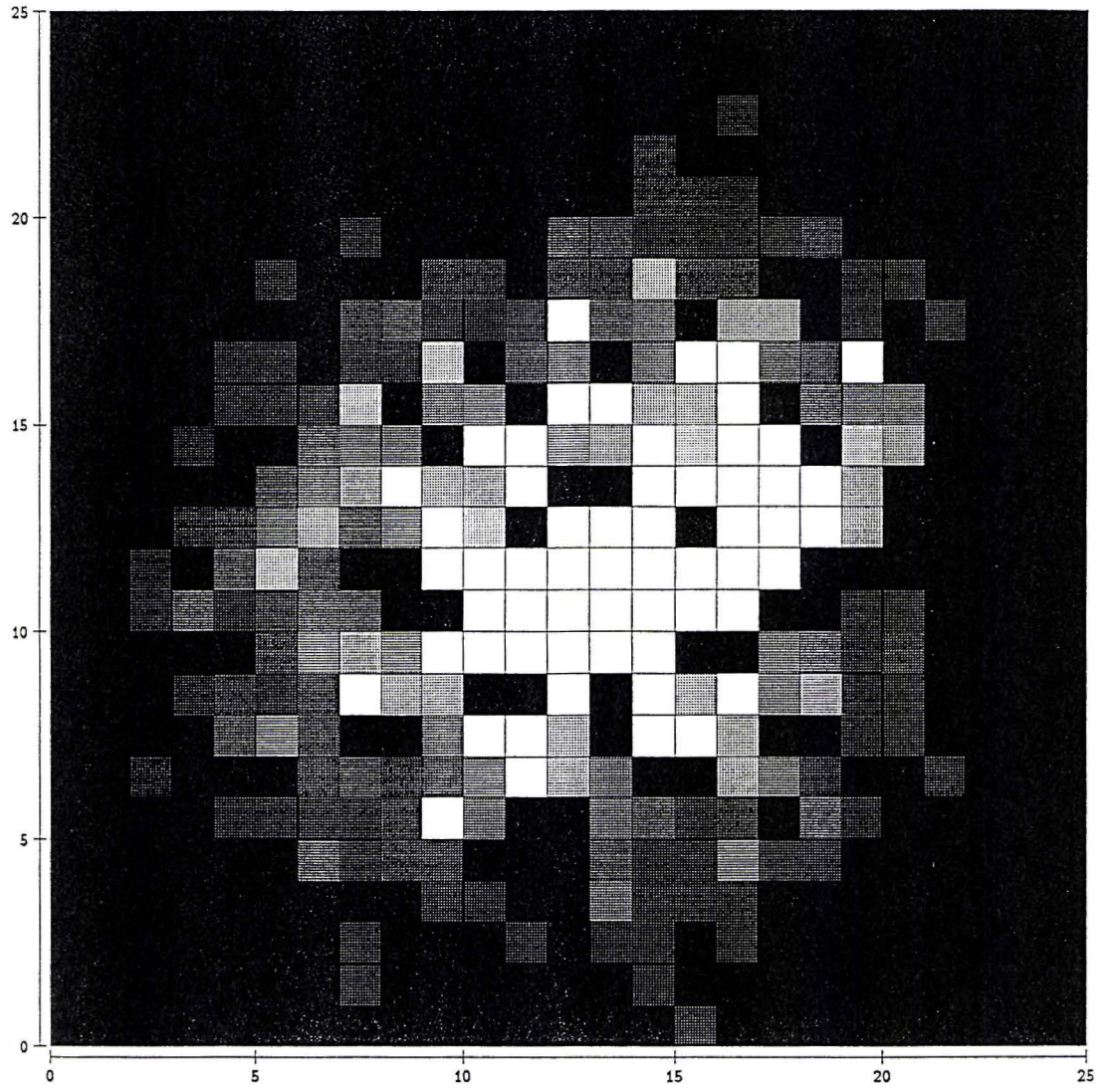

Fig. 3-10-A. The simulation of diffusional transport process in the medium presented in Fig. 3-7-A (P0607B1) at 200 time steps. A particle was released in the middle, and spread out. Lighter color indicates the higher first order probability (concentration profile).

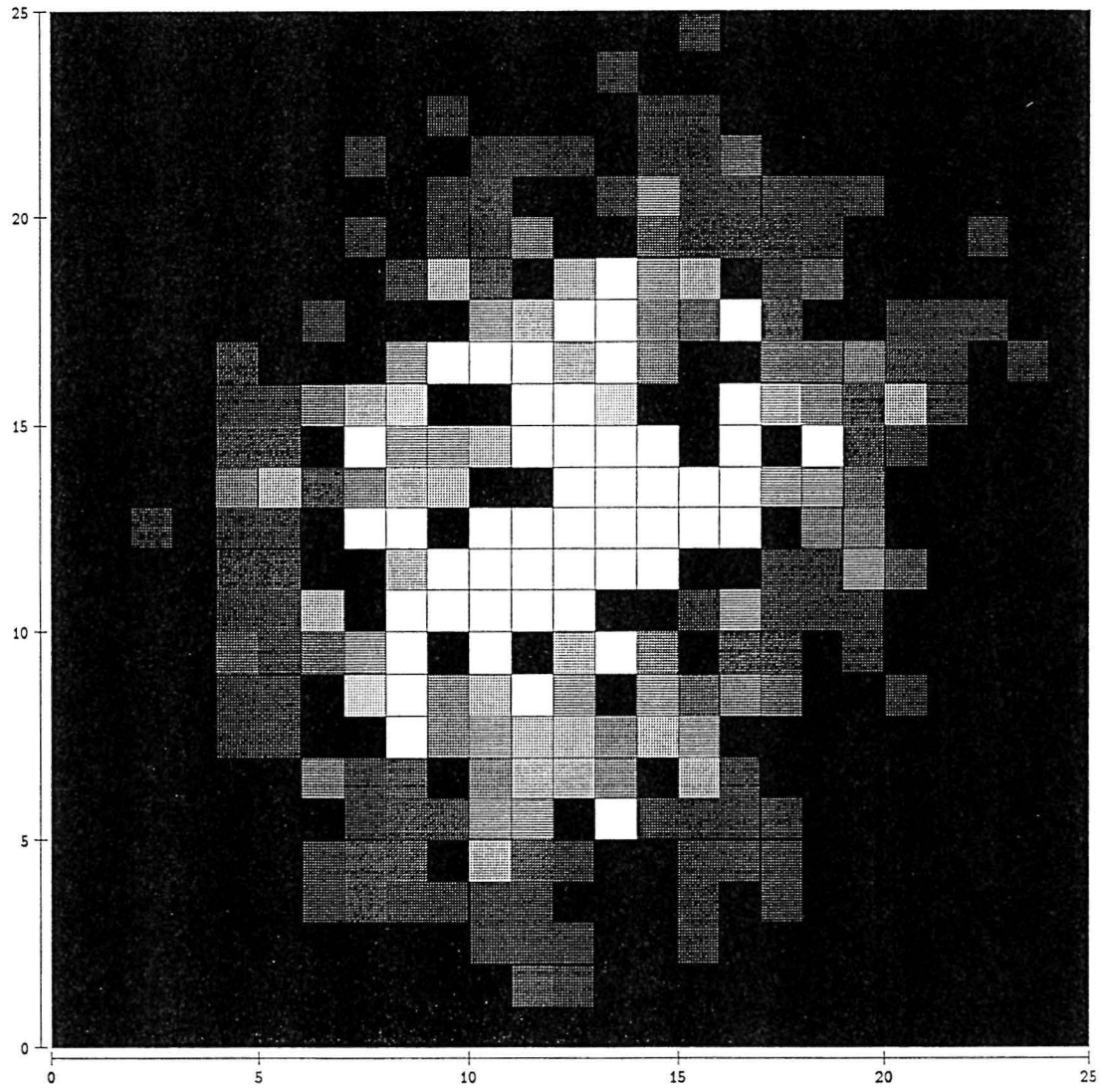

Fig. 3-10-B. The simulation of diffusional transport process in the medium presented in Fig. 3-7-B (P0607B2) at 200 time steps. A particle was released in the middle, and spread out. Lighter color indicates the higher first order probability (concentration profile).

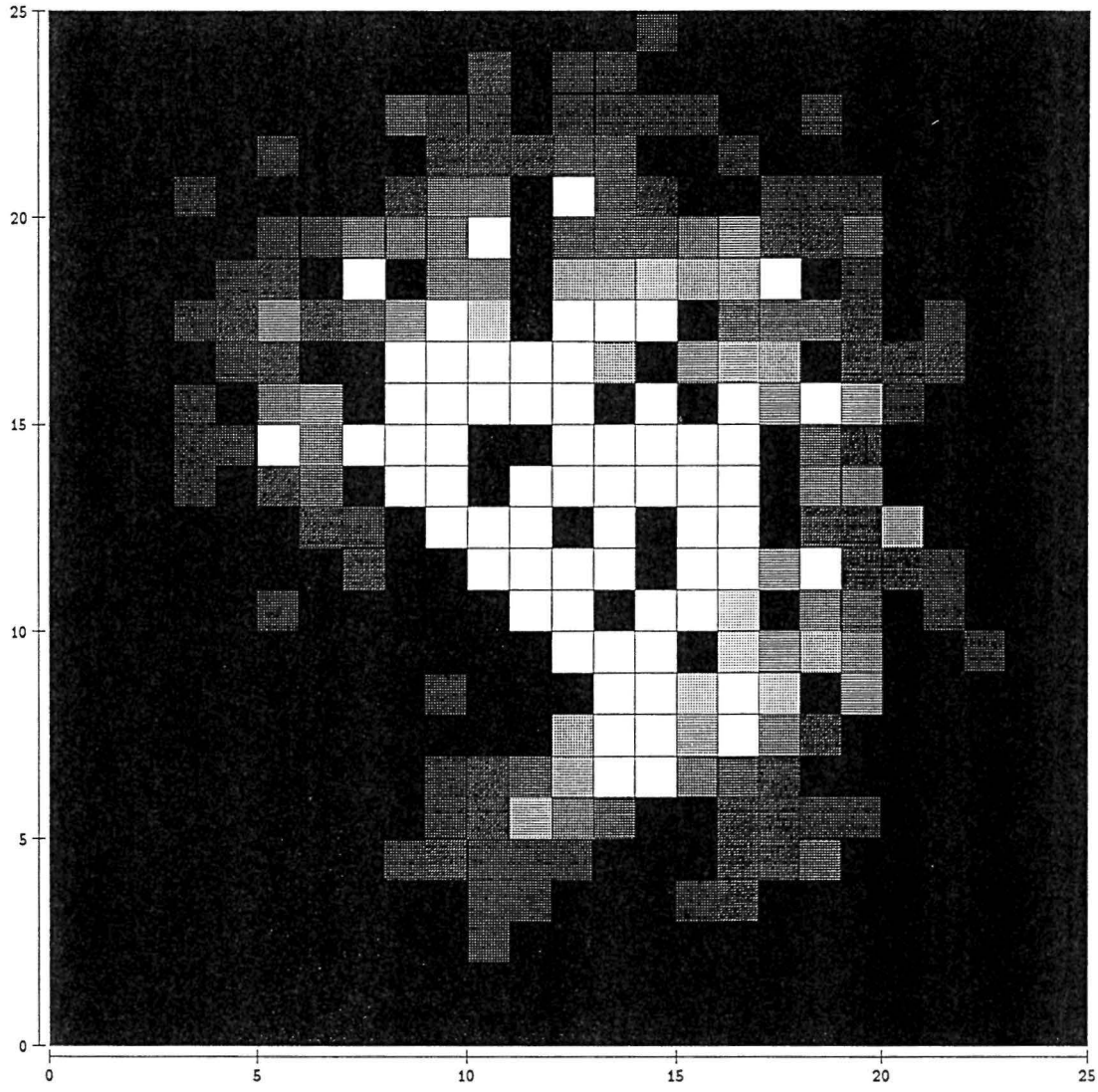

Fig. 3-10-C. The simulation of diffusional transport process in the medium presented in Fig. 3-7-C (p0607B3) at 200 time steps. A particle was released in the middle, and spread out. Lighter color indicates the higher first order probability (concentration profile).

conditions and the spatial heterogeneity of the permeable region of the medium. The three realizations with similar frequency distributions of the self-transition numbers showed quite different diffusion patterns (especially p0607B3). It is evident that the local heterogeneities around the source (Fig. 3-10) markedly influence the diffusion pattern during the early stages of diffusion.

The first and second spatial moments (Freyberg, 1986) were calculated (Fig.3-11 and 12) using the following equations

$$\mu_x(t) = \sum^{\forall x} x\, p[X(t)=x] \tag{3-95}$$

$$\mu_y(t) = \sum^{\forall y} y\, p[Y(t)=y] \tag{3-96}$$

$$M_{xx}(t) = \sum^{\forall x} x^2\, p[X(t)=x] \tag{3-97}$$

$$M_{yy}(t) = \sum^{\forall y} y^2\, p[Y(t)=y] \tag{3-98}$$

$$M_{xy}(t) = \sum^{\forall x,y} x\, y\, p[X(t)=x, Y(t)=y] \tag{3-99}$$

From the first spatial moment, it was found that there was an apparent convective flux (Fig. 3-11). This apparent convective flux is due to the noise (heterogeneity) induced flow and the impermeable boundary effect. The second central moments are calculated from the first moments and the second moments as follows.

$$\sigma_{xx}^2(t) = M_{xx}(t) - [\mu_x(t)]^2 \tag{3-100}$$

$$\sigma_{yy}^2(t) = M_{yy}(t) - [\mu_y(t)]^2 \tag{3-101}$$

$$\sigma_{xy}(t) = M_{xy}(t) - [\mu_x(t)\ \mu_y(t)] \tag{3-102}$$

The second central moment tensor is defined as

$$\sigma^2(t) = \begin{bmatrix} \sigma_{xx}^2(t) & \sigma_{xy}^2(t) \\ \sigma_{yx}^2(t) & \sigma_{yy}^2(t) \end{bmatrix} \tag{3-103}$$

The diffusion coefficient is generally defined as (Freyberg, 1986)

$$D = \frac{1}{2}\frac{d}{dt}\sigma^2(t) \tag{3-104}$$

In Fig. 3-12, the σ_{xx}^2, σ_{yy}^2, and σ_{xy}^2 are plotted against time step. The slope of the curves are proportional to the diffusion coefficients. Recall that the diffusion coefficient is a constant value for a homogeneous medium. However, in a heterogeneous environment, there is a certain time before the asymptotic diffusion coefficient is reached. Within this time, the diffusion coefficient exhibits time dependence (Montroll, 1964; Mitescu et al., 1978; Pandey et al., 1984). The time to reach the asymptotic behavior is generally known as the cross-over time, and the time-dependence of the diffusion coefficient has been studied extensively in percolation and fractal theories (Halvin and Ben-Avraham, 1987). Although the medium of 25 × 25, and the maximum time steps of 200, are probably too small

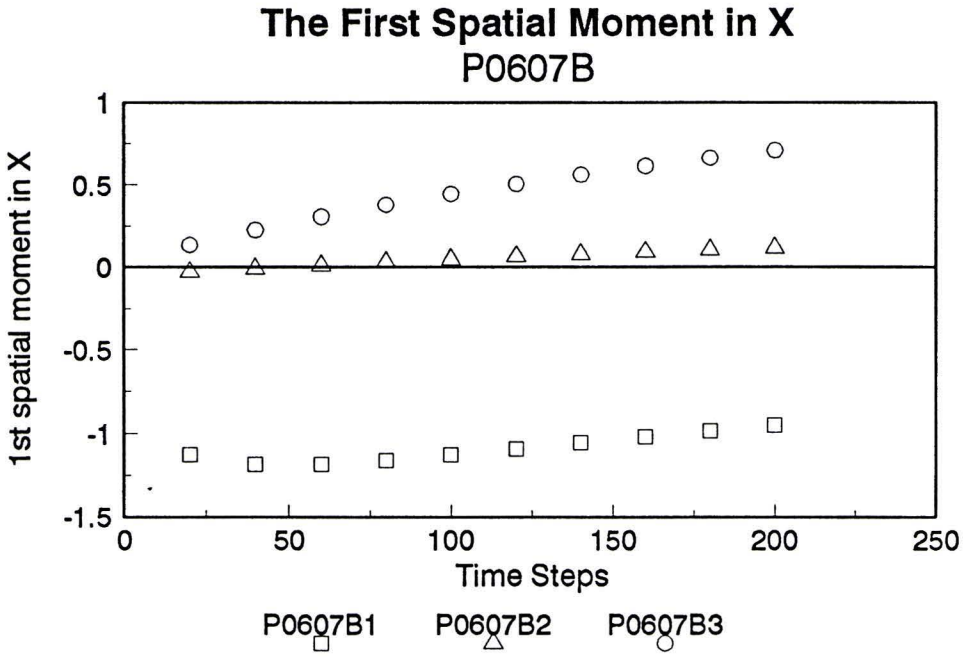

Fig. 3-11-A. The first spatial moments in x directions. Due to the heterogeneity, the center of the mass was not at the source (0,0).

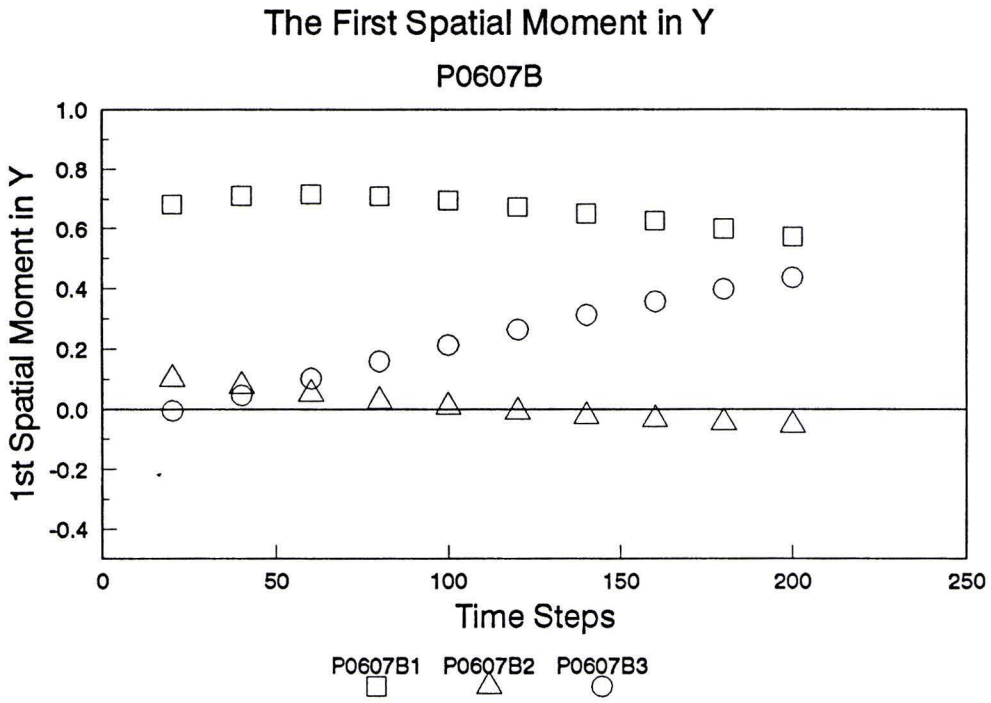

Fig. 3-11-B. The first spatial moments in y directions. Due to the heterogeneity, the center of the mass was not at the source (0,0).

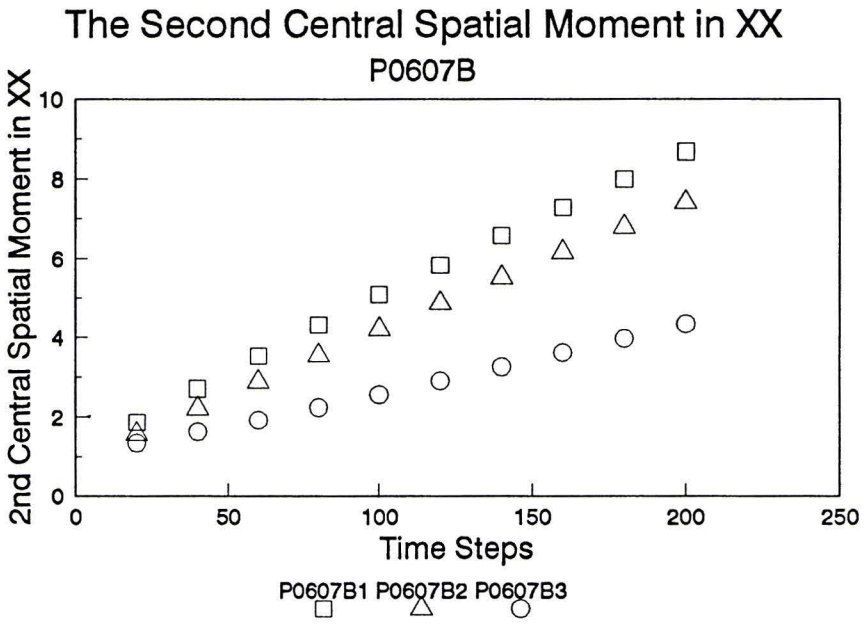

Fig. 3-12-A. The second central spatial moments in xx direction. The second moment is related to the spreading characteristics of the transport processes.

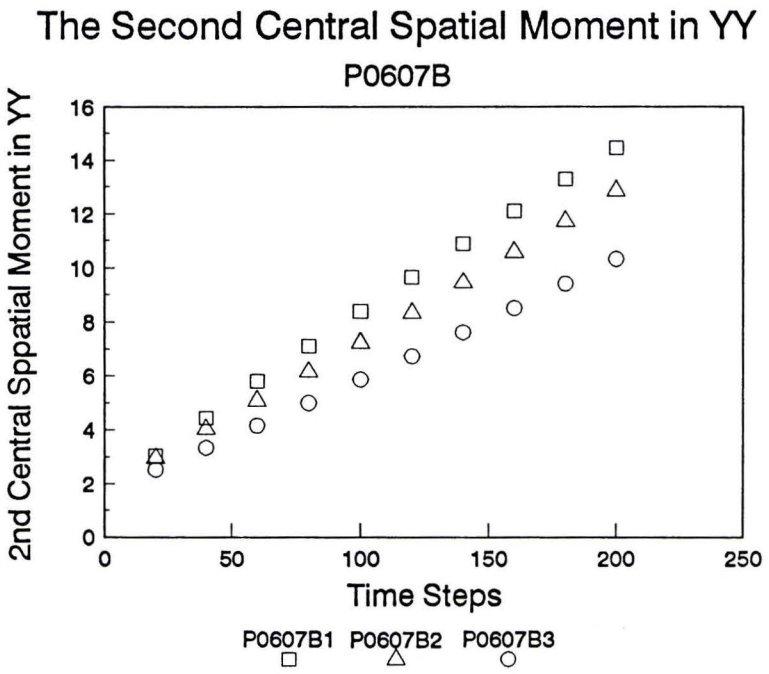

Fig. 3-12-B. The second central spatial moments in yy direction. The second moment is related to the spreading characteristics of the transport processes.

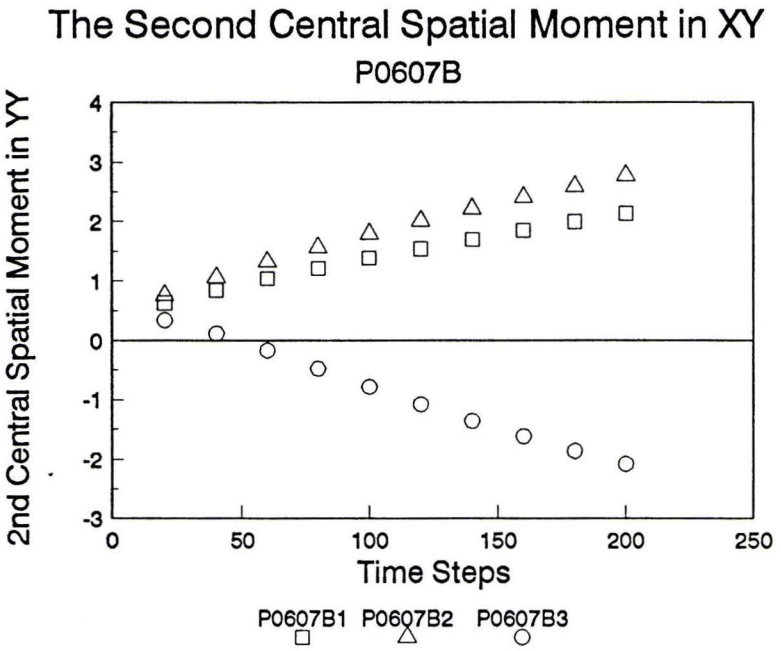

Fig. 3-12-C. The second central spatial moments in xy direction. The second moment is related to the spreading characteristics of the transport processes.

to discuss the asymptotic behavior of diffusion in heterogeneous medium, the slopes of the second central spatial moments became stable after 40 time steps (the slope of the second central spatial moment is proportional to the apparent diffusion coefficient). In other words, the apparent diffusion coefficient became almost a constant (time independent) after 40 time steps. Considering the complex appearance of the diffusion profile (Fig. 3-10), this stability of the second central moments is quite remarkable (this also means the insensitivity of the second spatial moment to the detailed spreading pattern).

Based on the spreading patterns (asymmetry, complex pattern), and the spatial moments (apparent drift, the anisotropy effect, i.e. the directional dependence of the spatial moments, and the differences between the realizations), the apparent heterogeneity effect seems to persist at much larger scale than the correlation scale of a few cells. To understand how the semi-variogram is related to solute transport phenomena, it is important to realize that a semi-variogram is an ensemble averaged measure of spatial correlation structure based on linear distance. Therefore, every spatial point in the medium has roughly the same statistical weight (although it depends on the number of points with distance "h" from the spatial point of interest), and the distance is measured only by the linear distance. On the other hand, the space explored by the solutes is dictated by the location of the source (point or non-point), the accessibility of the region for the solutes, the easiness of the access (e.g. the solutes generally moves from low diffusion coefficient region to high diffusion coefficient region, or the heterogeneity

induced drift), and so on. Therefore, even when the source is non-point, the statistics of the space that the solute see can be quite different from the statistics of the medium itself .

These simulations demonstrated how diffusional transport processes in spatially-heterogeneous medium with complex boundary condition can be modeled using the discrete Markov chain model. The simulation demonstrated the very complex features of diffusional transport processes in a heterogeneous medium. While the approach based on partial differential equation is elegant, the representations of complex geometries (the spatial variability/boundary condition) with smooth functions are extremely difficult. Accurate mathematical techniques are definitely essential to predict transport process in complex, heterogeneous media. Nevertheless what is lacking more is the precise information about the characteristics of the media. Though this chapter is devoted to the mesoscopic diffusional transport in heterogeneous media, a similar approach can be applied to the large-scale convective-dispersive transport in heterogeneous system.

Desorption Kinetics

In this section, the desorption of solute from a hypothetical mesoscopic heterogeneous sorbed phase which has spatially variable diffusional characteristics (self-transition densities) and complex boundary conditions will be simulated using the discrete Markov chain model. The main purpose of this simulation is to investigate the possible mechanisms for the rate-limiting desorption kinetics of

hydrophobic organic solutes from sorbed phase to the solution phase. As exemplified by the two-site/region model, the sorption/desorption process is often modeled with a discrete number of domains which are kinetically fast (nearly instantaneous) or slow (rate-limiting) at the time-scale of interest.

The slow kinetics are generally attributed to the diffusional transport of the solute either in organic matter or in narrow pores (Rao et al., 1980; Brusseau and Rao, 1989). Many mathematical models do not differentiate such processes (Nkedi-Kizza et al., 1984), and a careful experimental design is required to investigate these processes. While these mathematical models give semi-quantitative measure of the sorption/desorption kinetic characteristics, in reality, the sorbed phase most likely consists of energetically/geometrically heterogeneous matrix whose kinetic characteristics vary from instantaneous to extremely slow in continuous fashion due to various constraints. The experimental verification of the kinetic processes inside the sorbed phase are very difficult since 1) there exists a high degree of complexity, and 2) the process is in molecular to mesoscopic level which cannot be measured directly at macroscopic level. Therefore, most of our investigation has been limited to the approach of "looking at the sorbed phase from outside". However, it is still possible to simulate the mesoscopic structure of sorbed phase from our best knowledge, and study the possible kinetic processes which may occur in such sorbed phase, i.e., "looking inside the sorbed phase."

To effectively study the impact of the heterogeneity, it is essential to come up with a hypothetical medium which possesses the representative features of

heterogeneous media which affect the desorption behavior. It was hypothesized that slow desorption kinetics are caused by:

(1) the existence of long tortuous paths (the complex boundary condition effect)

(2) the existence of low diffusion coefficient sites which trap solutes (the effect of spatially heterogeneous diffusion characteristics)

Furthermore, the comparisons of the simulation with an idealized diffusion model and a mass transfer model were desired. Based on these considerations, the following modifications of the program P0607BM.C were made.

(1) a near circular sorbed phase

(2) more impermeable regions to create tortuous paths

To create the medium, the impermeable cells were placed first and aggregated, followed by the permeable cells with lower to higher self-transition probabilities. After the aggregation, a disc of 11 unit-cell-length radius was selected (Fig. 3-13). The frequency distribution of the self-transition numbers is given in Fig. 3-14. Note that there are a few paths which run across the sorbed phase. Since the transport to any 4 diagonal neighbors is not permitted, a path is connected as long as there exists at least one immediate neighbor. The self-transition number for the solution

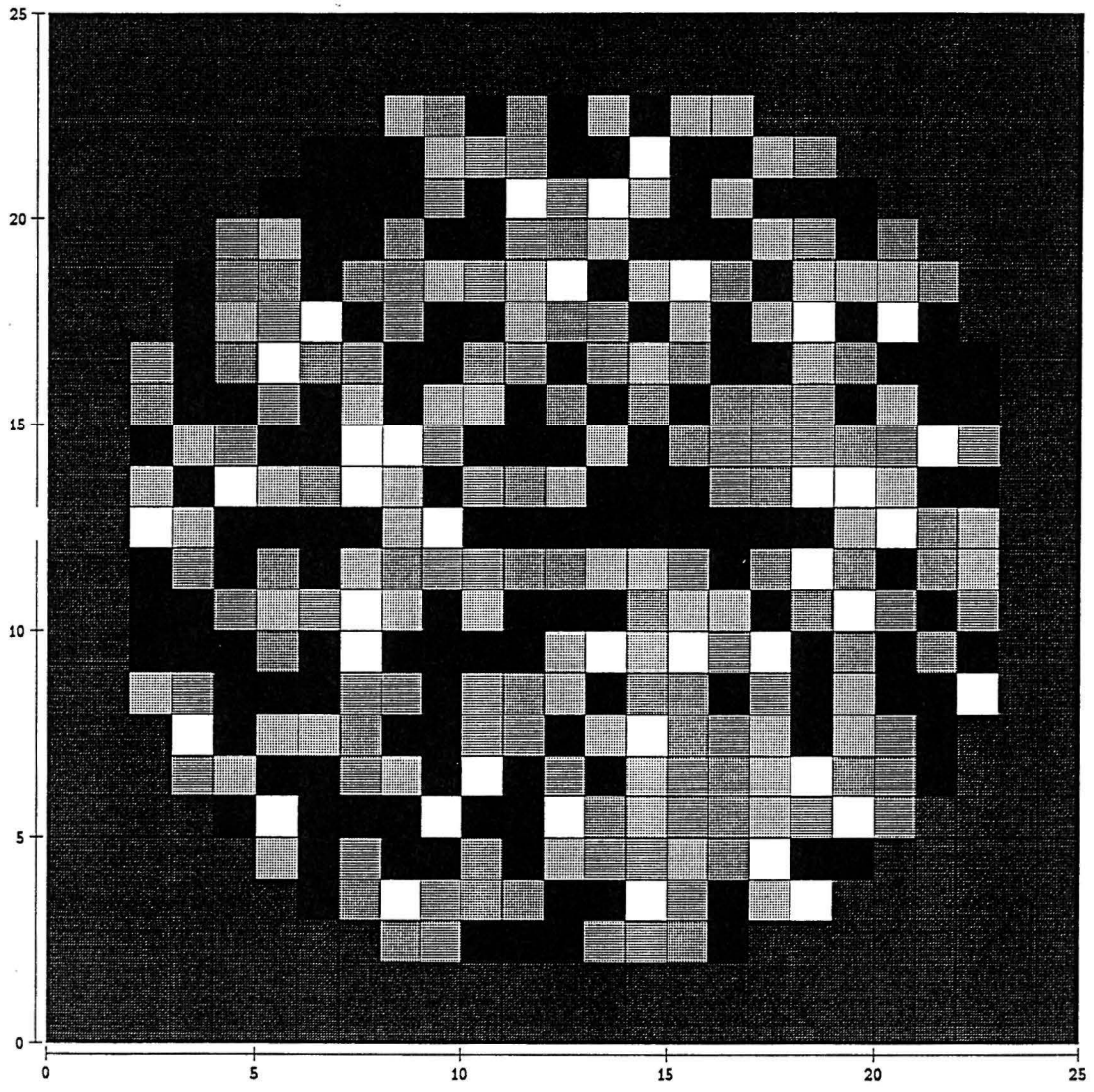

Fig. 3-13. A realization of near-spherical, hypothetical sorbed phase with spatially variable diffusional characteristics. Lighter region has higher self-transition number (lower diffusion coefficient).

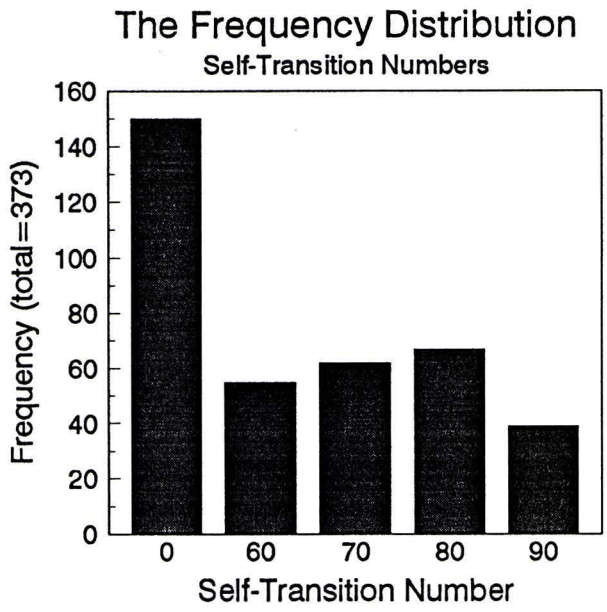

Fig. 3-14 The frequency distribution of the self-transition numbers of the medium given in Fig. 3-13.

phase (outside of the sorbed phase) was set to be 20 during the adsorption experiment, and then changed to 100 (trap) during the desorption experiment to eliminate any sorption of desorbed solute back to the sorbed phase.

Desorption kinetics were simulated as follows. At first, the sorbed phase was immersed into the solution phase (outside of the sorbed phase) where the probability of finding the solute in the solution phase was set to be uniform. This process corresponds to the sorption process which was required to establish the initial (near-equilibrium) distribution of the particles for the desorption study. The sorption from the solution phase was necessary to ensure that: 1) only the permeable cells accessible from the solution phase are occupied by the solute (There are permeable cells which are not accessible from the solution because they are surrounded by impermeable cells), and 2) The distribution of the solute particles mimics the actual thermodynamic equilibrium where the chemical potential in each cell is the same. Initially, there was no solute inside the sorbed phase. As the sorption proceeded, the probability of finding the solute inside the sorbed phase increased. At 1000 time steps, the change in the solute distribution in the sorbed phase became small (Fig. 3-15).

To initiate the desorption study, the distribution of the first order density inside the sorbed phase was recorded, and the total first-order density was renormalized to zero for the sorption phase. In the desorption simulation, the release of the solute from the sorbed phase to the solution phase was considered where the solution phase first order density was kept zero. When the concentration

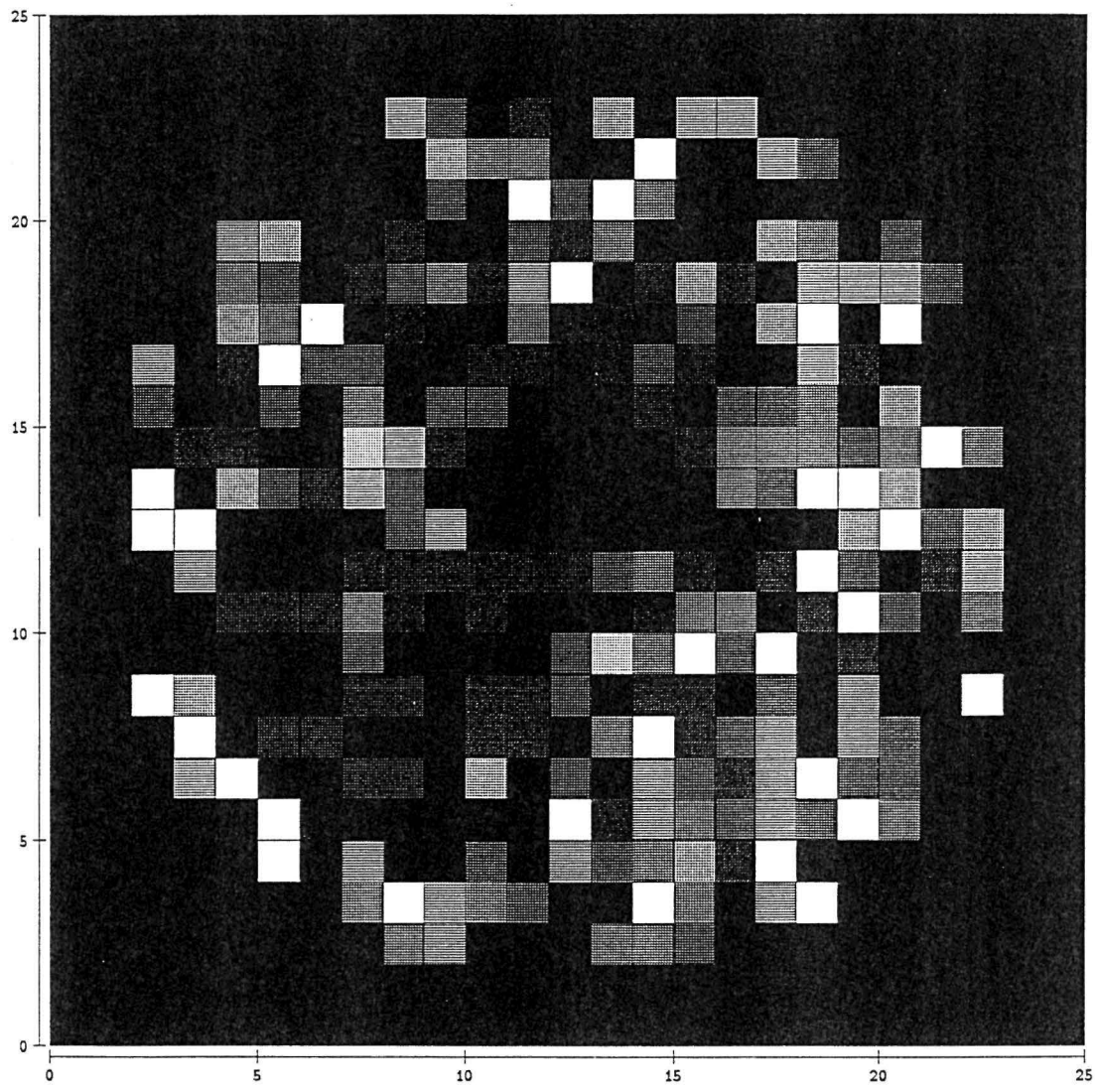

Fig. 3-15. The first-order probability density distribution (the concentration profile) at 1210 time-steps. The lighter the color, the higher is the probability (concentration). This is near equilibrium configuration.

of the solute in the solution phase is finite, the experimentally observable quantity is the apparent sorption/desorption kinetics which is the difference of the adsorption rate and the desorption rate. Zero concentration (zero first-order probability) boundary concentration essentially eliminates the adsorption from the solution phase to the sorption phase, and singles out the desorption process. The statistics of our interest is the probability that the solute traverses the interface between the sorbed phase and solution phase for the first time at time t (the first passage time) given the particle was inside the sorbed phase at time 0. If the first passage time probability, $p[x_b(t) \mid x_o(t=0)]$, is defined as the probability of crossing the boundary at location x_b at time t given the particle was located at location x_o inside the sorbed phase at time 0, the desorption probability becomes

$$\iint p[x_b(t) \mid x_o(t=0)]\ p(x_o)\ dx_o\ dx_b \qquad (3\text{-}105)$$

where the integrals are over the sorbed phase, x_o, and over the sorbed phase/solution phase boundary, x_b. In practice, the zero boundary condition was attained by placing a "trap" at the boundaries, x_b. A trap has the self transition probability of one. Therefore, once the particle moves to the trap, it cannot move out from the trap. The result of this simulation is given in Fig. 3-16 and 3-17.

Comparisons with Conventional Models

There are many models of desorption kinetics. To investigate the validity of these models, the result of the desorption simulation was compared with a few common models. The simulation mimics the desorption of a solute from two-

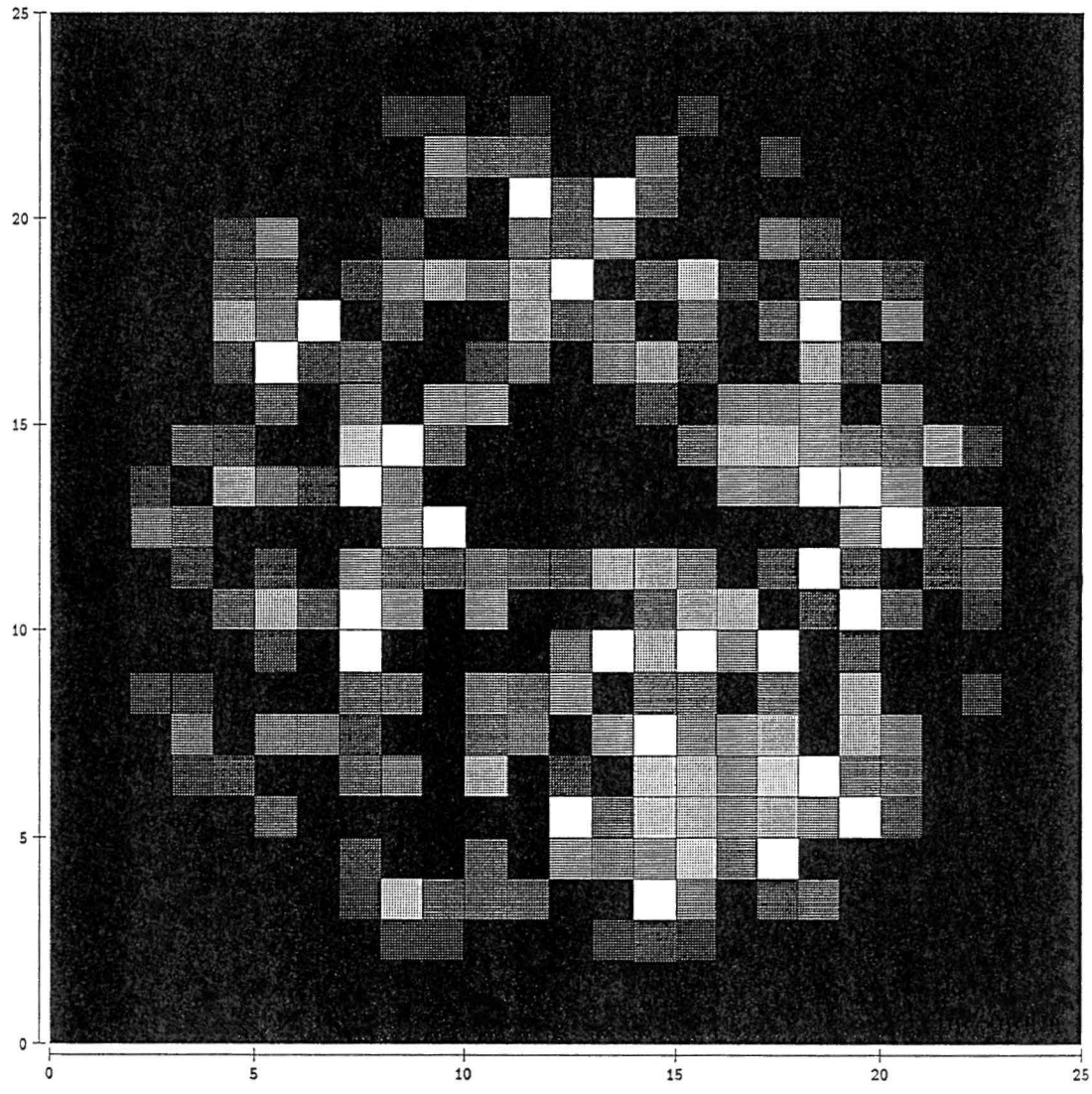

Fig. 3-16-A The result of the desorption simulation at 22 time steps. The lighter the color, the higher is the concentration. At this stage, approximately 85 % of the initial mass is left in the sobbed phase.

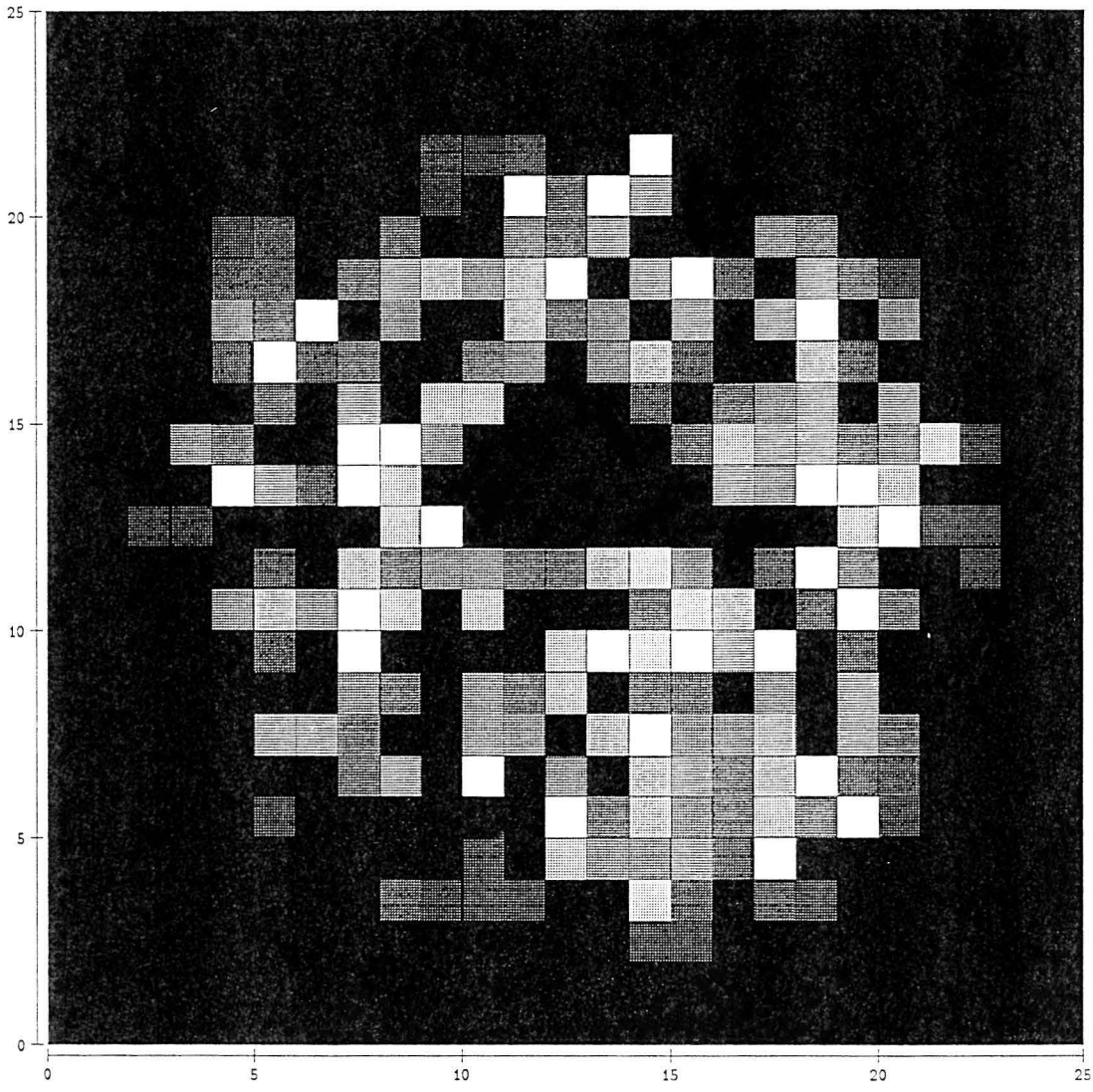

Fig. 3-16-B The result of the desorption simulation at 121 time steps. The lighter the color, the higher is the concentration. At this stage, approximately 70 % of initial mass is left inside the sobbed phase.

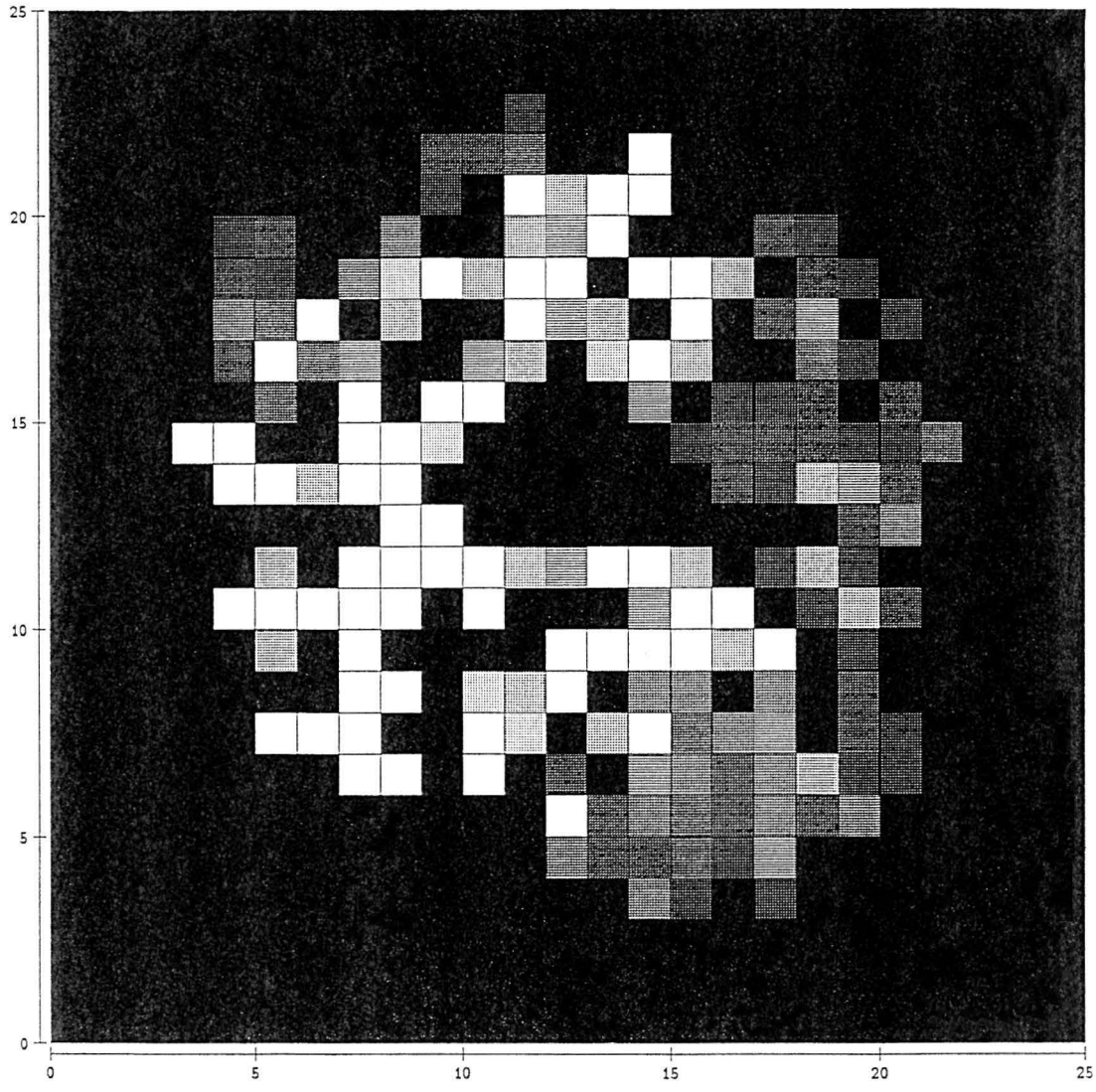

Fig. 3-16-C The result of the desorption simulation at 1210 time steps. The lighter the color, the higher is the concentration. At this stage, approximately 30 % of the initial mass is left in the sobbed phase.

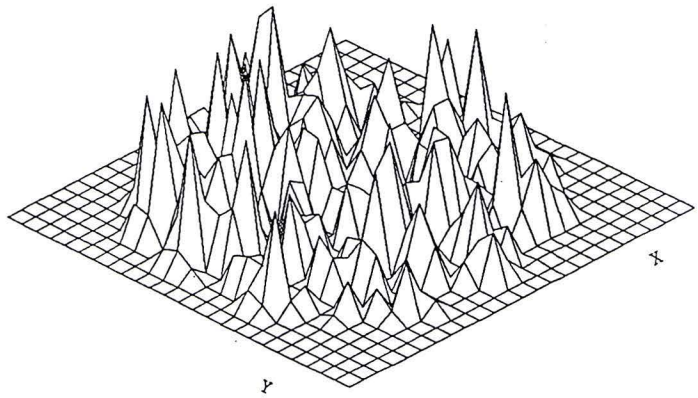

after 22 time steps

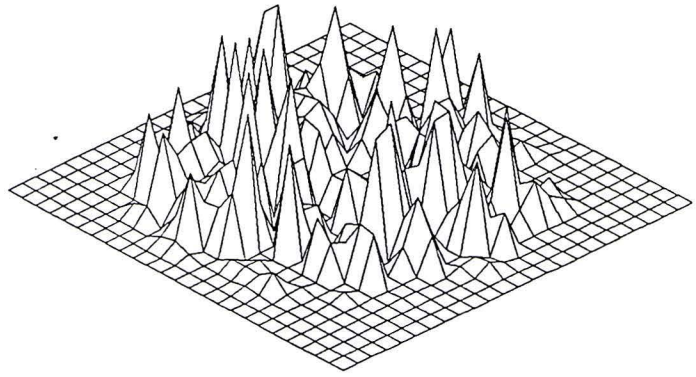

after 121 time steps

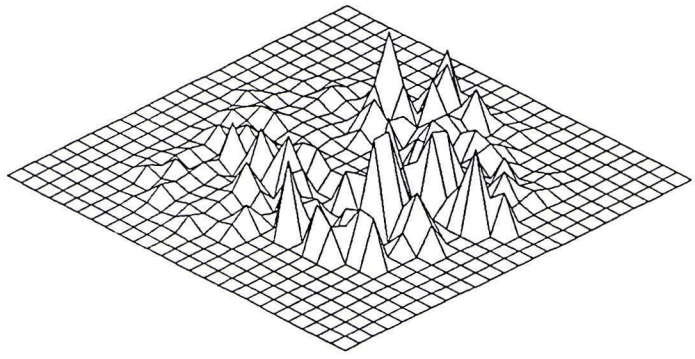

after 1210 time steps

Fig. 3-17. The 3-D representation of desorption processes. The height represents the concentration (the first-order probability density). The corresponding medium is given in Fig. 3-13.

dimensional porous sorption phase to the solution phase where the desorbed solute is immediately stripped away from the boundary.

The Mass Transfer Model

The mass transfer model generally assumes that the difference between the solution phase concentration and the sorbed phase concentration is linearly related to the sorption/desorption kinetics via a kinetic rate constant. For this simulation, the mass balance equation can be directly translated to the probability balance equation

$$\frac{dP^{sorbed}}{dt} = k\,[P^{solution} - P^{sorbed}] \qquad (3\text{-}106)$$

The sorption phase probabilities are considered to be uniform in the sorption phase. In this special case with zero boundary condition, the two-domain (sites/regions) model also simplifies to the desorption mass transfer model. The two-domain model assumes that there are two different regions/sites for sorption/desorption. One of them is essentially in instantaneous equilibrium with the solution phase, and the other is kinetically slower which is usually written as reversible first order sorption (Brusseau and Rao, 1989) as

$$\underset{solution}{\overset{equil.}{\rightleftharpoons}}\ domain\ 1 \underset{k_2}{\overset{k_1}{\rightleftharpoons}}\ domain\ 2 \qquad (3\text{-}107)$$

However, the zero solution phase concentration makes the concentration in the domain 1 to be zero throughout the simulation. Therefore, the only pertinent process is the desoption of solute from domain 2 to domain 1.

Diffusion Model

The diffusion model assumes the concentration gradient inside the sorbed phase as the driving force for the sorption/desorption kinetics. Since the shape of the sorbed phase and the distribution of the diffusion coefficient inside the sorbed phase are not known in ordinary macroscopic column scale experiment, the sorbed phase is often simplified as a spherical, uniform medium with corresponding effective diffusion equation. For the two-dimensional desorption simulation conducted in this research, however, the most pertinent model is the two-dimensional radial diffusion with zero concentration boundary condition and uniform concentration initial condition.

The governing equation is

$$\frac{\partial p(x,t)}{\partial t} = \frac{1}{r}\frac{\partial}{\partial r}\left[r\, D_{eff} \frac{\partial p(r,t)}{\partial r} \right] \qquad (3\text{-}108)$$

$$p(r,0) = p_o \qquad 0 < r < a \qquad (3\text{-}109)$$

$$p(a,t) = 0 \qquad 0 \le t \qquad (3\text{-}110)$$

The analytical solution of this partial differential equation is (Crank, 1975)

$$p(x,t) = \sum_{n=1}^{\infty} A_n J_o(\alpha_n r)\exp[-D_{eff}\alpha_n^2 t] \tag{3-111}$$

$$A_n = \frac{p_o \int_0^a J_o(r\alpha_n)\,dr}{\int_0^a r[J_o(r\alpha_n)]^2\,dr} \tag{3-112}$$

where $J_o(x)$ is the Bessel function of the first kind of order zero. α_ns are the roots of the Bessels function

$$J_o(a\alpha_n) = 0 \tag{3-113}$$

However, the experimentally measurable quantity is the overall desorption kinetics. The fraction of the mass, or the cumulative probability which has left the boundary at time t is given by (Crank, 1975)

$$\frac{F(t)}{F(\infty)} = 1 - \sum_{n=1}^{\infty} \frac{4}{a^2\alpha_n^2}\exp[-D_{eff}\alpha_n^2 t] \tag{3-114}$$

$$F(t) = 1 - \int \int_{x^2+y^2=r^2<a^2} p(x,y,t,r)\,dx\,dy \tag{3-115}$$

and $F(\infty) = 1$. Non-linear fitting programs were developed to fit the result with these two models.

The Results of Desorption Kinetics from Heterogenous Sorbed Phase

Figure 3-18 shows the total probability of finding the particle inside the sorbed phase as the function of time steps along with the best-fit diffusion and mass transfer model. The mass transfer model did not capture the simulation result well. On the other hand, the diffusion model seems to be adequate to model the overall desorption behavior. The close comparison of the simulation with the best-fit diffusion (D_{eff} = 0.0176±0.0002) model showed that the simulation has slightly faster initial desorption followed by slower kinetics. The reason for this kinetic behavior may be explained from the geometrical factor as well as the energetic factor. The geometrical factor influence the distribution of the diffusion path (tortuosity). There are a few paths which have very tortuous paths which seems to influence the slow desorption kinetics. The slow kinetics are also affected by the release from the local domain where the self-transition probability is high (i.e. lower diffusion coefficient) due to the energetic heterogeneity. Figure 3-16 shows the concentration profile during the desorption process at time steps 55. A significant amount of solutes exists at the lower right quadrant. After the 1210 time steps (Fig. 3-16), the solute left from the lower right quadrant, but was remaining in the narrow path region (left side).

The Effect of the Boundary Conditions

As depicted in Fig. 3-17 (3-D graphs of the spatial-coordinate versus the first-order densities (concentrations)), when the self-transition numbers (i.e. the

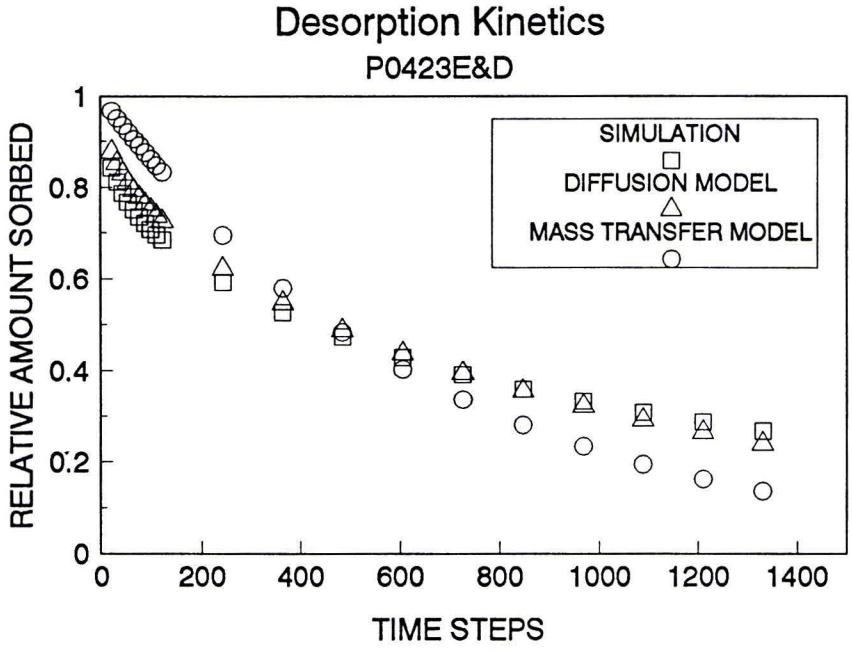

Fig. 3-18. The results of the desorption simulation. The relative mass in the sobbed phase is plotted against the time-steps. The mass-transfer model and the diffusion model were also fitted.

local diffusion coefficients) were spatially variable, the distribution of the solute inside the sorbed phase is strongly affected by the distribution of the self-transition numbers (Notice the sharp peaks of the concentration (the first order densities) at the high self-transition number cells). However, when the distribution of the self-transition number is turned off (uniform diffusion coefficient distribution), the desorption is determined by the diffusion path length, i.e. the distance from the solution phase (Fig. 3-19). To examine the effect of permeable space structure (the boundary or the diffusion path length effect) independent of the effect of the spatial variability of the self-transition numbers, the average self-transition number of the permeable space (the self-transition number of 74.0) was assigned to the permeable cells inside the sorbed phase. In this simulation, therefore, the self-transition numbers in the permeable cells were all 74.0. The computer desorption experiment was conducted on this medium. The desorption curve (Fig. 3-20) was very close to the desorption curve of the medium with the spatially-variable self-transition number, and was even closer to the diffusion model. Based on these desorption simulations, it was found that the distribution of solutes inside the sorbed phase (Fig. 3-21, Fig. 3-22) is influenced by both the structure of the permeable space as well as the distribution of the self-transition numbers. It was also evident that, despite the complex appearance of diffusion profile inside the sorbed phase, the overall desorption kinetics (the total mass of solutes coming out from the sorbed phase) is quite insensitive to the local heterogeneity of the diffusion path length (the boundary condition) and the spatially-variable

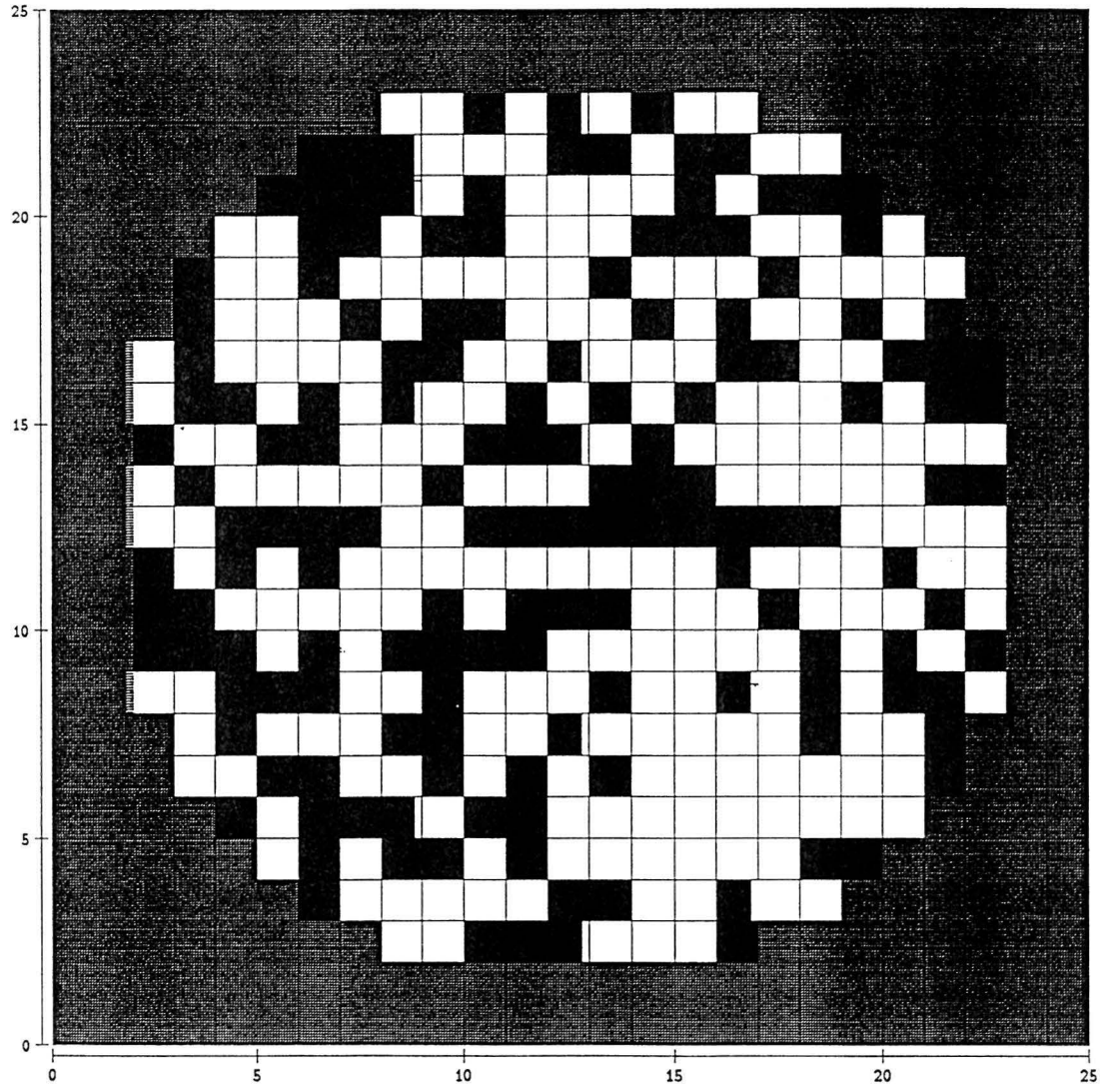

Fig. 3-19. A realization of the two dimensional, circular, sobbed phase with uniform self-transition (diffusion) characteristics. The spatial distribution of the impermeable cells are identical to the medium in Fig. 3-13. However, the self-transition numbers (the permeable space) are averaged to 74.0.

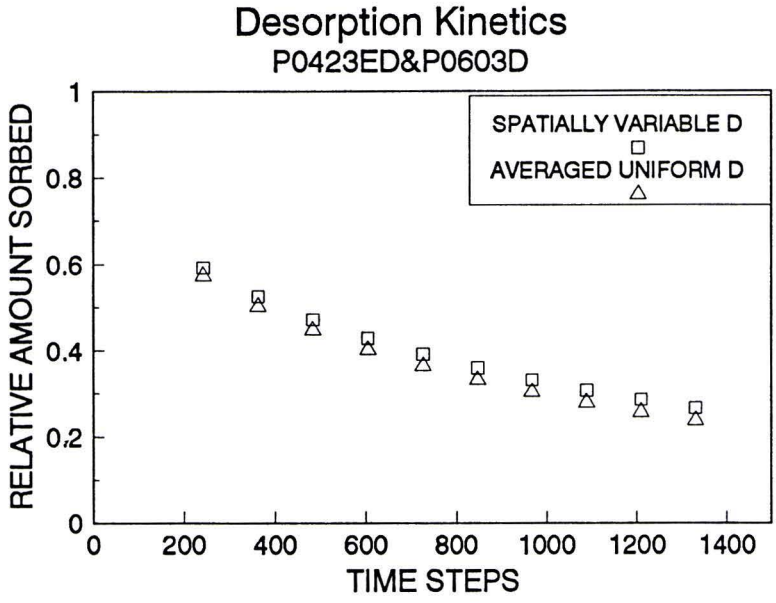

Fig. 3-20. The results of the desorption simulation. The relative mass in the sorbed phase is plotted against the time-steps. The results with (Fig. 3-13) and without (Fig. 3-19) the spatial distribution of the self-transition numbers are shown here.

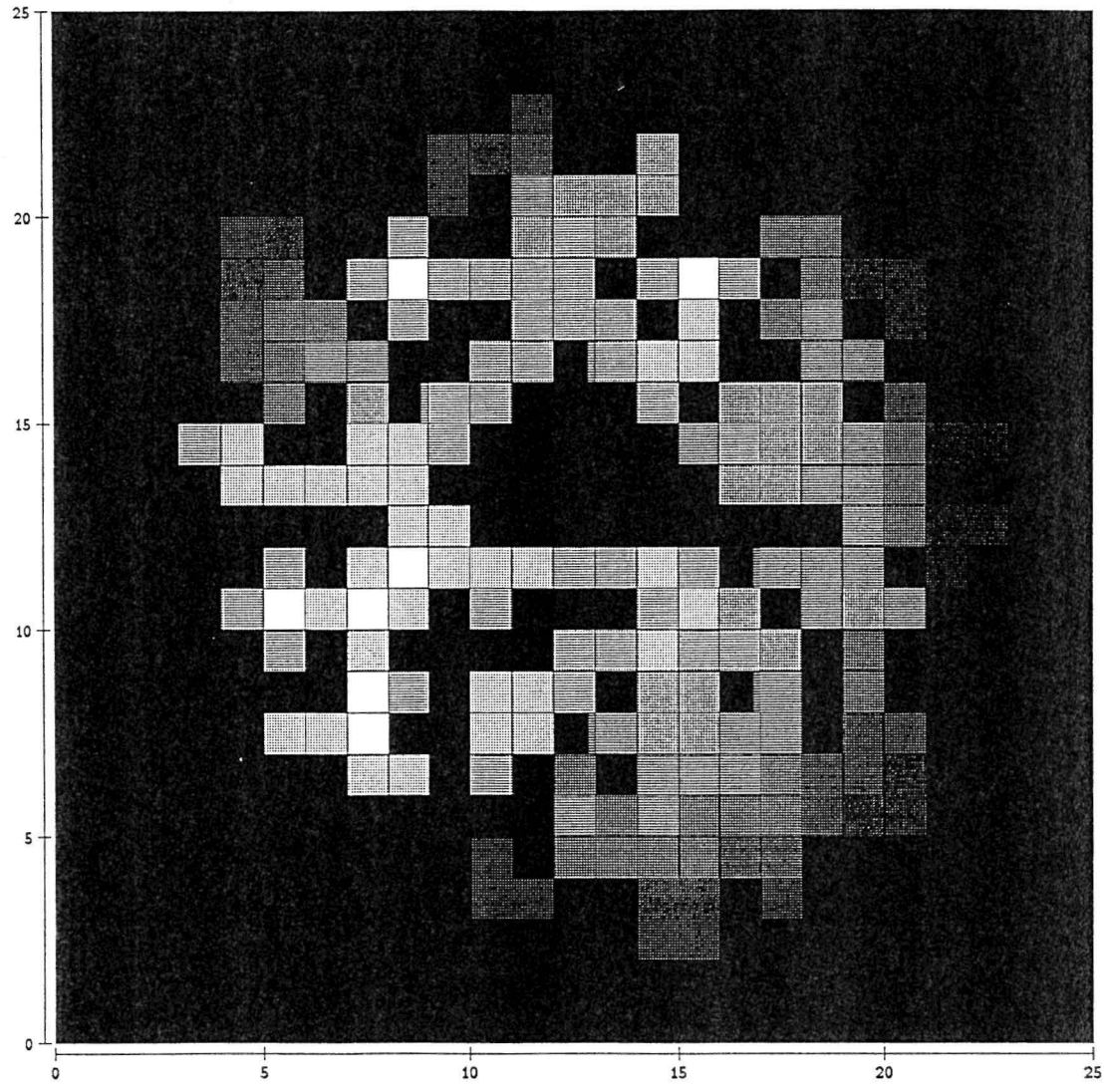

Fig. 3-21-A. The result of the desorption simulation at 242 time steps. The lighter the color, the higher is the concentration. Approximately 60% of the initial mass is left in the sobbed phase.

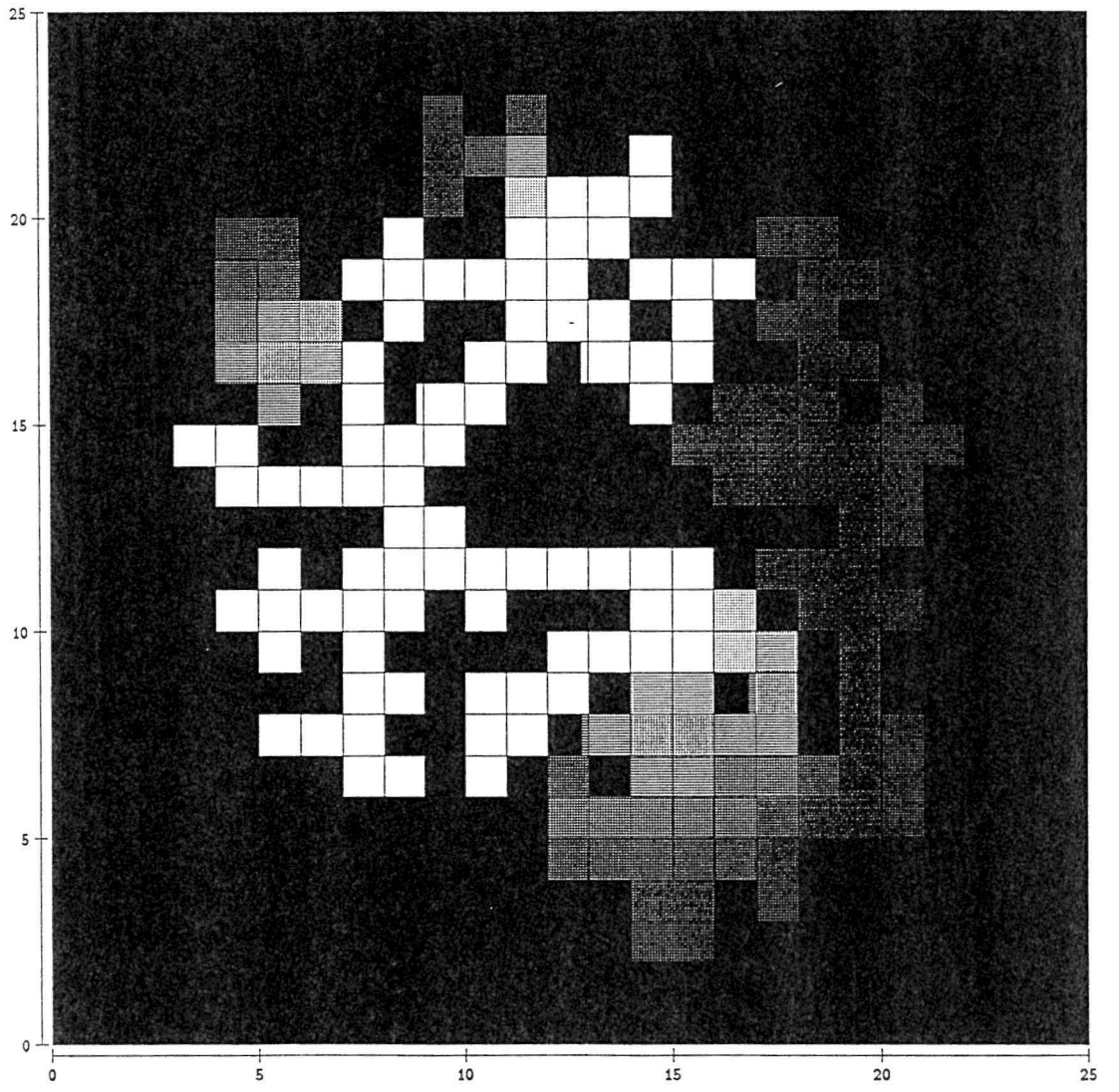

Fig. 3-21-B. The result of the desorption simulation at 1210 time steps. The lighter the color, the higher is the concentration. Approximately 30 % of the initial mass is left in the sobbed phase.

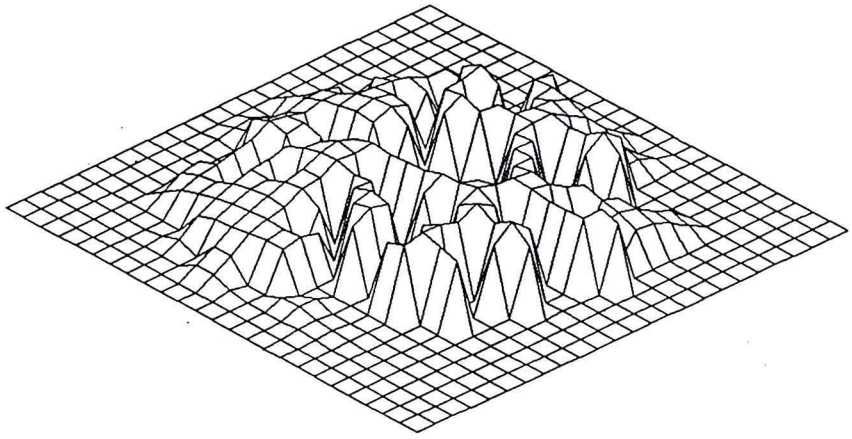

after 242 time steps

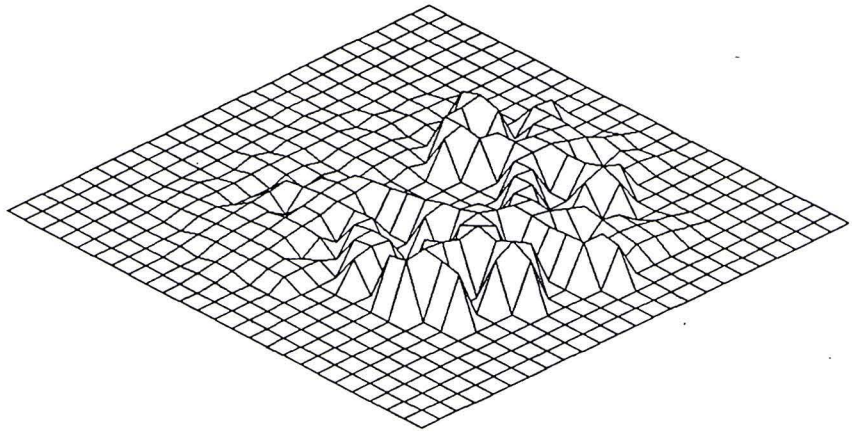

after 1210 time steps

Fig. 3-22. The 3-D representation of desorption processes. The height represents the concentration (the first-order probability density). The corresponding medium is given in Fig. 3-19.

self-transition numbers (diffusion coefficient). In these simulations, the heterogeneity effects seem to be rapidly averaged out at the macroscopic scale. This fact partially supports the approximation of actual desorption processes with idealized models, such as the diffusion model, or higher order mass transfer models (e.g. two site/region model). Furthermore, when the kinetics of the system consists of a series of local-scale nonequilibrium phenomena (diffusion), and when the overall kinetics exhibits a significant deviation from the idealized averaged model (diffusion model), the existence of extreme rate-limiting process (very long, tortuous path compared to other diffusion paths, and/or a local environment with extremely low diffusion coefficient compared to the other parts of the medium) can be expected. Therefore, the identifications of such rate-limiting processes become crucial to elucidate the overall desorption processes.

CHAPTER 4
CONCLUSIONS

In this dissertation, methods for describing complexity, and the means by which complexity affects the transport process were studied. It is extremely difficult to describe the complexity of natural systems in detail. However, depending on the need for the information of the heterogeneity (e.g. predicting the solute transport in field-scale heterogeneous media), various level of simplifications can be made.

In Chapter 2, sorption of vapors onto geometrically heterogeneous natural and synthetic sorbents were studied. One of the main objectives of this chapter was to describe geometrical heterogeneity of a natural sorbent surface in terms of a single parameter, known as the surface fractal dimension. To extract the information of the molecular level surface topology, equilibrium sorption isotherms of various probe molecules were used. Sorption is a process by which solute molecules interact with the sorbent in complex manner. The degree of the complexity of interaction is often overwhelming, and detailed theory is still limited to adsorption of simple solutes onto simple sorbents. However, it is possible to extract various information from sorption isotherms semi-quantitatively. In this research, molecules of different sizes were used as probes to explore the

molecular level surfaces of some natural and synthetic sorbents. Using the concept of surface fractal dimension, the surface roughness of the sorbents may be expressed in terms of the surface fractal dimensions, which is related to the functional dependence of the sorbent surface area (or the monolayer value) on the size of the probe. Roughly speaking, a high surface fractal dimension (close to 3) indicates highly convoluted surface, and low surface fractal dimension (close to 2) means the surface is nearly flat. Our goal is thus to experimentally determine the surface geometrical heterogeneity with the surface fractal dimension in a statistical sense.

The monolayer coverage method was thus adopted to investigate the surface fractal dimension. The monolayer coverage method estimates the surface fractal dimension from the functional relationship between the monolayer value, $N_m(\sigma)$ and the projected size of the probe, σ. The main difficulty in applying the monolayer coverage method arises from the difficulties of clearly defining and measuring or estimating the monolayer value, $N_m(\sigma)$, and the size of the probe molecule on the surface, σ.

In this research, three sorbents, kaolinite (KGa-1), silica-gel (SYLOID 244), and Borden aquifer sand were investigated. It was found that the estimation method for σ values also affected the fractal dimension significantly. Using the σ values estimated from the liquid density method, the surface fractal dimensions of KGa-1 and SYLOID 244 were 2.18 ± 0.09 and 2.56 ± 0.26, respectively. There is considerable uncertainty associated with the surface fractal dimension measured

with the monolayer coverage method. Therefore, in addition to the statistical character of the fractal dimension as the averaged measure of the surface roughness, the experimental uncertainty of at least ± 10 % should be reckoned in estimating the surface fractal dimension. Nevertheless, based on the knowledge of structures of the kaolinite and silica-gel, and based on the reported fractal dimensions of similar sorbents, the experimentally measured fractal dimensions seem to reflect the actual surface roughness quite well. The application of the same technique to a natural aquifer sand, Borden aquifer material, was not successful. The reasons were attributed to the compounded effects of irreversible sorption, hysteresis, the alteration of the surface characteristics by the impacts of sorption (penetration) of the probe, etc. The experimental difficulties of the surface fractal dimension may be minimized by adopting different measurement techniques (e.g. SAXS), and by characterizing the dimension in an integrated way.

In Chapter 3, transport processes in a heterogeneous medium were considered. The Langevin equation, the Fokker-Planck equation, and the Chapman-Kolmogorov equation were considered as fundamental approaches to solute transport processes. The relationship between these methods was clarified. Using the discrete Markov chain model, solute transport in a heterogeneous medium can be, in principle, simulated. In the Markov chain model, the driving force for the transport process, which is approximately proportional to the gradient of the thermodynamic intensive variables, is incorporated into the transition

probability matrix. In this dissertation, the detail of the transport mechanisms, i.e., mass, momentum, and energy balance, was not studied. Instead, the overall local dynamics of transport processes were approximated with Markovian transition probabilities. Accordingly, we assigned the estimated transition probability which lumps the detailed local transport dynamics parameters such as the average local convective flux, the local dispersion coefficient, and other parameters related to the higher local moments. The solute transport process can be derived by solving a matrix equation without conducting time consuming random-walk simulations.

In Chapter 3, the diffusional transport of hydrophobic organic solutes inside the sorbed phase was simulated in a hypothetical, two-dimensional, heterogeneous, porous medium. The hypothetical realizations of porous media were created using modified diffusion-limited-aggregation (DLA) type logic. It is not certain whether such a model can mimic a real mesoscopic porous medium like soil organic matter phase. However, the simulation of solute transport process in such a hypothetical heterogeneous medium can provide some insight into the actual transport processes in heterogeneous media. Spatial moment analysis was conducted to statistically characterize the transport processes. The discrete Markov chain model was also applied to scrutinize the desorption kinetics from a heterogeneous sorbed phase. A two-dimensional, circular heterogeneous sorbed phase was created using the modified DLA logic. Followed by adsorption from the surrounding bulk phase to the equilibrium configuration, the desorption of solute to zero concentration bulk phase was investigated. This simulation was compared

to the analytical solutions of the averaged diffusion model and the first-order mass transfer model. The result of the simulation could be adequately described with the diffusion model. However, the mass transfer model could not capture the desorption behavior well. The effect of the spatially variable self-transition numbers on the overall desorption characteristics was studied by replacing the spatially variable self-transition numbers in the permeable space with the statistical average value (spatially homogeneous). In this particular case, the overall desorption kinetics was not markedly influenced by the averaging of the self-transition numbers in the permeable space.

From the simulations in Chapter 3, it was concluded that the local transport process can be strongly influenced by the heterogeneity of the system. However, the overall, macroscopic transport parameters, such as the apparent diffusion coefficient (the second central moments), are reasonably stable due to the rapid averaging of heterogeneity effects over the time and space.

APPENDIX A
SORPTION ISOTHERM EQUATIONS

In macroscopic thermodynamics, the macroscopic phenomena are explained in terms of energy which comprises of various pairs of macroscopic internal variable and macroscopic external variable. However, to estimate the molecular level phenomena, in principle, we have to invoke some kind of microscopic mechanistic model. In this section, we will examine the B.E.T. isotherm equation from rather theoretical point of views. We will rely extensively on the B.E.T. isotherm equation to obtain the fractal dimensions of the sorbents. However, the applicability of the B.E.T. equation has not been discussed thoroughly. Therefore, this subsection is devoted for the understanding of the underlying picture of the B.E.T. theory.

The theoretical understanding of physisorption of monolayers of pure gases on homogeneous solids is now at a fairly rigorous molecular-statistical mechanics level. However, in spite of the significant progress, physical adsorption on heterogeneous solids remains unsolved problem. From the experimental point of view, the adsorption of single vapor still remains one of the best tools to obtain various surface characteristics such as surface area and pore distribution.

The Derivation of Langmuir and B.E.T. Equation

In this section, the B.E.T. equation will be derived from kinetic as well as the statistical mechanical models. While how the B.E.T. equation can be derived is an interesting academic exercise, the more interesting part is that the same equation can be derived from different physical models. This fact indicates that even the observed results can be explained with the proposed mechanistic model very well, the true physical nature of the system should be interpreted carefully.

In 1938, Langmuir derived an adsorption isotherm equation from the rates of evaporation and of condensation. The surface is assumed to consist of a certain number of sites S of which S_1 are occupied and $S_0 = S - S_1$ are not occupied. The rate of evaporation is taken to be proportional to S_1, and the rate of the condensation proportional to the bare surface S_0 and to the gas pressure P. At equilibrium, the rate of evaporation and the rate of condensation are equal

$$k_1 S_1 = k_2 P S_0 = k_2 P(S - S_1) \qquad \text{(A-1)}$$

Then

$$\theta = \frac{S_1}{S} = \frac{bP}{1+bP} \qquad \text{(A-2)}$$

where $b = k_2/k_1$ is the ratio of rate coefficients. This is the Langmuir equation.

The B.E.T. equation is essentially an extension of Langmuir equation to multilayer system. Let us denote S_i for the part of the surface which is covered with

i layers of the adsorbed molecule. We assume that the heat of sorption to the first layer is Q_1, and for all succeeding layers, it is equal to Q_V.

At equilibrium, we have

$$a_1 P S_0 = b_1 S_1 e^{-Q_1/RT} \tag{A-3}$$

for the adsorption equilibrium between the bare surface and the first layer, and for the succeeding surfaces,

$$a_i P S_{i-1} = b_i S_i e^{-Q_i/RT} \tag{A-4}$$

For the first layer

$$S_1 = yS_0 \;\; ; \;\; S_2 = xS_1 \tag{A-5}$$

and for the rest

$$S_i = x^{i-1} S_1 = yx^{i-1} S_0 = cx^i S_0 \tag{A-6}$$

where

$$y = \frac{a_1}{b_1} P e^{Q_1/RT} \;\; ; \;\; x = \frac{a_i}{b_i} P e^{Q_i/RT} \tag{A-7}$$

and

$$c = \frac{y}{x} = \frac{a_1 b_i}{b_1 a_i} e^{(Q_1 - Q_i)/RT} \tag{A-8}$$

We calculate the number of lattice points occupied by the adsorbed solute as

$$\frac{n}{n_m} = \frac{\sum_{i=1}^{\infty} iS_i}{\sum_{i=0}^{\infty} S_i} = cS_0 \frac{\sum_{i=1}^{\infty} ix^i}{S_0 + S_0 c \sum_{i=1}^{\infty} x^i} \qquad \text{(A-9)}$$

Then

$$\frac{n}{n_m} = \frac{cx/(1-x)^2}{1+cx/(1-x)} = \frac{cx}{(1-x)[1+(c-1)x]} \qquad \text{(A-10)}$$

where $x = P/P_0$.

These derivations are based on kinetic arguments. However, it is preferable to develop a much rigorous molecular level statistical mechanical adsorption model which is consistent with the B.E.T. equation since the nature of the model is seen more clearly and it is not necessary to assume any kinetic mechanism. The derivation given by Hill (1986) will be followed here. According to this model, a surface has M independent, distinguishable, and equivalent sites, on each of which an indefinite number of molecules can be adsorbed in a vertical pile. The each sorption site is characterized by the uniform potential well in which the adsorbed molecule is trapped.

The grand partition function is defined as

$$\begin{aligned} \Xi(V,T,\mu) &= \sum_{j,N} e^{-E_j(N,V)/kT} e^{N\mu/kT} \\ &= \sum_{N} \left[e^{N\mu/kT} \sum_{j} e^{-E_j(N,V)/kT} \right] \\ &= \sum_{N} Q(N,V,T) e^{N\mu/kT} \end{aligned} \qquad \text{(A-11)}$$

where Q(N,V,T) is the canonical partition function for fixed N (number of the molecules), V (volume of the ensemble), and T (temperature). Then the probability that a grand canonical ensemble (in contact with thermal and chemical potential reservoir) contains N molecules and is in the energy state $E_j(N,V)$ is

$$P_j(N,V,T,\mu) = \frac{e^{-E_j(N,V)/kT} e^{N\mu/kT}}{\Xi(V,T,\mu)} \tag{A-12}$$

If there is a total of N molecules bound on the M sites, and the number of sites having s molecules bound is a_s, then the canonical partition function for the system of M(V) sites, Q(N,M,T), becomes

$$Q(N,M,T) = \sum_{\forall a} \frac{M! q(0)^{a_0} q(1)^{a_1} \cdots q(m)^{a_m}}{a_0! a_1! \cdots a_m!} \tag{A-13}$$

where q(s) is the site partition function when s molecules are bound to the site,

$$q(s) = q_0 q_1 q_2 \cdots q_s \tag{A-14}$$

where $q_0 = 1$ and $q_1, q_2, \ldots$ are the partition function for the bottom layer, the 2nd layer and so forth. The grand partition function is

$$\begin{aligned} \Xi(N,M(V),T) &= \sum_N Q(N,M,T)\lambda^N \\ &= \sum_{\forall A} \frac{M! q(0)^{a_0} [q(1)\lambda]^{a_1} [q(2)\lambda^2]^{a_2} \cdots [q(m)\lambda^m]^{a_m} \cdots}{a_0! a_1! a_2! \cdots a_m! \cdots} \end{aligned} \tag{A-15}$$

where

$$\lambda = e^{\mu/kT} \tag{A-16}$$

Using the multinomial theorem, the grand partition function can be written as

$$\Xi(M,T,\lambda(\mu)) = \xi(\lambda,T)^M \tag{A-17}$$

with

$$\xi = \sum_{s=0} q(s)\lambda^s = q(0)+q(1)\lambda+\cdots q(m)\lambda^m \tag{A-18}$$

The average number of the molecules in the macroscopic system is

$$\langle N\rangle = \lambda\left(\frac{\partial \ln \Xi}{\partial \lambda}\right)_{M,T} = M\lambda\left(\frac{\partial \ln \xi}{\partial \lambda}\right)_{T} \tag{A-19}$$

Therefore the average number of molecules per M sites, i.e. the fraction of the coverage, is

$$\theta = \frac{\langle N\rangle}{M} = \lambda\left(\frac{\partial \ln \xi}{\partial \lambda}\right)_{T} = \frac{\sum_{s=0} s\, q(s)\lambda^s}{\sum_{s=0} q(s)\lambda^s} \tag{A-20}$$

By substituting the partition function for each layer

$$\theta = \frac{q_1\lambda+2q_1q_2\lambda^2+3q_1q_2q_3\lambda^3\cdots}{1+q_1\lambda+q_1q_2\lambda^2+q_1q_2q_3\lambda^3\cdots} \tag{A-21}$$

At this point, we assume that the partition functions for the second and higher layers are the same, $q_2 = q_3 = \ldots$ and so on.

Then

$$\begin{aligned}\theta &= \frac{q_1\lambda(1+2q_2\lambda+3q_2^2\lambda^2+\cdots)}{1+q_1\lambda(1+q_2\lambda+q_2\lambda^2+\cdots)} \\ &= \frac{q_1\lambda}{(1-q_2\lambda+q_1\lambda)(1-q_2\lambda)} \\ &= \frac{cx}{(1-x+cx)(1-x)}\end{aligned} \tag{A-22}$$

where

$$\begin{aligned}c &= q_1/q_2 \\ x &= q_2\lambda = q_2 e^{\mu_d/kT} P = P/P_0\end{aligned} \tag{A-23}$$

This is the B.E.T equation.

From the kinetic model, it is impossible to see the molecular level picture of the B.E.T. model. However, based on the statistical mechanical derivation, it is obvious that this model is highly idealized and physically unrealistic. This is very interesting since the kinetic derivation appears to be acceptable in macroscopic scale. The model assumptions may be summarized as

(1) The sorption is reversible.

(2) The sorption is localized.

(3) The surface is flat.

(4) The sorption occurs vertically, and there is no horizontal interaction between the sorbed molecules.

(5) The heat of sorption between the bare surface and the sorbed molecule in the first layer is uniform across the surface.

(6) The heat of sorption associated with the successive multilayer formation is uniform and does not depend on the distance from the surface.

Gregg and Sing (1982) give extensive discussion of the validity of B.E.T. equation. A real surface probably differs from this idealized picture for

(1) energetic factor: the heat of sorption (the potential well) is not uniformly distributed, and there is horizontal interaction between the sorbed molecules.

(2) geometric factor: the surface is not flat.

The statistical mechanical derivation illustrated that it is desired to redevelop a model based on the molecular dynamics and statistical mechanics if the surface and the nature of solute-sorbent/solute-solute interactions are well characterized in the molecular level. Furthermore, it may become possible to relate various spectroscopic evidences with macroscopic sorption data in the future. The B.E.T. theory is clearly inadequate, and the parameters obtained from the B.E.T. equation inevitably entail ambiguities. However, it is impractical or impossible to characterize the surface of natural sorbent in such rigorous manner. Furthermore, the development of molecular level sorption theory from molecular dynamics or statistical mechanical argument is beyond the scope of this study which deal with complex surfaces.

As alternative approaches, potential theories, such as Polaynyi equation, D-R equation and F-H-H equation have also been investigated extensively. In potential theory, sorption is explained from the differential molar work of

adsorption. According to Dubinin's idea, the process involved is volume filling of the micropores rather than layer-by-layer adsorption on the surface (pore wall). However, to obtain the estimate of a specific surface area, the B.E.T. theory is at least qualitatively straightforward. Therefore, the modification of Langmuir or B.E.T. type treatments to account for the energetic and geometric heterogeneities have been also pursued. For example, when the heat of sorption is not uniform, we can incorporate the site energy distribution into the basic isotherm equation, θ(Q, P, T) as

$$\Theta(P,T) = \int_0^\infty \theta(Q,P,T) f(Q)\, dQ \qquad \text{(A-24)}$$

Unfortunately, it is difficult to determine the energy distribution independently. In general, the surface heterogeneity tends to mask the effect of monolayer completion, and the measured heat of sorption exhibits gradual change with the surface coverage (Gregg and Sing, 1982).

In addition to the energetic heterogeneity (jaroniec and Madey, 1988), when the surface is not flat, the other assumption made in Langmuir or B.E.T. equations will be violated. The focus of this study is on the geometric heterogeneity, i.e. then sorption on rough surfaces. In fact there is few general models which can account for the geometric heterogeneities of the sorbents. The difficulty of the geometric heterogeneity is the mathematical description of such geometric heterogeneity. For the heterogeneity associated with the energy, it is probably possible to adopt the concept of Boltzmann distribution which relates the probability of finding a particle

in different energy states, along with the p.d.f. of the energy distribution. On the other hand, there has been no simple parameter to represent the geometrical heterogeneity before the theory of fractal dimension. However, as we saw in the previous section, the development of fractal theory seems to enable us to parameterize the geometrical heterogeneity. Several investigators have proposed modified B.E.T equations for fractal surfaces. In the B.E.T. theory, the amount of the solute sorbed per unit mass of the sorbent was estimated from the monolayer value, N_m, the energetic term, C, and the partial pressure of the solute at the given temperature. In addition to these parameters, in fractal isotherm equations, the fractal dimension, D, also determines the sorption characteristics. For example, Fripiat et al. (1986) assumed a law for the ratio of the moles in the ith layer (n_i) to moles in the first layer (n_1), n_i/n_1, to be approximately equal to $i^{-(D/2)}$. They derived an expression

$$\frac{N}{N_m} = \frac{C\sum_{i=1}^{n} i^{2-D} \sum_{j=1}^{n} x_j}{1 + C\sum_{i=1}^{n} x^i} \qquad \text{(A-25)}$$

where $x = P/P_0$.

Cole et al. (1986) have derived an another expression

$$\frac{N}{N_m} = \frac{Cx}{1-x}(D-2)\int_1^{\infty} m^{1-D} \frac{1-(m+1)x^m + mx^{m+1}}{1+(C-1)x-Cx^{m+1}}\, dm \qquad \text{(A-26)}$$

According to these equations, the fractal dimension does affect the monolayer value from which the surface fractal dimension is calculated. For example, Sokolowska et al. (1989) reported the results obtained from the classical B.E.T. equation and the fractal B.E.T. equation (Fripiat et al., 1986). However, according to Fripiat (1989), the effect of the surface fractal dimension at low relative pressure range ($p/p_o < 0.25$) is small, especially when the surface fractal dimension is lower than 2.5 (Fripiat et al., 1986). To ensure this, a few preliminary assessments were conducted by fitting the experimental data with both the classical B.E.T. equation as well as the B.E.T. equation given by Fripiat et al, (1986). The result showed that the use of fractal B.E.T. equation increased the monolayer value, $N_m(\sigma)$, about 7 to 9 percent for the kaolinite data. Since all data points shifted to the same direction, the effect on dimension is believed to be small. As the last example of modified B.E.T. equation, Sokolowska (1989) extended the fractal isotherm equation to the energetic heterogeneous case by incorporating the energy distribution function. In principle, this is an isotherm equation for both geometrically and energetically heterogeneous system. However, this equation also suffers from some of the unrealistic assumptions in the B.E.T. theory.

APPENDIX B
DESORPTION ISOTHERMS

Fig. B-1. Desorption of H2O from KGa-1

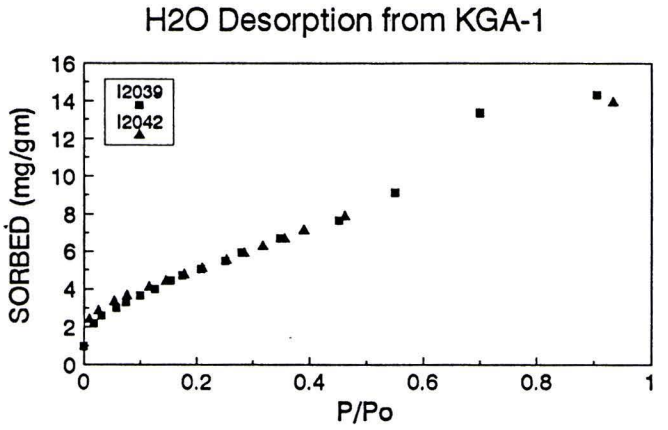

Fig. B-2. Desorption of benzene from KGa-1

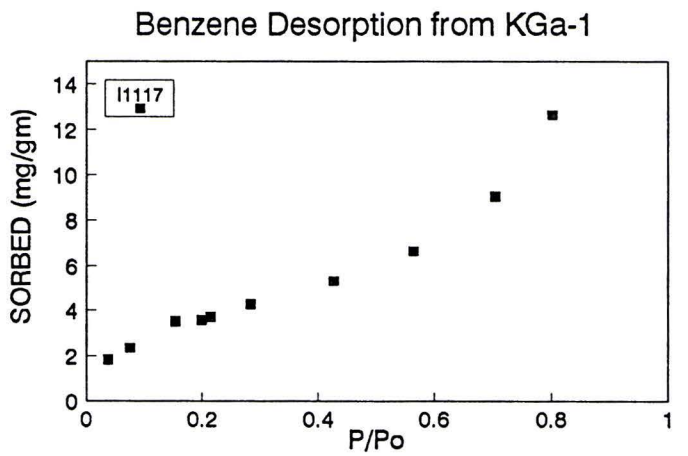

Fig. B-3. Desorption of p-xylene from KGa-1

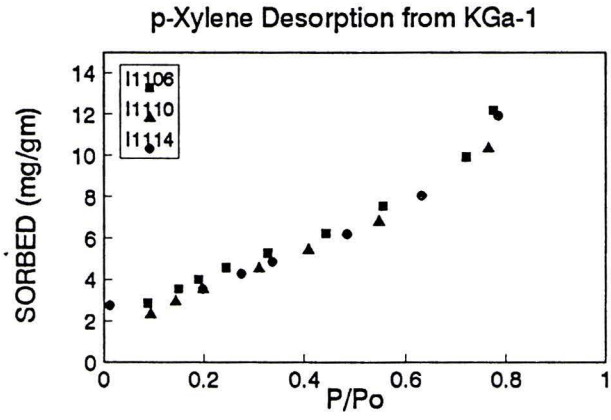

Fig. B-4. Desorption of hexane from KGa-1

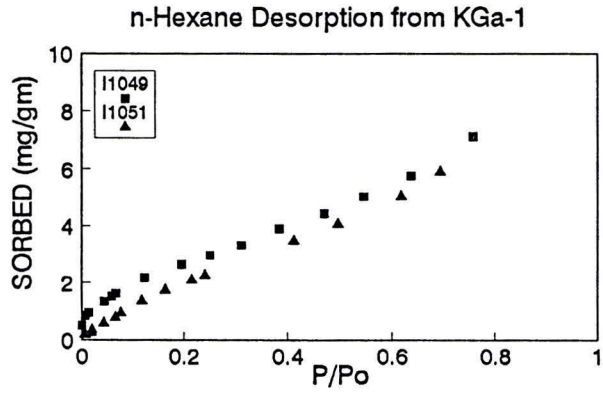

Fig. B-5. Desorption of octane from KGa-1

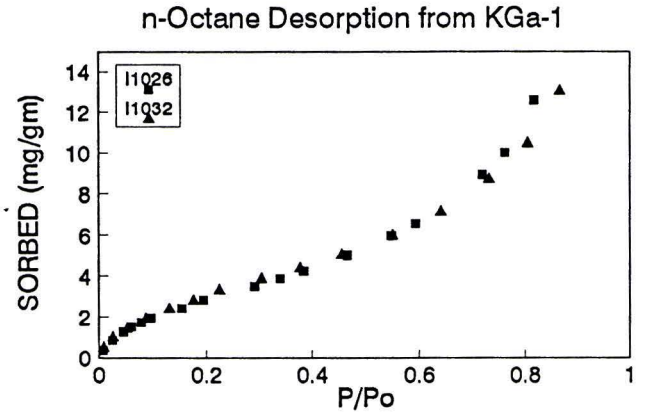

Fig. B-6. Desorption of H2O from silica-gel

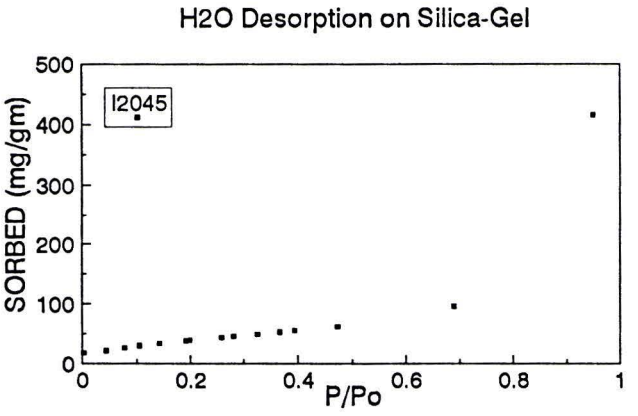

Fig. B-7. Desorption of benzene from silica-gel

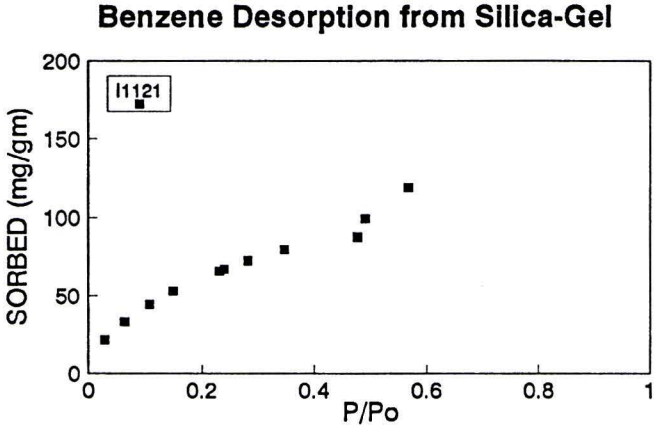

Fig. B-8. Desorption of p-xylene from silica-gel

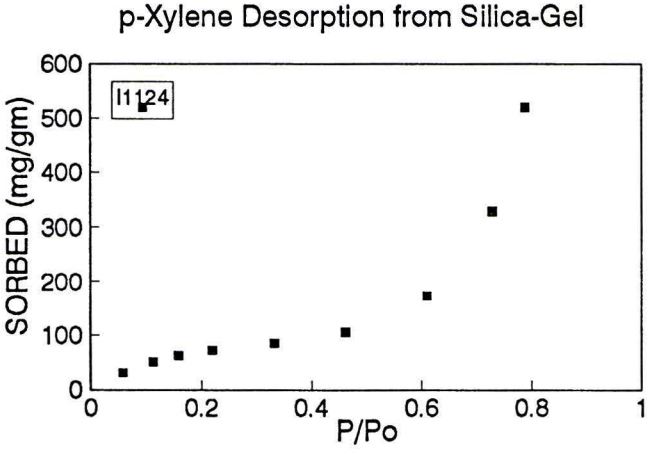

Fig. B-9. Desorption of hexane from silica-gel

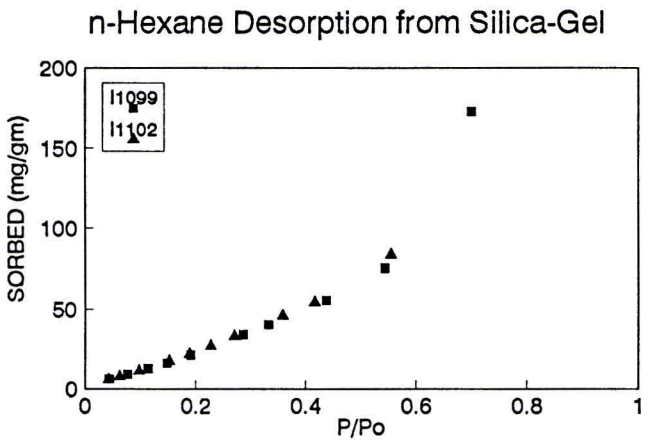

Fig. B-10. Desorption of octane from silica-gel

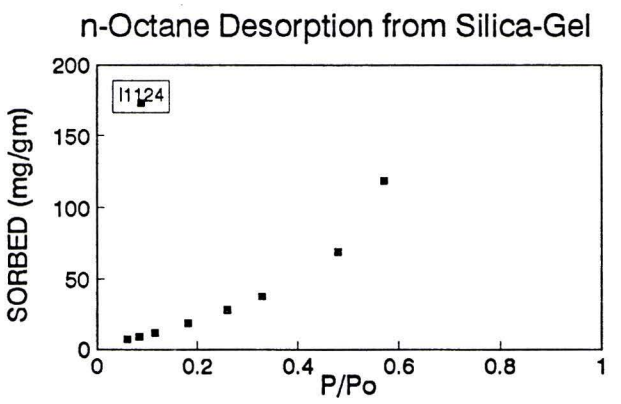

Fig. B-11. Desorption of H2O from Borden aquifer material

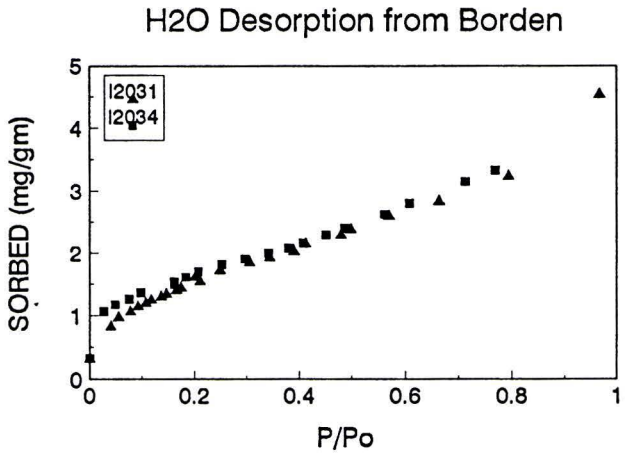

Fig. B-12. Desorption of benzene from Borden aquifer material

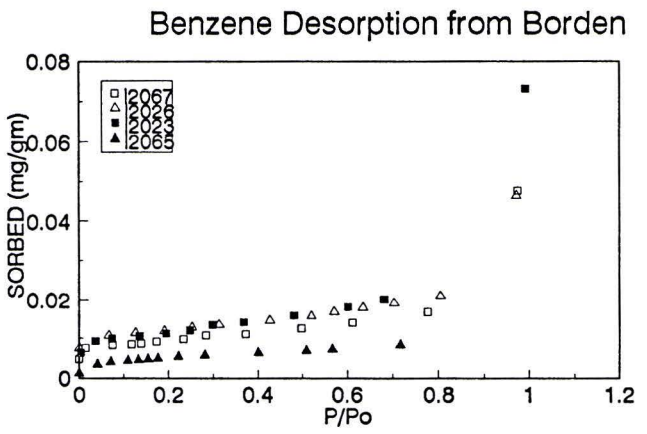

Fig. B-13. Desorption of pentane from Borden aquifer material

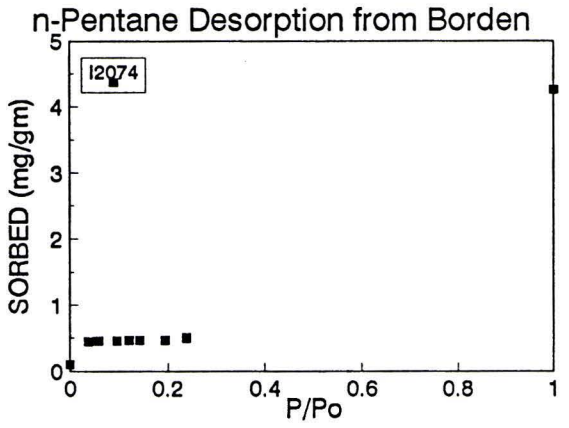

Fig. B-14. Desorption of p-xylene from Borden aquifer material

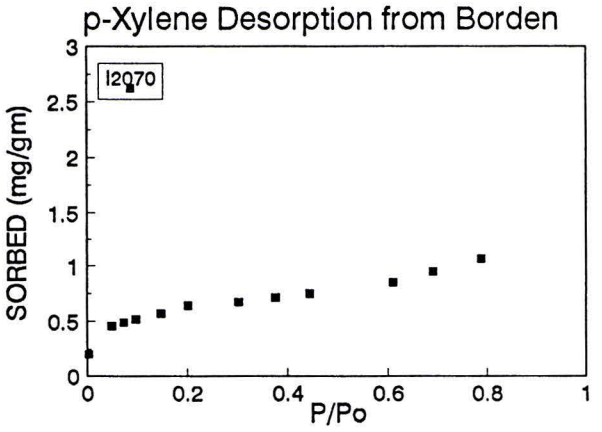

Fig. B-15. Desorption of hexane from Borden aquifer material

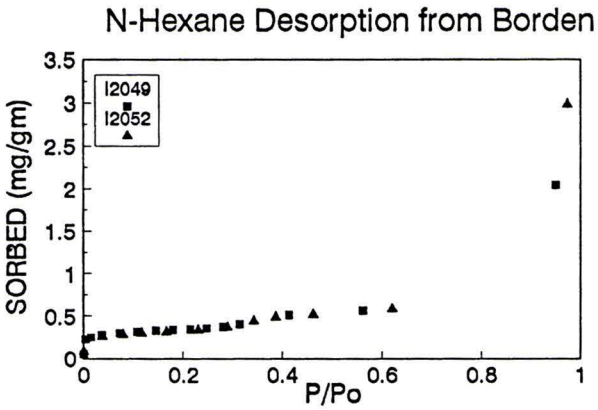

Fig. B-16. Desorption of heptane from Borden aquifer material

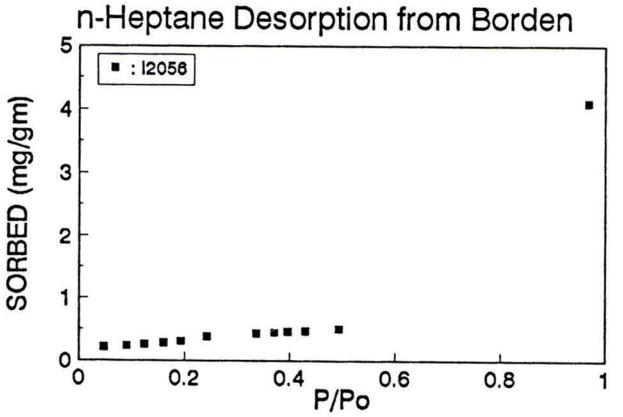

Fig. B-17. Desorption of octane from Borden aquifer material

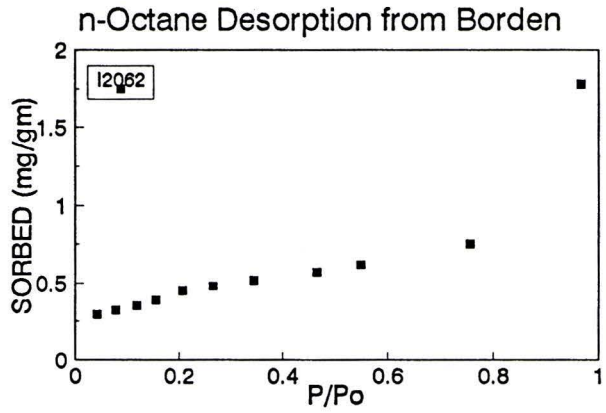

APPENDIX C
DISCRETE MARKOV CHAIN MODEL COMPUTER CODE

```
/* CREATE MEDIUM WITH DIFFUSION-LIMITED AGGREGATION */
/* P0607BM1.C */
#include stdio
#include math
#include stdlib
#include time
short medium[27][27];
short search[729][4];
double base=2.0;
double expo=31.0;
float uniform(float);
int random(int);

main()
{
        int i,j,k,l,m,n,q,r,s;          /* for loop counter */
        int Neighbour;                  /* the number of neighbour */
        float uni;                      /* dummy variable for uniform() */
        int rnd;                        /* dummy variable for random() */
        int x,y;                        /* coordinate for the medium */
        int maxx=28;                    /* size of space in x direction */
       int maxy=28;                     /* size of space in y direction */
        int occ_d[6][3];                /* number of cell occupied & d */
        int agg_time=2000;              /* total time for aggregation */
        int oldx, oldy;                 /* coordinate for the particle */
        int newx, newy;                 /* coordinate for the particle */
        FILE *fp1;                      /* file name pointer */

/* open output files for the medium and diffsuion */
        if ((fp1=fopen("p0607b1.med","w+"))==NULL) {
                perror("fopen\n");
                printf("could not open file-1\n");
                exit();
        }

/* ++++++++++++++++++++++++++++++++++++++++++++++++++++++++++*/
/* initialize the medium */
        for (i=1; i<maxx; i=i+1) {
        for (j=1; j<maxy; j=j+1) {
                medium[i][j]=0;}
```

```
        }

/* initial distribution for all particles */
        occ_d[1][1]=170;
                occ_d[1][2]=60;
        occ_d[2][1]=160;
                occ_d[2][2]=70;
        occ_d[3][1]=150;
                occ_d[3][2]=80;
        occ_d[4][1]=79;
                occ_d[4][2]=90;
        occ_d[5][1]=170;
                occ_d[5][2]=100;

/* allocate high d cells with DLA */
        for (j=1; j<5; j=j+1) {
                i=5-j;
                printf("%d\n",i);
                printf("d=%d\n",occ_d[i][2]);
/* search for opening */
        for (m=1; m<730; m=m+1) {
                search[m][2]=0;
                search[m][3]=0;
        }
        s=0;
        for (m=1; m<maxx; m=m+1) {
        for (n=1; n<maxy; n=n+1) {
                if (medium[m][n]==0) {
                        s=s+1;
                        search[s][1]=s;
                        search[s][2]=m;
                        search[s][3]=n;
                }
        }
        }
        k=1;
        while (k<occ_d[i][1]+1) {
                l=(int)(uniform(uni)*s);
                x=search[l][2];
                y=search[l][3];
                if (medium[x][y]==0) {
                        medium[x][y]=occ_d[i][2];
                        k=k+1;
                }
```

```
        }
/* start aggregation */
        l=0;
        while (l<agg_time) {
                oldx=(int)(uniform(uni)*(maxx-1));
                oldy=(int)(uniform(uni)*(maxy-1));
        if (medium[oldx][oldy]==occ_d[i][2]) {
        Neighbour=0;
        for (q=0; q<2; q=q+1) {
        for (r=0; r<2; r=r+1) {
                Neighbour=Neighbour+medium[oldx+q-1][oldy+r-1];
        }
        }
        if (Neighbour==0) {
                        newx=oldx+random(rnd);
                        newy=oldy+random(rnd);
        if (newx<1) {
                newx=newx+maxx-1;
        }
        if (newy<1) {
                newy=newy+maxy-1;
        }
        if (newx>maxx-1) {
                newx=newx-maxx+1;
        }
        if (newy>maxy-1) {
                newy=newy-maxy+1;
        }
                if (medium[newx][newy]==0) {
                        medium[oldx][oldy]=0;
                        medium[newx][newy]=occ_d[i][2];
                }
        }
        }
        l=l+1;
        }

        } /* the end of the d loop */

        k=0;

        for (m=2; m<maxx-1; m=m+1) {
        for (n=2; n<maxy-1; n=n+1) {
        k=k+1;
```

```
        if (medium[m][n]==0) {
                medium[m][n]=occ_d[5][2];
        }
        if (medium[m][n]==100) {
                medium[m][n]=0;
        }
        fprintf(fp1,"%d,%d,%d,%d\n",k,m-1,n-1,medium[m][n]);
        }
        }

        fclose(fp1);
}

float uniform(float uni)
{
        float p,q;
        srand((unsigned)time(NULL));
        p=(float)rand();
        q=(float)pow(base,expo);
        uni=p/q;
        return uni;
}

int random(int rnd)
{
        float r, uni;
        r=uniform(uni);
        if (r<0.5) {
                rnd= 1;
        }
        else rnd= -1;
        return rnd;
}



/* MARKOVIAN TRANSITION PROBABILITY DENSITY - RANDOM WALK */
/* DISTRIBUTION OF PARTICLE AFTER N MONTE-CARLO STEPS */
/* 2-D CASE */
/* P0607BD1.C */
#include stdio
#include math
#include time
int local[626][5];                      /* node,coordinate,D */
```

```
double transit_1[626][626];          /* transition prob. density matrix */
double transit_i[626][626];          /* PI^(time_intvl) matrix */
double transit_t[626][626];          /* PI^(diff_time) matrix */
double transit_p[626][626];
double density_1[626];               /* initial density of the particles */
double density_t[626];               /* density of particle at diff_time */
double evolution[626][13];           /* time-evolution of density */
void PImatrix(void);                 /* subroutine for PI matrix */
void PIintvl(void);                  /* subroutine for PI^(intvl) */
void INIdens(void);                  /* subroutine for density_1[] */
double base=2.0;
double expo=31.0;
int time_intvl=20;
int d;
int number_node;                     /* number of non-zero node */
FILE *fp1,*fp2;                      /* input/output file pointer */
main()
{
        int i,j,k;                   /* loop counter */
        float uni;                   /* dummy variable for uniform() */
        int x,y,node;                /* coodinate */
        int max_time=200;            /* maximum diffusion steps */
        int max_step=10;
        int max_x=26;
        int max_y=26;
        int dt_step;                 /* diffusion time step */
/* open output file */
        if ((fp1=fopen("p0607b1.out","w+"))==NULL) {
                perror("fopen\n");
                printf("could not open file\n");
                exit();
        }
        if ((fp2=fopen("p0607b1.med","r+"))==NULL) {
                perror("fopen\n");
                printf("could not open file-2\n");
                exit(); }

/* randomize the RNG */
        srand((unsigned)time(NULL));

/* initialize the node[][] */
        i=0;
        while ((fscanf(fp2, "%d,%d,%d,%d\n",&node,&x,&y,&d)!=EOF)) {
        i=i+1;
```

```
        local[i][1]=node;
        local[i][2]=x;
        local[i][3]=y;
        local[i][4]=d;
        }
        number_node=i+1;

/* create the transition probability density matrix */
        PImatrix();

/* create the PI^(time_intvl) */
        PIintvl();

/* create the initial density */
        INIdens();

/* initialize transit_p[][] */
        for (i=1; i<number_node; i=i+1) {
        for (j=1; j<number_node; j=j+1) {
                transit_p[i][j]=transit_i[i][j];
        }
        }

/* calculate the density at diff-time step */
        for (dt_step=1;dt_step<max_step+1;dt_step=dt_step+1){

/* matrix multiplication */
        for (i=1; i<number_node; i=i+1) {
        for (j=1; j<number_node; j=j+1) {
        for (k=1; k<number_node; k=k+1) {
        transit_t[i][j]=transit_t[i][j]+transit_p[i][k]*transit_i[k][j];
        }
        }
        }
/* density(time) calculation */
        for (i=1; i<number_node; i=i+1) {
        for (k=1; k<number_node; k=k+1) {
        density_t[i]=density_t[i]+density_1[k]*transit_t[k][i];
        }
        }
/* density result */
        for (i=1; i<number_node; i=i+1) {
                evolution[i][dt_step]=density_t[i];
                density_t[i]=0.0;
```

```
        }
/* initialize transit_p[][] */
        for (i=1; i<number_node; i=i+1){
        for (j=1; j<number_node; j=j+1){
                transit_p[i][j]=transit_t[i][j];
                transit_t[i][j]=0.0;
        }
        }

        } /* the end of dt_step loop */

/* output */
        for (i=1; i<number_node; i=i+1) {
        fprintf(fp1, "%d,%d,%d,%d,",i,local[i][2],local[i][3],local[i][4]);
        for (j=1; j<11; j=j+1) {
                fprintf(fp1, "%f,",evolution[i][j]);
        }
        fprintf(fp1, "\n");
        }

        fclose(fp1);
        fclose(fp2);
}

void PImatrix(void)
{
        int i,j;
        int f;
        double p;
        double total[626];
        int sq_x,sq_y,sq_sum;
        float r;
        for (i=1; i<number_node; i=i+1) {
                total[i]=0.0;
        for (j=1; j<number_node; j=j+1) {
                transit_1[i][j]=0;
                sq_x=(local[i][2]-local[j][2])*(local[i][2]-local[j][2]);
                sq_y=(local[i][3]-local[j][3])*(local[i][3]-local[j][3]);
                sq_sum=sq_x+sq_y;
               r=sqrt(sq_sum);
                f=local[i][4];
                p=f*0.01;
                transit_1[i][j]=0;
                if (r==0.0){transit_1[i][j]=p;}
```

```
                if (r<1.1&&r>0){transit_1[i][j]=(1-p)/4;}
                if (local[j][4]==0) {transit_1[i][j]=0.0;}
                total[i]=total[i]+transit_1[i][j];
        }
        for (j=1; j<number_node; j=j+1) {
                if (total[i]!=0.0) {
                transit_1[i][j]=transit_1[i][j]/total[i];
                }
        }       }
}

void PIintvl(void)
{
        int i,j,k,t;
        for (i=1; i<number_node; i=i+1) {
        for (j=1; j<number_node; j=j+1) {
                transit_p[i][j]=transit_1[i][j];
        }
        }
        for (t=1; t<20; t=t+1) {
        for (i=1; i<number_node; i=i+1) {
        for (j=1; j<number_node; j=j+1) {
        for (k=1; k<number_node; k=k+1) {
        transit_t[i][j]=transit_t[i][j]+transit_p[i][k]*transit_1[k][j];
        }
        }
        }
        for (i=1; i<number_node; i=i+1){
        for (j=1; j<number_node; j=j+1){
                transit_p[i][j]=transit_t[i][j];
                transit_t[i][j]=0.0;
        }
        }
        }
        for (i=1; i<number_node; i=i+1) {
        for (j=1; j<number_node; j=j+1) {
                transit_i[i][j]=transit_p[i][j];
                transit_p[i][j]=0.0;
        }
        }
}

void INIdens(void)
{
```

```
        int i;
        for (i=1; i<number_node; i=i+1) {
                density_1[i]=0;
                if (local[i][1]==313) {density_1[i]=1.0;}
        }
}
```

APPENDIX D
DISTRIBUTION OF SELF-TRANSITION NUMBER

First of all, we will consider how the self-transition number is related to the diffusion coefficient. The simple 1-D case will be discussed here. Suppose that the motion of the solute particle per unit time can be approximated with three states; one step to the left, one step to the right, or remains at the same position. For a symmetrical random walk, the transition probabilities are $p_1 = (1-p)/2$ (left), $p_3 = (1-p)/2$ (right) and $p_2 = p$ respectively (p is the self-transition probability). After n time steps, the probability of making k_1 steps to the left, k_2 steps remained the same place, and k_3 steps to the right is given by a multinomial distribution which can be approximated (DeMoivre-Laplace theorem) as

$$\frac{n!}{k_1!\,k_2!\,k_3!}\,p_1^{k_1}\,p_2^{k_2}\,p_3^{k_3} \approx \frac{\exp\left(-\frac{1}{2}\left[\frac{(k_1-np_1)^2}{np_1}+\frac{(k_2-np_2)^2}{np_2}+\frac{k_3-np_3)^2}{np_3}\right]\right)}{\sqrt{(2\pi n)^2\,p_1\,p_2\,p_3}} \qquad \text{(D-1)}$$

Similarly, when the transition is represented with two states probability of Bernoille trial, to the left, p, and to the right, q = 1-p, the distribution of the particle after n time steps is represented with binomial distribution which is approximated with a normal distribution using DeMoivre-Laplace theorem.

$$\frac{n!}{k_1!\ k_2!} p^{k_1} q^{k_2} = \frac{1}{(2\pi npq)^{1/2}} \exp\left[-\frac{(k_1 - np)^2}{2npq}\right] \qquad \text{(D-2)}$$

Then the variance and the transition probability is related as

$$\sigma^2 = npq \qquad \text{(D-3)}$$

where t is the time corresponding to the n time steps. The relationship between the variance and the apparent diffusion coefficient is given as

$$\sigma^2 = 2Dt \qquad \text{(D-4)}$$

Therefore, it is reasonable to expect Gaussian distribution from simple random walk simulation. In other words, the self-transition number is related to the diffusion coefficient.

The transition probability, $p[x_2(t=t_{i+1}) \mid x_1(t=t_i)]$ is defined as the probability that the given particle (solute) is transported from x_1 to x_2 in unit time step. Therefore a transition probability itself is not a mechanical parameter. However, it is important to understand what a transition probability represents. As an example,, we consider the mesoscopic diffusion-like transport of solute in sorbed phase.

In the sorbed phase, the solvent is assumed to be stagnant (immobile). The motion of the solute particle is thus induced by the thermal motion of the particle and the numerous collisions among the molecules. Various factors influence the transition probability, or the apparent diffusion coefficient of the local environment. The diffusion-dominated solute transport environment may be viewed as pores

filled with stagnant water, surrounded by reactive walls. Then the following factors are identified.

(1) Diffusion takes place in solution phase.

(2) There are tortuous paths.

(3) There is the interaction between solute and the local environment (local sorption).

The corresponding local transport equation (homogeneous case) is written as

$$\frac{\partial M}{\partial t} = D(\tau,\theta)\ \nabla^2 C \qquad \text{(D-2)}$$

$$M = C + S \qquad \text{(D-3)}$$

M represents the mass in the control volume, which is the sum of the mass in the solution phase and local sorbed phase, C, and the mass in the local sorbed phase, S, per unit control volume. Note that in this description, the concentrations are expressed in terms of mass per unit control volume rather than per unit volume of solution or per unit mass of soil. Also remember that this equation could be describing the solute transport inside the macroscopic sorbed phase domain. Therefore, the solution phase in this domain is not the bulk solution phase, but rather stagnant, immobile phase. $D(\tau,\theta)$ is the diffusion coefficient of the local medium under the given water content, θ, and the tortuosity factor, τ. Therefore, $D(\tau,\theta)$ account for the factors (1) and (2) mentioned above. The local sorption factor is often treated separately, partly to account for the non-linear (concentration dependent) sorption behavior. For simplicity, let assume that the local interaction

energy between the solute and local sorption site/domain, $\Delta\epsilon$, is concentration independent. If we assume Boltzmann distribution, the probability that the local sorption coefficient, K = S / C is proportional to $\exp(-\Delta\epsilon/RT)$, where R is the gas constant, and T is the temperature. Then the apparent diffusion coefficient which includes the all three factors can be written as $D(\tau, \Delta\epsilon, \theta, ...) = D(\tau,\theta)/(1+K(\Delta\epsilon))$. The relationship between the apparent diffusion coefficient and the transition probability can be estimated from DeMoivre-Laplace, or from the law of large numbers.

The distribution of the self-transition number is, thus, related to the joint distributions of the $\Delta\epsilon$ (the local interaction energy), θ (the local water content), τ (the local tortuosity factor).

REFERENCE LIST

Adamson,A.W., 1990, Physical Chemistry of Surfaces, 5th edition, John Wiley and Sons, Inc., New York

Alymore,L.A.G., Sills,I.D., and Quirk,J.P., 1970, Surface area of homoionic illite and montmorillonite clay minerals as measured by the sorptions of nitrogen and carbon dioxide, Clays and Clay Minerals, 18:91-96

Augustijn,D.C.M., 1993, Chemodynamics of Complex Waste Mixtures: Applications to Contamination and Remediation of Soils and Aquifer Media, Ph.D. dissertation, University of Florida

Avnir,D., Farin,D., and Pfeifer,P., 1983, Chemistry in noninteger dimension between two and three, II. Fractal surfaces of adsorbents, J. Chem. Phys., 79:3566-3571

Avnir,D., Farin,D. and Pfeifer,P., 1984, Molecular fractal surfaces, Nature, 308:261-263

Avnir,D. Farin,D., and Pfeifer,P., 1985, Surface geometric irregularity of particulate materials: The fractal approach, J. Coll. Interface Sci., 103:112-123

Bale,H.D. and Schmidt,P.W, 1984, Small-angle x-ray-scattering investigation of submicroscopic porosity with fractal properties, Physics Rev. Lett., 53:596-599

Ball,W.P., Buehler,Ch., Harmon,T.C., MacKay,D.M., and Roberts,P.V., 1990, Characterization of a sandy aquifer material at the grain scale, J. Contami. Hydrol., 5:253-295

Bartoli,F., Philippy,R., Doirisse,M., Niquet,S. and Dubuit,M., 1991, Structure and self-similarity in silty and sandy soils: The fractal approach, J. Soil Science, 42:167-185

Bhattacharya,R.N., and Gupta,V.K., 1990, Application of central limit theorems to solute dispersion in saturated porous media : From kinetic to field scales, In: Dynamics of Fluids in Hierarchical Porous Media, edit. J.H. Cushman, Academic Press, San Diego

Brown,G., Newman,A.C.D., Rayner,J.H., Weir,A.H., 1985, The structure and chemistry of soil clay minerals, in The Chemistry of Soil Constituents, edit Greenland,D.J. and Hayes,M.H.B, pp 29-178, John Wiley and Sons, Chichester

Brusseau,M.L. and Rao,P.S.C., 1989, Sorption nonideality during organic contaminant transport in porous media, Critical Reviews in Environmental Control, 19:33-99

Callen,H.B., 1985, Thermodynamics and an Introduction to Thermostatistics, John Wiley and Sons, New York

Carter,D.L., Mortland.M.M. and Kemper,W.D., 1986, Specific surface area, in Methods of Soil Analysis: Part 1 - Physical and Mineralogical Methods, 2nd. edit., edit. Klute,A., pp 413-423, American Society of Agronmy / SoilScience Society of America, Wisconsin

Chiou,C.T., Kyle,D.E. and Malcolm,R.L., 1988, Sorption of vapors of some organic liquids on soil humic acids and its relation to partitioning of organic compounds in soil organic matter, Environ. Sci. and Technol., 22:298-303

Chu,S-Y., and Sposito,G., 1980, A derivation of the macroscopic solute transport equations for homogeneous, saturated, porous media, Water Resources Research, 16:542-546

Clint,J.H., 1972, Adsorption of n-alkane vapours on graphon, J. Chem. Soc. Faraday Trans. I., 68:2239-2246

Cohen,W.H. and Knight,B.H., 1947, Adsorption phenomena in soils with special reference to their surface area, J. Soc. Chem. Ind., 66:357-364

Crank,J., 1975, The Mathematics of Diffusion, Clarendon Press, Oxford, 1975

Durbin,P.A., 1983, Stochastic Differential Equations and Turbulent Dispersion, NASA Reference Publication 1103

Falconer,K.J., 1989, Fractal Geometry: Mathematical Foundations and Applications, Wiley, New York

Farin,D. and Avnir,D., 1989, The fractal nature of molecular-surface interactions and reactions, in The Fractal Approach to Heterogeneous Chemistry, edit. Avnir,D. pp271-293, John Wiley and Sons Ltd., New York

Farin,D. Volpert,A. and Avnir,D., 1985, Determination of adsorption conformation from surface resolution analysis, J.Amer.Chem.Soc., 107:3368-3370

Feder,J., 1988, Fractals, Plenum Press, New York

Fripiat,J.J., 1989, Porosity and adsorption isotherms, in The Fractal Approach to Heterogeneous Chemistry, edit. Avnir, pp331-340, John Wiley and Sons Ltd.,New York

Fripiat,J.J., Gatineau,L. and van Damme,H., 1986, Multilayer physical adsorption on fractal surfaces, Langmuir, 2:562-567

Freyberg,D.L., 1986, A natural gradient experiment on solute transport in a sand aquifer, 2, Spatial moments and the advection and dispersion of nonreactive tracers, Water Resources Research, 22:2031-2046

Gregg,S.J. and Sing,K.S.W., 1982, Adsorption, Surface Area, and Porosity, Academic Press, London

Halvin,S. and Ben-Avraham,D., 1987, Diffusion in disordered media, Advances in Physics, 36:695-798

Hill,T.H., 1986, Introduction to Statistical Thermodynamics, Dover, New York

Jaroniec,M. and Madey,R., 1988, Physical Adsorption on Heterogeneous Solids, Elsevier, Amsterdam

Jepson,W.B. and Rowse,J.B., 1975, The composition of kaolinite - an electron microscope microprobe study, Clay and Clay Minerals, 23:310-317

Joy,A.S., 1953, Methods and techniques for the determination of specific surface area by gas adsorption, Vacuum, 3:254-278

Jury,W.A., Sposito,G. and White,R., 1986, A Transfer function model of solute transport through soil 1. Fundamental concepts, Water Resources Research, 22:243-247

Kaye,B.H., 1989, Image analysis techniques for characterizing fractal structures, in The Fractal Approach to Heterogeneous Chemistry, edit. Avnir,D. pp55-66, John Wiley and Sons, New York

Knighton,R.E. and Wagnet,R.J., 1987, Simulation of solute transport using a continuous time Markov process 1. Theory and steady state approximation, Water Resources Research, 23(10):1911-1916

Laszlo,E., 1972, The Systems View of the World, Braziller, New York

Little,L.H., 1966, Infrared Spectra of Adsorbed Species, Academic Press, New York

Mandelbrot,B.B., 1982, The Fractal Geometry of Nature, W.H. Freeman, New York

Mandelbrot,B.B. and van Ness,J.W., 1968, Fractional Brownian motions, fractional noises and applications, SIAM Review, 10:422-437

McClellan,A.L. and Harnsberger,H.F., 1967, Cross-sectional area of molecules adsorbed on solid surfaces, J. Coll. Interf. Sci., 23:577-599

Mitescu,C.D., Ottavi, H. and Roussenq, J., 1978, Diffusion on percolation lattices: The labyrinthine ant, In Electrical Transport and Optical Properties of Inhomogeneous Media, edit. Garland,J.C. and Tanner,D.B., pp 377-81, American Institute of Physics, New York

Montroll,E.W., 1964, Random walks on lattices, Proc. Symp. Apply. Math., 16, 193-220

Mortensen,R.E., 1969, Mathematical problems of modeling stochastic nonlinear dynamic systems, J. Stat. Phys., 2:271-296

Nakanishi,K. and Soga,N, 1988, Adsorption on alcohol vapors on alkoxide-derived silica-gels, J. Non-Cryst. Solids, 100:399-403

Nkedi-Kizza,P., Bigger,J.W., Selim,H.M., van Genuchten,M.Th., Wierenga,P.J., Davidson,J.M., and Nielson,D.R., 1984, On the equivalence of two conceptual models for describing ion exchange during transport through an aggregated Oxisol, Water Resour. Res., 20, 1123-1130

Ogilvy,J.A., 1991, Theory of Wave Scattering from Random Rough Surface, A. Hilger, Philadelphia

Orcel,G., 1987, The Chemistry of Silica Sol-Gel, Ph.D. dissertation, University of Florida

Pandey,R.B., Stauffer,D., Margolina,A., and Zabolitzky,J.G., 1984, Diffusion on random systems above, below and at their percolation threshold in two and three dimensions, J. Stat. Phys., 34, 427-450

Papoulis,A., 1991, Probability, Random Variables, and Stochastic Processes, McGraw-Hill, New York

Pfeifer,P., 1987, Characterization of surface irregularity, in Preparative Chemistry using Supported Reagents, edit. Laszlo,P., pp13-33, Academic Press, San Diego

Pfeifer,P., 1988, Fractals in surface science: scattering and thermodynamics of adsorbed films, in Chemistry and Physics of Solid Surfaces VII, edit. Vanselow,R., pp 283-305, CRC press, New York

Pfeifer,P. and Avnir,D., 1983, Chemistry in noninteger dimensions between two and three. I. Fractal theory of heterogeneous surface, J.Chem.Phys., 79:3558-3565 .

Pfeifer,P., Avnir,D. and Farin,D., 1984, Scaling behavior of surface irregularity in the molecular domain: From adsorption studies to fractal catalysis, J. Stat. Phys., 36:699-716

Pfeifer,P. Johnston,G.P., Deshpande,R., Smith,D.M., and Hurd,A.J., 1991, Structure analysis of porous solids from preadsorbed films, Langmuir, 7:2833-2843

Pfeifer,P. and Obert,M., 1989, Fractals : Basic concepts and terminology, in The Fractal Approach to Heterogeneous Chemistry, edit. Avnir,D., pp11-43, John Wiley and Sons Ltd., New York

Pines-Rojanski,D., Huppert,D., and Avnir,D., 1987, Pore-size effects on the fractal distribution of adsorbed acceptor molecules as revealed by electronic energy transfer on silica surface, Chem. Phys. Letter, 139:109-115

Rao,P.S.C., Jessup,R.E., Rolston,D.E., Davidson,J.M., and Kilcrease,D.P., 1980, Experimental and mathematical description of nonadsorbed solute transfer by diffusion in spherical aggregates, Soil Sci. Soc. Am. J., 44:684-688

Reif,F., 1965, Fundamentals of Statistical and Thermal Physics, McGraw-Hill, New York

Rice,J.A., and Lin,J-S., 1993, Fractal nature of humic material, Environ. Sci. and Technol., 27:413-414

Rietman,E., 1989, Exploring the Geometry of Nature: Computer Modeling of Chaos, Fractals, Cellular Automata, and Neural Networks, Windcrest Books, Blue Ridge Summit, PA

Rieu,M., and Sposito,G., 1991, Relation pression capillaire-teneure en eau dans les milleux poreux fracgmentes et identification du caractere fractal de la structure des sols, C. R. Acad. Sci. Paris, 312 II:1483-1489

Rojanski,D., Huppert,D., Bale,H.D., Dacai,X., Smith,P.W., Farin,D., Seri-Levy,A., and Avnir,D., 1986, Integrated fractal analysis of silica: Adsorption, electronic energy transfer, and small-angle x-ray scattering, Phys. Rev. Lett., 56:2505-2508

Ross,S.B., Smith,D.M., Hurd,A.J. and Schaefer,D.W., 1988, Surface roughness in vapor phase aggregates via adsorption and scattering techniques, Langmuir, 4:977-982

Rothman,D.H., 1988, Cullular-automaton fluids: A model for flow in porous media, Geophysics, 53:509-518

Schaefer,D.W., 1984, Fractal geometry of silica condensation polymers, Phys. Rev. Lett., 53:1383-1386

Schrödinger,E., 1967, What is Life? & Mind and Matter, Cambridge Unviersity Press, New York

Serra,J.P, 1982, Image Analysis and Mathematical Morphology, Academic Press, London

Serra,R., Andretta,M., Compiani,M. and Zanarini,G., 1986, Physics of Complex Systems : The Mesoscopic Approach to Fluctuations, Non-linearity and Self-Organization, Pergamon

Sokolowska,Z., Stawinski,J., Patrykiejew,A. and Sokolowski,S., 1989, A note on fractal analysis of adsorption process by soils and soil minerals, International Agrophysics, 5:3-12

Sposito,G., Gupta,V.K., and Bhattacharya,R.N., 1983, Foundational theories of solute transport in porous media: A critical review, In: Flow Through Porous Media, edit. Pinder,G.F., pp. 76-85, CML Publishing, Southhampton, England

Swalen,J.D., Allara,D.L., Andrade,J.D., Chandross,E.A., Garoff,S., Israelachvili,J., McCarthy,T.J., Murray,R., Pease,R.F., Rabolt,J.F., Wynne,K.J. and Yu,H., 1987, Molucular monolayers and films, Langmuir, 3:932-950

Takayasu,H. and Takayasu,M., 1988, What is Fractal?, Diamond, Tokyo

Tatsumi,J., Yamauchi,A. and Kono,Y., 1991, Fractal analysis of plant root systems, Annals of Botany, 64:499-503

Tikhonov,A.N. and Arsenin,V.Y., 1977, Solutions of Ill-Posed Problems, edit. John, F., V.H. Winston & Sons, Washington D.C.

Tisscot,B. and Ungerer,Ph., 1989, 14th international meeting on organic geochemistry: Introductory talk, Organic Geochemistry, 16:XXV-XLV

Tyler,S.W. and Wheatcraft,S.W., 1990, Fractal processes in soil water retention, Water Resources Research, 26:1047-1054

Uffink,G.J.M., 1989, Application of Kolmogorov's backward equation in random walk simulations of groundwater contaminant transport, In: Contaminant Transport in Groundwater Proceedings of the International Symposium on Contaminant Transport in Ground Water, edit. Kobus,,H.E. and Kinzelbach,H., pp 283-290, A.A. Balkema, Rotterdam

van Damme,H., Levitz,P., Fripiat,J.J., Alcover,J.F., Gatineau,L. and Bergaya,F., 1985, Clay minerals: A molecular approach to their (fractal) microstructure, Springer Proceedings in Physics, 5:24-30

van Kampen,N.G., 1981a, Stochastic Processes in Physics and Chemistry, North-Holland, New York

van Kampen,N.G., 1981b, Ito versus Stratonovich, J. Stat. Phys., 24:175-187, 1981

Vicsek,T. 1989, Fractal Growth Phenomena, World Scientific, New Jersey

Wijnen,P.W.J.G., Beelen,T.P.M., Rummens,K.P.J., Saeijs,H.C.P.L., de Haan,J.M., van de Ven,L.J.M. and Santen,R.A., 1991, The molecular basis of aging of aqueous silica gel, J. Coll. Interf. Sci., 145:17-32

Wolfram,S., 1986, Cellular automaton fluids 1: Basic theory, J. Stat. Phys., 45:471-526

Yates,S.R. and Yates,M.V., 1990, Geostatistics for Waste Management: A User's Manual for the GEOPACK (Version 1.0) Geostatistical Software system, U.S. E.P.A., Ada, OK

Young,I.M. and Crawford,J.W., 1991, The Fractal structure of soil aggregates: Its measurement and interpretation, J. Soil Sci., 42:187-192

BIOGRAPHICAL SKETCH

Itaru Okuda was born in 1964 in Nagoya, Japan. He studied environmental science at Tokyo University of Agriculture and Technology, and earned the B.S. degree in 1987. From 1987 to 1989, he attended the University of California at Riverside. Under the supervision of Dr. W.J. Farmer, he received M.S. degree in soil science (soil chemistry) in 1989. Since 1989, he has been studying soil chemistry/physics at University of Florida.

I certify that I have read this study and that in my opinion it conforms to acceptable standards of scholarly presentation and is fully adequate, in scope and quality, as a dissertation for the degree of Doctor of Philosophy.

P.S.C. Rao, Chair
Graduate Research Professor of Soil and Water Science

I certify that I have read this study and that in my opinion it conforms to acceptable standards of scholarly presentation and is fully adequate, in scope and quality, as a dissertation for the degree of Doctor of Philosophy.

C.T. Johnston
Associate Professor of Soil and Water Science

I certify that I have read this study and that in my opinion it conforms to acceptable standards of scholarly presentation and is fully adequate, in scope and quality, as a dissertation for the degree of Doctor of Philosophy.

R.D. Rhue
Associate Professor of Soil and Water Science

I certify that I have read this study and that in my opinion it conforms to acceptable standards of scholarly presentation and is fully adequate, in scope and quality, as a dissertation for the degree of Doctor of Philosophy.

C.W. Park
Assistant Professor of Chemical Engineering

I certify that I have read this study and that in my opinion it conforms to acceptable standards of scholarly presentation and is fully adequate, in scope and quality, as a dissertation for the degree of Doctor of Philosophy.

K. Hatfield
Assistant Professor of Civil Engineering

I certify that I have read this study and that in my opinion it conforms to acceptable standards of scholarly presentation and is fully adequate, in scope and quality, as a dissertation for the degree of Doctor of Philosophy.

W.D. Graham
Assistant Professor of Agricultural Engineering

This dissertation was submitted to the Graduate Faculty of the College of Agriculture and to the Graduate School and was accepted as partial fulfillment of the requirements for the degree of Doctor of Philosophy.

August 1993

Dean, College of Agriculture

Dean, Graduate School